



Università degli Studi di Ferrara

DOTTORATO DI RICERCA IN SCIENZE DELL'INGEGNERIA

CICLO XXII

COORDINATORE Prof. TRILLO STEFANO

**A F.E. UPPER BOUND LIMIT ANALYSIS MODEL FOR MASONRY
CURVED AND 3D STRUCTURES, WITH AND WITHOUT FRP-
REINFORCEMENT**

Settore Scientifico Disciplinare ICAR/08

Dottorando

Dott. [Enrico Milani](#)

Tutori

Prof. [Antonio Tralli](#)

Dott. [Gabriele Milani](#)

Anni 2007/2009

Doctoral Thesis submitted in fulfilment of the requirements for the Degree of
Doctor of Philosophy

Ph.D. Program:

Università degli Studi di Ferrara

Dipartimento di Ingegneria

Dottorato di Ricerca in Scienze dell'Ingegneria Civile

Thesis Supervisors:

Prof. Antonio Tralli – Università degli Studi di Ferrara, Italy

Dr. Gabriele Milani – Politecnico di Milano, Italy

Public Defence: Ferrara, Italy, March 26, 2010

Board of Examiners:

Prof. Antonio Tralli - Università degli Studi di Ferrara, Italy

Prof. Elio Sacco - Università degli Studi di Cassino, Italy

Prof. Renato Lancellotta – Politecnico di Torino, Italy

Acknowledgments

The work has been carried out at the Engineering Department of the University of Ferrara under the supervision of Prof. Antonio Tralli and Dr. Gabriele Milani.

I am grateful to Prof. Tralli, for his advice and useful suggestions.

I would like to thank Dr. Milani Gabriele for the hard work done together and under his guide.

I would like to record my thanks to Prof. Claudio Alessandri and Ing. Vincenzo Mallardo from the faculty of Architecture of the University of Ferrara, who followed the beginning of my work with interest and friendship.

A very special thanks goes out to all my friends, in particular to Luca. We have always shared good times and unforgettable happy moments.

He has been, is and always will be my reference point.

Finally, a great thank to all my family Ermanno, Patrizia, Marco, Mirco, Michela, Andrea, Leonardo, Giuseppe, Nicolina e Dina.

Thanks God for giving me such a beautiful family. They gave me the education and handed down the most important life values. They taught me the love of knowledge. They have always encouraged and helped me a lot. I love you.

SOMMARIO

Lo scopo della seguente tesi è di proporre un nuovo efficiente modello numerico basato sul teorema cinematico dell'analisi limite, per lo studio di volte e strutture in muratura con o senza fibrorinforzi in FRP.

L'approccio consiste in 2 Step. Al primo step si definiscono le superfici di rottura della struttura in muratura senza FRP attraverso una procedura di analisi limite. Si considera una cella rappresentativa costituita da un elemento centrale collegato con gli altri elementi attraverso delle interfacce rigide-plastiche (giunti di malta).

Nel secondo step le superfici di rottura vengono implementate in un innovativo codice agli elementi finiti per l'analisi al collasso di volte o interi edifici in muratura.

ABSTRACT

The aim of this thesis is to propose a new efficient numerical tool, based on the kinematic theorem of limit analysis, for the study of masonry shell and 3D structures with or without FRP reinforcement.

The approach consists of two steps. In step I unreinforced masonry strength domains are obtained with a FE limit analysis procedure applied to a representative element of volume constituted by a central brick interacting with its six neighbours by means of rigid plastic interfaces (mortar joint). In step II, the unreinforced strength domains are implemented in a novel upper bound FE limit analysis code for the analysis at collapse of entire masonry curved and 3D structures.

Contents

| | |
|---|-----------|
| Chapter 1 Introduction | 1 |
| 1.1 Masonry curved elements..... | 5 |
| 1.2 Masonry reinforced with FRP..... | 8 |
| 1.3 References..... | 11 |
| | |
| Chapter 2 Masonry curved shells homogenized failure surfaces | 17 |
| 2.1 Homogenization background..... | 19 |
| 2.2 Derivation of masonry homogenized failure surfaces by means of a FE discretization of the unit cell..... | 29 |
| 2.3 Numerical results..... | 38 |
| 2.3.1 Parabolic arches by Vermeltfoort..... | 38 |
| 2.3.2 Ribbed cross vault..... | 44 |

| | | |
|--|---|------------|
| 2.3.3 | Emi-spherical dome..... | 49 |
| 2.3.4 | Cloister vault | 52 |
| 2.4 | Conclusion..... | 58 |
| 2.5 | References..... | 59 |
| Chapter 3 Limit analysis of masonry vaults by curved shell Finite Elements | | 63 |
| 3.1 | The curved triangular F. E. model..... | 64 |
| 3.1.1 | Basic assumptions..... | 64 |
| 3.1.2 | Six-nodes curved shell elementary..... | 65 |
| 3.1.3 | Plastic flow relationships and power dissipation. | 71 |
| 3.1.4 | The Linear Programming (LP) problem..... | 73 |
| 3.2 | Structural examples..... | 74 |
| 3.2.1 | Barrel rectangular vault..... | 75 |
| 3.2.2 | Skew arch..... | 78 |
| 3.2.3 | Ribbed cross vault..... | 84 |
| 3.2.4 | Hemispherical dome..... | 88 |
| 3.3 | Conclusion..... | 93 |
| 3.4 | References..... | 99 |
| Chapter 4 Upper Bound limit analysis model for FRP-reinforced masonry curved structures | | 101 |
| 4.1 | The structural level F. E. model..... | 103 |
| 4.1.1 | Basic assumptions..... | 103 |
| 4.1.2 | 6-noded wedge masonry element..... | 103 |

| | |
|--|------------|
| 4.1.3 Plastic flow relationships and power dissipation. | 104 |
| 4.1.4 3-noded flat FRP elements (triangles)..... | 109 |
| 4.1.5 FRP/masonry interfaces (delamination)..... | 113 |
| 4.2 Structural examples..... | 120 |
| 4.2.1 Parabolich arch..... | 123 |
| 4.2.2 Ribbed cross vault..... | 133 |
| 4.2.3 Hemispherical dome..... | 138 |
| 4.2.4 Cloister Vault..... | 144 |
| 4.3 Conclusion..... | 147 |
| 4.4 References..... | 150 |
| | |
| Chapter 5 Application of numerical model proposed on an entire masonry building | 153 |
| | |
| 5.1 Masonry test structure: geometry description..... | 154 |
| 5.1.1 Reinforced building..... | 155 |
| 5.1.2 Loading condition and material properties..... | 155 |
| 5.2 Numerical results..... | 159 |
| 5.2.1 X direction..... | 159 |
| 5.2.2 Y direction..... | 167 |
| 5.3 Conclusion..... | 173 |
| 5.4 References..... | 174 |
| | |
| Chapter 6 Conclusion | 177 |

References

181

Chapter 1.

Introduction

The recent earthquakes occurred in Umbria and Marche (Italy 1997-1998), Molise (Italy 2002) and Abruzzo (Italy 2009) indicated that the historical Italian buildings, essentially constituted by masonry structures, are scarcely resistant to horizontal loads and highly vulnerable to seismic actions. Such inadequate behavior of brickwork under earthquakes is a common issue of masonry buildings in many countries worldwide. Inadequate resistance under seismic actions may be observed also for curved masonry structures, as for instance vaults, domes and arches, which typically are designed to withstand vertical loads under membranal regimes only. Great impact on the scientific community and on common people had the collapse of one vault of the S. Francesco Basilica in Assisi during Umbria earthquake (26 September 1997), which caused both the death of 4 persons and an unquantifiable artistic loss, due to the almost total destruction of frescos realized by the great Italian medieval artist Cimabue.

The need of designing efficient and non invasive strengthening interventions to masonry structures in seismic area appeared almost immediately clear to all technicians involved in the reconstruction of collapsed vaults after Umbria and Marche earthquakes. Therefore, the utilization of FRP strips as reinforcement instead of conventional methods seems the most suitable solution for the seismic upgrading, thanks to the limited invasiveness, durability and good performance at failure [1]-[7] of carbon fibers.

Despite the great importance and the increasing diffusion of such innovative strengthening technique, no numerical models devoted to the prediction of the ultimate load bearing capacity of vaults and entire masonry buildings reinforced with FRP strips are nowadays available. The international scientific community is producing and has recently proposed several numerical models for the analysis of masonry structures with and without FRP but the problem is still open. The difficulty in modeling masonry structures depends on many causes; among the others, the most important are of course, the heterogeneous character of masonry (since it is a regular assemblage of blocks between which mortar joints are laid) and the brittle behavior of joints. Another important remark is that a general approach, able to predict the ultimate load bearing capacity of masonry under in- and out-of-plane loads is still far to be proposed. Especially in presence of out-of-plane actions, the important role of compressive membrane actions has not been taken into account with sufficient care, probably because experimental tests mainly deal with pure flexion (maybe a consequence of the complexity of the experimentation in presence of multiple loads). Sophisticated numerical methods began to emerge during the last decade, and have been used as valuable tools for the analysis of masonry, see for instance the works by Lourenço et al. [8], [9], [10], Berto et al. [11], [12], [13], Luciano and Sacco [14], [15], [16] Marfia and Sacco [17],

Gambarotta and Lagomarsino [18],[19], Pietruszczak and Ushaksarei [20], [21] and Massart et al. [22].

In general, numerical models are based on three different approaches: micro-modeling, macro-modeling and homogenization.

The micro-modeling consists in representing separately mortar joint sand units. In some cases, reasonable simplifications have been introduced, for example utilizing zero-thickness interfaces for the joints (see for instance Lourenço and Rots [10] and Lotfi and Shing [23]). An evident drawback of this approach, which in some cases limits its applicability to small panels, is connected to the necessity of modeling separately units and mortar. Of course, micro-modeling allows to capture a point-to-point prediction of stress and strain state on masonry panels to compare with experimental evidences. On the other hand, the difficult applicability of this method for the structural analysis of complex walls belonging to existing real buildings is evident. The alternative macro-modeling is intended for large-scale structural calculations. With this end in mind, it does not make any distinction between masonry units and joints, so averaging the effect of mortar through the formulation of a fictitious continuous material [24]. Among the others, it is worth mentioning the classical approach which models masonry as a no tension material (NTM). In this framework, many technical and theoretical papers have been published in the past thirty years, mostly by Italian researchers [25]-[29]. In spite of the attractive simplicity of the mechanical assumptions of this approach, robust numerical tools seem to be difficult to obtain, even if some FE codes have been recently implemented with success [30],[31]. Furthermore, even if the classical theorems of limit analysis can be extended to NTM (see [28]) some difficulties are still present. In particular:

- The origin of the axes in the stress space ($\boldsymbol{\sigma} = \mathbf{0}$) belongs to the boundary of the strength domain, so making the use of standard FE packages difficult.
- It should be noted that a key aspect which determines the strength of masonry panels subjected to horizontal actions is friction between the blocks, as pointed out in [32]; as a consequence, constitutive equations for masonry are generally non associated (see for instance [33]). Furthermore, even if an associated flow rule is assumed, a plane stress state in which shear stress and a vertical compressive pressure are acting, while horizontal normal stress is absent (typical situation for load-bearing shear walls), provides a positive principal stress, not admissible for a NTM.

Several other models belonging to macro-modeling can be found in the technical literature, some of which with a marked phenomenological nature. In order to take into account some distinctive aspects of masonry, such as anisotropy in the inelastic range and the post-peak softening behavior, closely related to the constituent materials (mortar and units) and to its geometry (bond pattern, thickness of joints, etc.), some recent macro-models have been “ad hoc” developed (see [8] and [12] for instance), featuring orthotropic elastic-plastic behavior with softening. Usually, the mechanical properties required by the model are derived from experimental data and the results are limited to the conditions under which the data are obtained. Obviously, the introduction of new materials might require a different set of experimental programs.

The third alternative is represented by the application of homogenization. It consists in identifying an elementary cell, which generates an entire panel by regular repetition. There are, indeed, important contributions for masonry in the inelastic range. For instance, Luciano and Sacco [14] proposed a brittle damaging model characterized by a unit cell composed by blocks, mortar and a finite number

of fractures on the interfaces. Massart [34] and Anthoine and Pegon [35] adopted a finite element approach to represent the non linear behavior of the homogenized material, assuming either elastic plastic or damaging constitutive laws for blocks and mortar. Nevertheless, this kind of FE approach requires a great computational effort, since the field problem has to be solved numerically for every time step in any Gauss point. De Buhan and de Felice in [36] proposed a suitable model for a homogenized limit analysis of masonry by means of the kinematic theorem, where the blocks are supposed infinitely resistant and the joints interfaces of zero thickness with a pure Mohr Coulomb failure criterion.

Limit analysis combined with homogenization appears very attractive because it is able to reproduce some distinctive aspects of masonry, such as the anisotropy at collapse and the scarce tensile strength, requiring only a reduced number of mechanical parameters of the constituent materials. Moreover, limit analysis can be easily applied to entire panels, once we dispose of the homogenized strength domains for masonry.

1.1 Masonry curved elements

Masonry curved elements -as for instance arches, domes and vaults- represent one of the most diffused structural typologies in historical buildings of both Eastern and Western architecture. Moreover, the growing interest in the preservation and rehabilitation of historic constructions has created a need for the development of new efficient tools for the analysis and the evaluation of load-bearing capacity of these structures.

The first “scientific” graphical attempts for the study of the equilibrium of masonry domes go back to the early 18th century and are due to, e.g. Bouguer (1734), Bossut (1778) and Mascheroni (1785), who stated simple mono-dimensional equilibrium

equations, neglecting the role of circumferential forces. Anyway, what appeared clear from the beginning, was that cracking occurs on curved masonry elements in presence of self-weight and of very low tensile stresses. In this context, a considerable improvement in the analysis of spherical domes was achieved when Levy (1888) proposed a graphical analysis aimed at finding the circle on which circumferential forces vanish. For an exhaustive history of the theories of masonry vaults we remand to the classical treatise of Benvenuto [37]. Nowadays it can be affirmed (Huerta [38]) that “the modern theory of limit analysis of masonry structures, which has been developed mainly by Heyman [39], is the tool to understand and analyze masonry structures”.

Despite the considerable research efforts done in the last decades and the wide spreading of Finite Elements programs (FE), traditional approaches based on the assumption of a 1D behavior (Heyman [40], Oppenheim et al. [41], Pesciullesi et al. [42]) are still the most diffused in engineering practice. In this context, modern and efficient computerized models have been presented in the framework of both thrust lines method (O’Dwyer[43], Block et al. [44]) and limit analysis (Roca et al. [45]), to predict possible collapse modes of masonry arches and axis-symmetrical domes.

On the other hand, when dealing with the study of complex 2D curved masonry shells, thrust lines methods and at hand calculations are hardly applicable: therefore, FE approaches in the inelastic range have been preferred for these kind of problems, assuming for masonry either a no tension (Lucchesi et al. [46] and [47]), a damaging (Creazza et al. [48] and [49]) or an orthotropic elasto-plastic behavior with low tensile resistance (Lourenço et al. [9], Lourenço [10]).

In the present degree, a novel finite element approach for the limit analysis of masonry vaulted structures is presented. A six-nodes triangular curved element is used in order to correctly take into account, as far as possible, the actual geometry

of the vault. For the sake of simplicity, a kinematic approach with possible velocity discontinuities along the edges of adjoining elements is considered. On the other hand, it has been demonstrated (see Sloan and Kleeman [50]) that the introduction of discontinuities at the interfaces between contiguous elements is suitable for the analysis at collapse of purely cohesive or cohesive-frictional materials, which is the case of masonry. Following a general approach widely diffused in the technical literature for the analysis of masonry flat plates (Sinha [51]) plastic dissipation is allowed only at the interfaces (generalized cylindrical hinges) between adjoining elements. In this way an upper bound of the collapse multiplier is obtained, since, looking at the dual formulation, the admissibility of the stress state is imposed (i.e. the thrust surface is obliged to be inside the vault depth when a no tension material is considered) only at the element boundaries. In order to take into account all possible deformation modes along triangles edges (i.e. rotation, stretching, and sliding) it is assumed that plastic dissipation occurs as a combination of bending, torsion, out-of-plane shear and membrane actions. Such an assumption is necessary when dealing with thick masonry shells (Reissner-Mindlin hypotheses). When in- and out-of-plane sliding phenomena occur, masonry exhibits a typical frictional behavior, which should be represented by non-associated flow rules. Despite this consideration, as it will be discussed throughout the Chapter 3, an associate flow rule is here adopted for the interfaces, in order to tackle large scale engineering problems with homogenization combined with simple LP routines. Thus, plastic dissipation is evaluated assuming for the interfaces between adjoining elements an upper bound approximation of masonry failure surfaces, obtained by means of a standard UB finite element procedure, once that a suitable elementary cell is identified for the curved texture under consideration. It is worth noting that, for double-curvature shell like masonry domes, the identification of an elementary cell which generates the whole structure it is not always possible. However, in these

cases, the technically meaningful simplification of assuming masonry constituted by the assemblage of bricks with variable sizes (depending on the value of principal curvatures) can be adopted.

This is the reason why, in the Chapter 2 a simple heuristic method based on a compatible identification between discrete model and equivalent continuum is preferred. In Chapter 2 the upper bound FE homogenization procedure adopted to obtain an upper bound approximation of the actual failure surfaces for masonry vaults is presented. Several examples of curved REV (parabolic arch, ribbed cross vault, hemispherical dome, barrel vault) are analyzed and discussed in detail. The anisotropy induced by the non null curvature of the REV is particularly evident if compared with results obtained in the flat case.

1.2 Masonry reinforced with FRP

As previously discuss, the utilization of FRP strips as reinforcement instead of conventional methods seems the most suitable solution for their limited invasiveness, durability and good performance at failure for the rehabilitation of domes and entire masonry building.

Nevertheless, it is worth noting that, despite the great importance and the increasing diffusion of such innovative strengthening technique, few numerical models devoted to the prediction of the ultimate load bearing capacity of out-of-plane loaded FRP-reinforced masonry [52][53] are nowadays at disposal.

Very recently, limit state approaches have been attempted for masonry arches also in presence of FRP reinforcement strips, see e.g. Caporale et al. [54] and Roca et al. [45].

As a matter of fact, non linear complex damaging models (e.g. [15]) should be used for the analysis FRP reinforced masonry. The FRP delamination from the support is, indeed, typically brittle, as well as the tensile cracking of mortar joints. These aspects preclude, in principle, the utilization of limit analysis, which is based on the assumption of perfect plasticity for the constituent materials.

Despite the aforementioned limitations connected to the hypotheses at the base of the approach proposed, following also what suggested in the Italian Code CNR-DT200 [55], limit analysis may be useful for design purposes, to provide a fast and reliable estimation of collapse loads at a structural level. On the contrary, no information is given by limit analysis concerning displacements reached near collapse. However, such displacements are relatively small and a rough estimation could be obtained by means of an elastic analysis of the structure modelling the crack pattern previously evaluated by means of limit analysis.

The most important effect of a generic strengthening intervention executed with FRP strips is, indeed, to preclude the formation of the failure mechanism which causes the collapse of the unreinforced structure, with the subsequent formation of a new collapse mechanism different from the un-strengthened case, with higher internal dissipation. Obviously, “hand” calculations may not be performed easily for complex structures, especially in presence of curved shells with unsymmetrical loads. Therefore, the adoption of an upper bound approach combined with FEM seems particularly suited for the prediction of FRP-masonry behavior prone to collapse.

The most suitable way for the analysis of FRP reinforced walls is the utilization of a two-steps approach based on homogenization concepts. First step, relying in the simplified homogenization of unreinforced masonry with a curved representative volume element has been widely illustrated in Chapter 2 and the reader is referred there for a proper discussion of the limitations and the capabilities of the method.

In the second step the macroscopic anisotropic strength domains obtained in Chapter 2 are implemented in a novel upper bound FE limit analysis code for the analysis at collapse of entire FRP reinforced masonry curved structures. Rigid infinitely resistant wedge-shaped 3D elements are used to model masonry at structural level. The utilization of 3D elements is suitable to simulate the flexural strength increase obtained by the introduction of FRP strips. On the other hand, wedge-shaped elements are utilized with the aim of reproducing possible diagonal out-of-plane failures, due to the development of cracks (caused by bending and torsion) which zigzag between contiguous bricks.

FRP strips are modelled by means of triangular rigid elements. Masonry and FRP layers interact by means of interfacial tangential actions between triangles (FRP) and wedges (masonry). Furthermore, a possible limited tensile strength for the FRP reinforcement is considered at the interfaces between adjoining triangular elements. In this way, both delamination phenomenon at the FRP/masonry interface and FRP tensile failure may be taken into account. Despite the fact that delamination is a typical fragile phenomenon, an equivalent ultimate shear strength for FRP/masonry interfaces is assumed in the framework of limit analysis, following formulas provided by the recent Italian norm CNR-DT 200 [55] for the peak delamination strength. It has to be emphasized that the limit analysis approach here proposed is based on the use a perfectly-plastic material response for masonry and for the FRP/masonry interface, i.e. softening effect and limited ductility cannot be considered.

In order to validate the numerical model proposed, a number of different structural examples are analyzed, consisting of two arches tested by Vermeltfoort [56] without reinforcement, a masonry ribbed cross vault by Faccio et al. [57], a hemispherical dome and a cloister vault, both tested by Foraboschi [58] in presence and absence of reinforcement (Chapter 3). Finally in Chapter 5 a set of numerical

simulations on an entire building reinforced with FRP strips and experimentally tested until collapse by Yi et al. [59],[60] is reported in presence and absence of reinforcement.

Results obtained with the model proposed fit well both experimental data and alternative non linear FEM simulations results. From an overall analysis of the performance of the numerical tool proposed, it can be deduced that the approach presented may be a valuable software for practitioners involved in an inexpensive evaluation of ultimate loads of masonry buildings reinforced with FRP strips

1.3 References

- [1] Corradi M, Borri A, Vignoli A. *Strengthening techniques tested on masonry structures struck by the Umbria–Marche earthquake of 1997–1998. Construction and Building Materials* 2002; 16: 229–239.
- [2] Schwegler G. *Masonry construction strengthened with composites in seismically endangered zone. In Proc.: 10th European Conference on Earthquake Engineering, Wien 1994: 2299–2303.*
- [3] Eshani MR. *Strengthening of earthquake damaged masonry structures with composite materials. In Proc.: Nonmetallic (FRP) reinforcement for concrete structures. Proceedings of the Second International RILEM Symposium FRPRCS-2 1997; 681–687.*
- [4] Saadmantesh H. *Fiber composites of new and existing structures. ACI Structural Journal* 1991; 91(3): 346–354.
- [5] El-Dakhakhni WW, Hamid AA, Hakam ZHR, Elgaaly M. *Hazard. mitigation and strengthening of unreinforced masonry walls using composites. Composite Structures* 2006; 73: 458–477.
- [6] Pendhari SS, Kant T, Desai YM. *Application of polymer composites in civil construction: A general review. Composite Structures* 2008; 84(2): 114–124.
- [7] Triantafillou TC. *Composites: a new possibility for the shear strengthening of concrete, masonry and wood. Composites Science and Technology* 1998; 58: 1285–1295
- [8] Lourenço PB. *An orthotropic continuum model for the analysis of masonry structures. Report 03.21.1.31.27 1995, University of Delft, Delft, Holland.*

-
- [9] Lourenço PB, de Borst R, Rots JG. A plane stress softening plasticity model for orthotropic materials. *Int. J. Num. Meth. Eng.* 1997;40: 4033-4057.
- [10] Lourenço PB, Rots JG. A multi-surface interface model for the analysis of masonry structures. *ASCE Jour. Eng. Mech.* 1997;123(7): 660-668.
- [11] Berto L, Saetta A, Scotta R, Vitaliani R. An orthotropic damage model for non linear masonry walls analysis: irreversible strain and friction effects. *Third International Seminar Structural Analysis of Historical Constructions*. Guimaraes, Portugal, 2001.
- [12] Berto L, Saetta A, Scotta R, Vitaliani R. An orthotropic damage model for masonry structures. *International Journal for Numerical Methods in Engineering* 2002; 55(22): 127-157.
- [13] Berto L, Saetta A, Scotta R, Vitaliani R. Shear behaviour of masonry panel: parametric FE analyses. *Int. Jour. Solids Struct.* 2004;41(16-17): 4383-4405.
- [14] Luciano R, Sacco E. Homogenization technique and damage model for old masonry material. *Int. Jour. Solids Struct.* 1997; 34(24):3191-3208.
- [15] Luciano R, Sacco E. Damage of masonry panels reinforced by FRP sheets. *Int. Jour. Solids Struct.* 1998; 35(15): 1723-1741.
- [16] Luciano R, Sacco E. A damage model for masonry structures. *Eur. Jour. Mech.-A/Solids* 1998; 17(2): 5-303.
- [17] Marfia S, Sacco E. Modeling of reinforced masonry elements. *Int. Jour. Solids Struct.* 2001; 38(24-25): 4177-4198.
- [18] Gambarotta L, Lagomarsino S. Damage models for the seismic response of brick masonry shear walls. Part I: the mortar joint model and its applications. *Earthquake Engineering and Structural Dynamics* 1997: 26; 423-439.
- [19] Gambarotta L, Lagomarsino S. Damage models for the seismic response of brick masonry shear walls. Part II: the continuum model Introduction and its applications. *Earthquake Engineering and Structural Dynamics* 1997: 26; 440-462.
- [20] Ushaksaraei R, Pietruszczak S. Failure criterion for structural masonry based on critical plane approach. *J. Eng. Mech.* ASCE 2002; 128(7): 769 –778.
- [21] Pietruszczak S, Ushaksaraei R. Description of inelastic behavior of structural masonry. *Int. Jour. Solids Struct.* 2003; 40(15): 4003-4019.
- [22] Massart TJ, Peerlings RHJ, Geers MGD. Mesoscopic modeling of failure and damage-induced anisotropy in brick masonry. *Eur. Jour. Mech.-A/Solids* 2004; 23(5): 719-735.
- [23] Lotfi HR, Shing PB. Interface model applied to fracture of masonry structures. *Jour. Struct. Eng.* ASCE 1994; 120(1): 63-80.
- [24] Heyman J. The stone skeleton. *Int. J. Solids Structures* 1966; 2: 249-279.

- [25] Romano G, Romano M. *Sulla soluzione di problemi strutturali in presenza di legami costitutivi unilateri*. Atti Acc. Naz. Linc. 1979; Serie VIII, Vol. LXVII.
- [26] Como M, Grimaldi A. *A unilateral model for limit analysis of masonry walls*. II Meeting on Unilateral Problems in Structural Analysis. CISM Courses and Lectures, Springer Verlag 1985; 288:223-238.
- [27] Del Piero G. *Constitutive equation and compatibility of the external loads for linear elastic masonry-like materials*. Meccanica 1989; 24: 150-162.
- [28] Del Piero G. *Limit analysis and no-tension materials*. Int. J. of Plasticity 1998; 14:259-271.
- [29] Di Pasquale S. *New trends in the analysis of masonry structures*. Meccanica 1992; 27: 173-184.
- [30] Alfano G, Rosati L, Valoroso N. *A numerical strategy for finite element analysis of no-tension materials*. Int. Jour. Num. Meth. Eng. 2000; 48: 317-350.
- [31] Cuomo M, Ventura G. *A complementary energy formulation of notension masonry-like solids*. Comp. Meth. Appl. Mech. Eng. 2000; 189: 313-339.
- [32] Giuffrè A. *Lecture sulla Meccanica delle murature storiche*. Kappa Eds., Rome, 1990.
- [33] Ferris M, Tin Loi F. *Limit analysis of frictional blocks assemblies as a mathematical problem with complementarity constraints*. Int.J. Mech. Sci. 2001; 43: 209-224.
- [34] Massart TJ. *Multi-scale modeling of damage in masonry structures*. PhD Thesis University of Bruxelles 2003.
- [35] Pegon P, Anthoine A. *Numerical strategies for solving continuum damage problems with softening: application to the homogenization of masonry*. Computers and Structures 1997; 64(1-4): 623-642.
- [36] de Buhan P, de Felice G. *A homogenisation approach to the ultimate strength of brick masonry*. Journal of the Mechanics and Physics of Solids 1997; 45(7): 1085-1104.
- [37] Benvenuto E. *An introduction to the history of structural mechanics. Volume II: vaulted structures and elastic systems* 1991; 307-554, Springer-Verlag Berlin-New-York.
- [38] Huerta S. *Mechanics of masonry vaults: the equilibrium approach*. In: Proc. Historical Constructions 2001, P.B. Lourenço & P. Roca (Eds.), Guimarães PT.
- [39] Heyman J. *The safety of masonry arches*. International Journal of Mechanical Sciences 1969; 43: 209-224.
- [40] Heyman J. *Equilibrium of shell structures*. Oxford, Oxford University Press 1977.

-
- [41] Oppenheim I J, Gunaratnam D J, Allen R H. *Limit State Analysis of Masonry Domes*. *Journal of Structural Engineering ASCE* 1989; 115: 868-882.
- [42] Pesciullesi C, Rapallini M, Tralli A, Cianchi A. *Optimal spherical masonry domes of uniform strength*. *Journal of Structural Engineering ASCE* 1997; 123: 203-209.
- [43] O'Dwyer D. *Funicular analysis of masonry vaults*. *Computers & Structures* 1999; 73 (1-5): 187-197.
- [44] Block P, Ciblac T, Ochsendorf J. *Real-time limit analysis of vaulted masonry buildings*. *Computers & Structures* 2006; 84(29-30): 1841-1852.
- [45] Roca P, Lopez-Almansa F, Miquel J, Hanganu A. *Limit analysis of reinforced masonry vaults*. *Engineering Structures* 2007; 29: 431-439.
- [46] Lucchesi M, Padovani C, Pasquinelli G, Zani N. *On the collapse of masonry arches*. *Meccanica* 1997; 32: 327-346
- [47] Lucchesi M, Padovani C, Pasquinelli G, Zani N. *The maximum modulus eccentricity surface for masonry vaults and limit analysis*. *Mathematics and Mechanics of Solids* 1999; 4: 71-87.
- [48] Creazza G, Saetta A, Matteazzi R, Vitaliani R. *Analyses of masonry vaults: a macro approach based on three-dimensional damage model*. *Journal of Structural Engineering ASCE* 2002; 128(5): 646-654.
- [49] Creazza G, Saetta A, Matteazzi R, Vitaliani R. *Analyses of masonry vaulted structures by using a 3-D damage model*. *European Congress on Computational Methods in Applied Sciences and Engineering, ECCOMAS 2000, Barcelona, SP*.
- [50] Sloan S W, Kleeman P W. *Upper bound limit analysis using discontinuous velocity fields*. *Computer Methods in Applied Mechanics and Engineering* 1995; 127(1-4): 293-314.
- [51] Sinha B P. *A simplified ultimate load analysis of laterally loaded model orthotropic brickwork panels of low tensile strength*. *Journal of Structural Engineering ASCE* 1978; 56B(4), 81-84.
- [52] Korany Y, Drysdale R. *Load-Displacement of Masonry Panels with Unbonded and Intermittently Bonded FRP. I: Analytical Model*. *J. Compos. for Constr.* 2007; 11(1): 15-23.
- [53] Milani G. *Homogenized limit analysis of FRP-reinforced masonry walls out-of-plane loaded*. *Computational Mechanics* 2009; 43(5): 617-639.
- [54] Caporale A, Luciano R, Rosati L. *Limit analysis of masonry arches with externally bonded FRP reinforcements*. *Computer Methods in Applied Mechanics and Engineering* 2006; 196: 247-260.

-
- [55] *CNR-DT200. Guide for the design and construction of externally bonded FRP systems for strengthening existing structures. C.N.R., National Research Council, Italy, 2006.*
- [56] *Vermeltoort A V. Analysis and experiments of masonry arches. In: Proc. Historical Constructions 2001, P.B. Lourenço & P. Roca (Eds.), Guimarães PT.*
- [57] *Faccio P, Foraboschi P, Siviero E. Masonry vaults reinforced with FRP strips [In Italian: Volte in muratura con rinforzi in FRP]. L'Edilizia 1999; 7/8: 44-50.*
- [58] *Foraboschi P. Masonry structures externally reinforced with FRP strips: tests at the collapse [in Italian]. In: Proc. I Convegno Nazionale "Sperimentazioni su Materiali e Strutture", Venice 2006.*
- [59] *Yi T, Moon FL, Leon RT, Khan LF. Lateral load tests on a two story unreinforced masonry building. ASCE J Struct Engrg 2006;132(5): 643–52.*
- [60] *Yi T, Moon FL, Leon RT, Khan LF. Analyses of a two-story unreinforced masonry building. ASCE J Struct Engrg 2006;132(5): 653–62.*

Chapter 2.

Masonry curved shells homogenized failure surfaces

The study of masonry vaults should take into account the essentials of the material “masonry” -i.e. heterogeneity, almost no resistance to tension combined with a good compressive strength and a high friction coefficient- as well as the overall importance of the geometry for achieving the equilibrium.

In particular, the definition and the use of suitable material constitutive laws for masonry remains an open issue. In the recent past, several authors (e.g. Luciano and Sacco [1], Pegon and Anthoine [2], Massart et al. [3]) proposed different complex modelling strategies for the analysis of masonry structures in the non-linear field. As a rule, three different approaches are possible, usually known as macro-modelling, micro-modelling and homogenization.

While in micro-modelling (e.g. [4]) a separate discretization of bricks and mortar (usually reduced to interfaces) is assumed, macro-models (e.g. [5]) substitute the

heterogeneous material with a fictitious anisotropic homogeneous one, thus needing much less time to be performed in complex non linear analyses, but requiring a calibration of the model with expensive experimental data fittings. Homogenization (e.g. [6] [1] [8] [9]) may be regarded as a compromise between micro and macro-modelling, since macroscopic masonry behavior is obtained solving suitable boundary value problems on the unit cell, thus taking into account constituent materials mechanical properties and geometry only at the micro-scale.

The aim of this Chapter is to present the upper bound FE homogenization procedure adopted to obtain an upper bound approximation of the actual failure surfaces for masonry vaults. In particular a FE limit analysis discretization of the elementary cell with 7 brick elements and mortar-joints reduced at the interface is used. The failure surfaces obtained, are implemented at the macro-scale level in an upper bound FE limit analysis code to obtain the collapse load and deformed shape at the collapse of entire masonry shells (Chapter 3 and Chapter 4).

Obviously, it should be remarked that rigorous homogenization can not be easily applied in the case of curved structures, since the identification of both a curved elementary cell and suitable periodicity conditions on boundaries is not an easy task. This is the reason why, in the present chapter a simple heuristic method based on a compatible identification between discrete model and equivalent continuum is preferred. In section 2.1 and 2.2 the upper bound FE homogenization procedure adopted to obtain an upper bound approximation of the actual failure surfaces for masonry vaults is presented. In sub-section 2.3 several examples of curved REV's (parabolic arch, ribbed cross vault, hemispherical dome, barrel vault) are analyzed and discussed in detail. The anisotropy induced by the non null curvature of the REV is particularly evident if compared with results obtained in the flat case.

2.1 Homogenization background

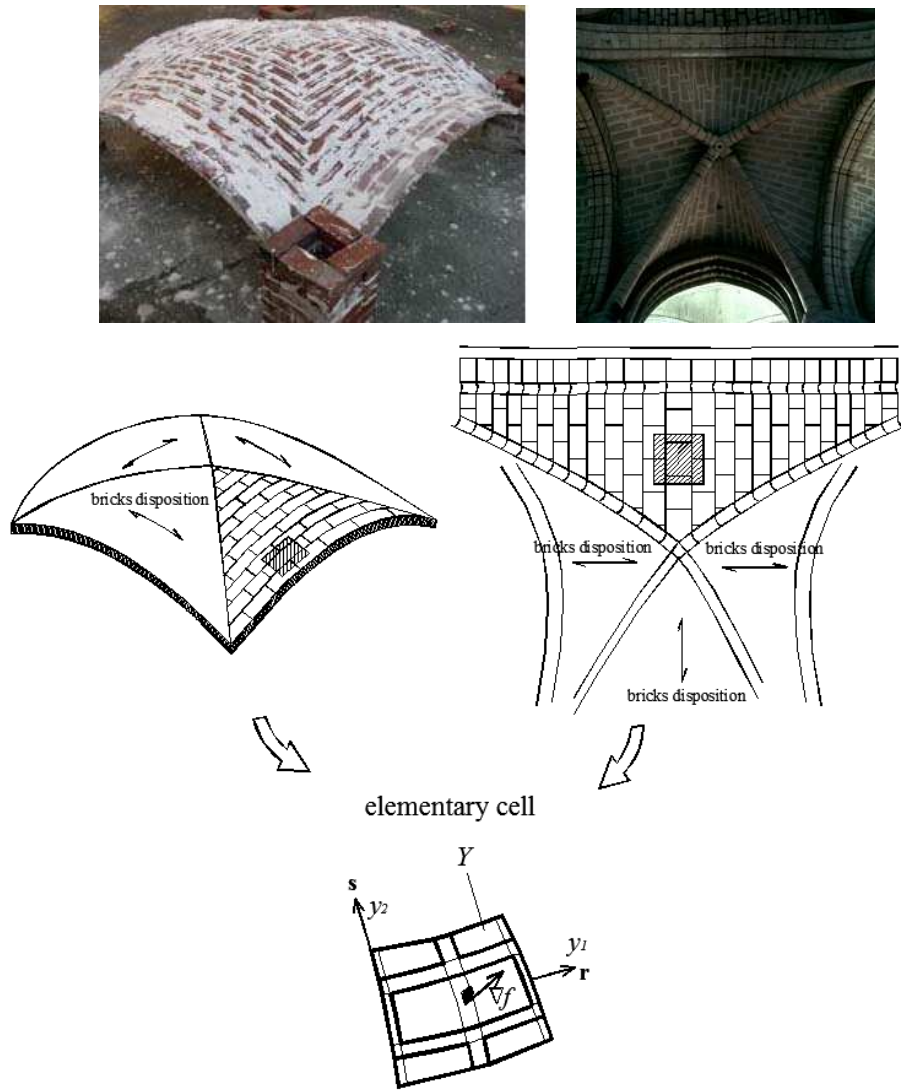


Figure 2.1: Typical double curvature shell structures (Ω) and different bricks dispositions.

In this section, a FE procedure for obtaining in- and out-of-plane masonry failure surfaces in case of curved shells is outlined. A linearization with several planes of such surfaces will be then implemented in the 3D kinematic FE limit analysis code described in the following chapter for a kinematic limit analysis of entire masonry shells.

The general case of curved masonry vaults constituted by a finite number of infinitely differentiable surfaces $f_i(\mathbf{x})$ is considered (Figure 2.1 and Figure 2.2). Since in the homogenized FE procedure, plastic dissipation on the interfaces between adjoining elements can occur as a combination of in-plane actions, bending moment, torsion and out-of-plane shear, Reissner-Mindlin thick plate hypotheses are adopted (Cecchi et al. [10], Cecchi and Milani [11]). It must be noted that the introduction of a limited shear strength under out-of-plane actions could play an important role for instance in presence of monolithic arches and thin shells subjected to concentrated loads, for which failure can occur for out-of-plane sliding of the blocks, Figure 2.3 (Drosopoulos et al. [12]).

Masonry is a composite material made by units bonded together with mortar joints. In most cases of building practice, units and mortar are periodically arranged, i.e. walls are constituted by the regular repetition of bricks bonded with joints. When dealing with flat panels, such periodicity allows to consider an entire structure Ω as the repetition of a suitable representative element of volume Y (REV or elementary cell) – see Figure 2.4. Y contains all the information necessary for describing completely the macroscopic behaviour of Ω . In particular, if a running bond pattern is considered, as shown in Figure 2.4, it has been shown that a rectangular elementary cell may be adopted.

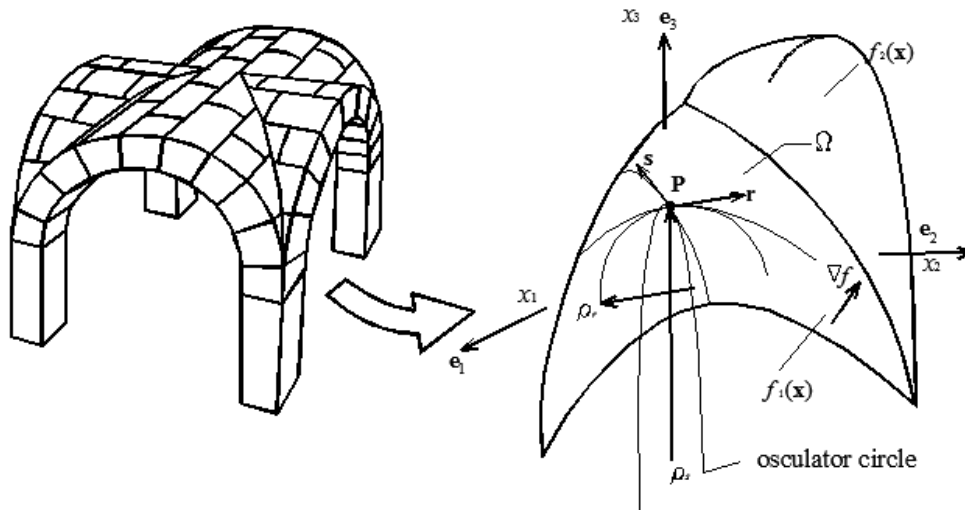


Figure 2.2: Typical double curvature shell structures Ω constituted by more than one infinitely differentiable surface (e.g. f_1, \dots, f_4). In the figure principal curvature radii at a point \mathbf{P} are also represented (ρ_s and ρ_r).

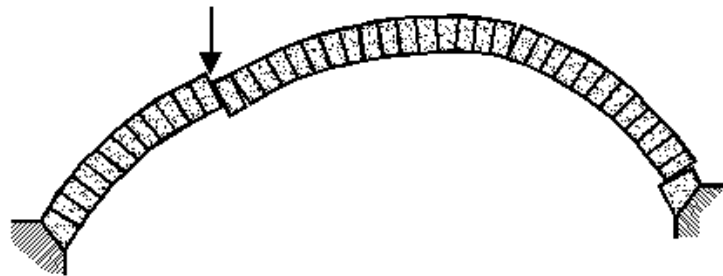


Figure 2.3: Possible sliding of a thick arch.

On the other hand, when a curved masonry surface Ω , identified at a point \mathbf{P} by the two principal curvatures $1/\rho_s$ and $1/\rho_r$ Figure 2.2 is considered, it is very straightforward to conclude that it is not always possible to rigorously consider Ω

as a regular repetition of the elementary volume Y , thus precluding in principle the utilization of homogenization in the most general case. Nevertheless, a heuristic but technically suitable approach is to identify in any case a representative volume element, as depicted in Figure 2.4, which generates the double curvature shell by repetition.

Without loss of generality, let us consider a masonry shell constituted by a finite number of regular curved surfaces Ω . In correspondence of a point \mathbf{x} of Ω , two versors \mathbf{r} and \mathbf{s} can be identified, corresponding to two orthogonal directions disposed parallel to the principal curvature planes of the vault in \mathbf{x} , see Figure 2.4.

Let the principal curvature radii along \mathbf{r} and \mathbf{s} be denoted with $\rho_s(\mathbf{x})$ and $\rho_r(\mathbf{x})$ respectively. Internal actions acting at each point $\mathbf{x} \in \Omega$ are constituted by both in-plane (meridian, hoop and shear stresses) and out-of-plane (meridian, parallel bending and torsion) actions.

When $\rho_r(\mathbf{x}) \rightarrow \infty$ and $\rho_s(\mathbf{x}) = \rho_s \forall \mathbf{x} \in \Omega$, the special cases of cross vaults, barrel and cloister vaults are obtained. For all these cases of technical interest, the curved elementary cell Y shown in Figure 2.5 can be identified, which generates the curved surface by repetition.

Furthermore, we define on Y the local curved frame of reference $y_1 - y_2 - y_3$, with y_3 normal to the vault middle surface, y_1 and y_2 parallel to \mathbf{r} and \mathbf{s} respectively (see Figure 2.4). For this special sub-class of problems, rigorous homogenization theory can be applied in combination with classic limit analysis theorems for the evaluation of the homogenized in- and out-of-plane strength domain S^{hom} of masonry.

Despite the fact that classic homogenization theory has never been applied to masonry vaults, but only to flat walls, homogenization concepts has been recently used, for instance, by Slinchenko and Verijenko [13] for lattice shells of revolution,

for cylindrical shells by Andrianov et al. [14] and by Habbal [15] in the case of 1D wrinkled arches.

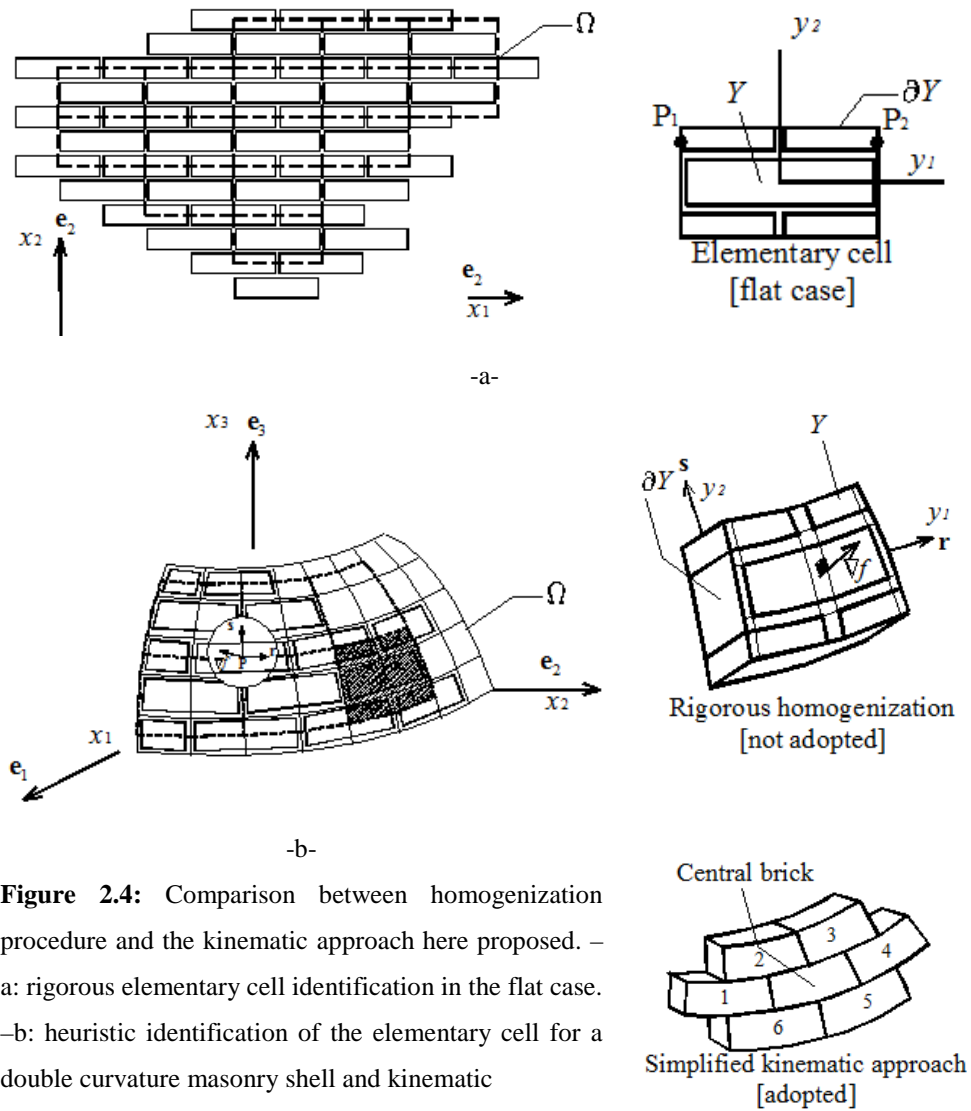


Figure 2.4: Comparison between homogenization procedure and the kinematic approach here proposed. – a: rigorous elementary cell identification in the flat case. – b: heuristic identification of the elementary cell for a double curvature masonry shell and kinematic

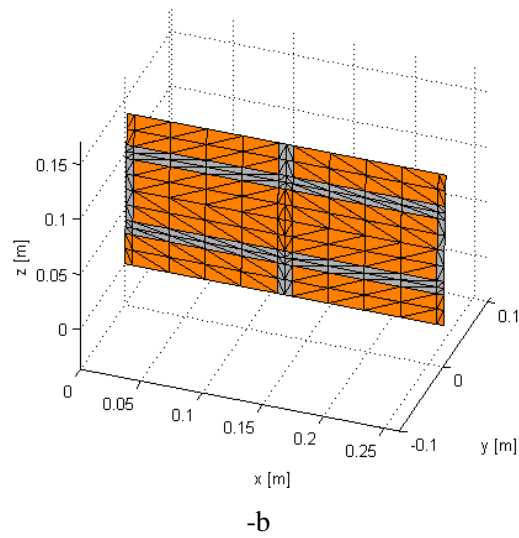
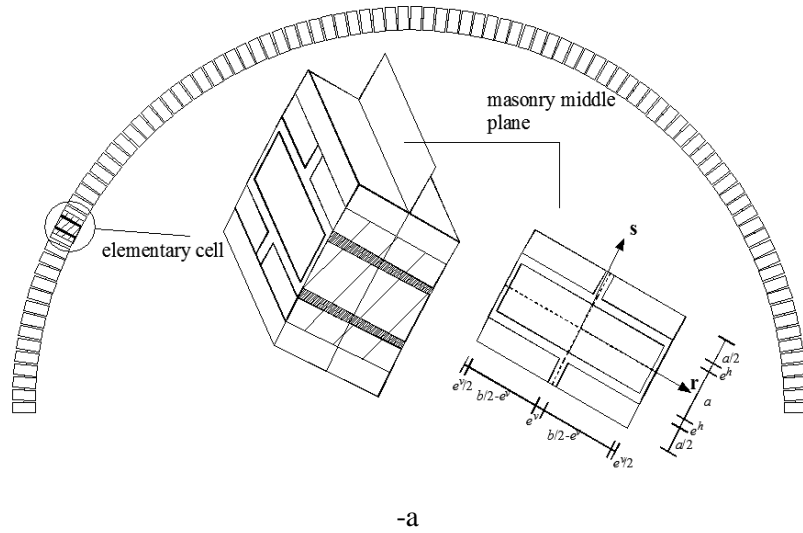


Figure 2.5: -a: Unit cell for a barrel vault with $\rho_s(\mathbf{x}) = \rho_s = 2 \text{ m}$. -b: Arch ($\rho_s = 2 \text{ m}$) elementary cell and its discretization by means of 288 FE flat triangular elements.

As a rule, when dealing with curved structures, equilibrium equations in the unit cell have to be written in a non Cartesian frame of reference, thus being substantially different with respect to the flat case.

The basic idea of the homogenization procedure consists in introducing averaged quantities representing the macroscopic membrane actions and strain tensors (respectively \mathbf{N} and \mathbf{E}) for in-plane actions, the macroscopic bending moment and curvature tensors for the out-of-plane problem (respectively \mathbf{M} and $\boldsymbol{\chi}$) and the out-of-plane sliding and shear (respectively Γ_3 and \mathbf{T}_3) defined as follows (here the direction 3 is assumed perpendicular to the masonry middle plane, Figure 2.4):

$$\begin{aligned}
 \mathbf{E} = [E_{ij}] &= \langle \boldsymbol{\varepsilon} \rangle = \frac{1}{V} \int_V \boldsymbol{\varepsilon}(\mathbf{u}) dV \quad (i, j = 1, 2) \\
 \mathbf{N}/t = [N_{ij}/t] &= \langle \boldsymbol{\sigma} \rangle = \frac{1}{V} \int_V \boldsymbol{\sigma} dV \quad (i, j = 1, 2) \\
 \boldsymbol{\chi} = [\chi_{ij}] &= \langle \partial \boldsymbol{\varepsilon} / \partial \mathbf{y} \rangle = \frac{1}{V} \int_V \frac{\partial \boldsymbol{\varepsilon}(\mathbf{u})}{\partial \mathbf{y}} dV \quad (i, j = 1, 2) \\
 \mathbf{M}/t = [M_{ij}] &= \langle \boldsymbol{\sigma} y_3 \rangle = \frac{1}{V} \int_V \boldsymbol{\sigma} y_3 dV \quad (i, j = 1, 2) \\
 \Gamma_3 = \langle \boldsymbol{\gamma}_3 \rangle &= \langle [\partial u_3 / \partial y_1 + \partial u_1 / \partial y_3; \partial u_3 / \partial y_2 + \partial u_2 / \partial y_3] \rangle = \frac{1}{V} \int_V \boldsymbol{\gamma}_3 dV \\
 \mathbf{T}_3/t = \langle \boldsymbol{\tau}_3 \rangle &= \langle [\boldsymbol{\sigma}_{13}; \boldsymbol{\sigma}_{23}] \rangle = \frac{1}{V} \int_V \boldsymbol{\tau}_3 dV
 \end{aligned} \tag{2.1}$$

where V is the volume of the elementary cell, t the transverse thickness, \mathbf{u} is the displacements vector (components u_i), $\boldsymbol{\varepsilon}$ and $\boldsymbol{\sigma}$ stand for the local quantities (stress and strain tensors with components ε_{ij} and σ_{ij} respectively) and $\langle * \rangle$ is the averaging operator. It is worth noting that, in this way, the behaviour of a moderately thick shell (Reissner-Mindlin hypotheses) may be modelled.

Anti-periodicity and periodicity conditions are imposed respectively to the stress field $\boldsymbol{\sigma}$ and the displacement field \mathbf{u} :

$$\begin{cases} \mathbf{u} = \tilde{\mathbf{E}}\mathbf{y} + \tilde{\boldsymbol{\chi}}\mathbf{y} + \tilde{\boldsymbol{\Gamma}}\mathbf{y} + \mathbf{u}^{\text{per}} & \mathbf{u}^{\text{per}} \text{ on } \partial Y \\ \boldsymbol{\sigma}\mathbf{n} & \text{anti-periodic on } \partial Y \end{cases} \quad (2.2)$$

where:

- \mathbf{u}^{per} stands for a periodic displacement field;
- ∂Y is the cell internal boundary (see Figure 2.4);
- $\tilde{\mathbf{E}} = [\mathbf{E} \quad \mathbf{0}; \quad \mathbf{0}^T \quad 0]$ ($\mathbf{0}$ is a 2×1 zero vector);
- $\tilde{\boldsymbol{\chi}} = \begin{bmatrix} y_3\boldsymbol{\chi} & \mathbf{0} & (1/2\boldsymbol{\chi}[y_1 \quad y_2]^T)^T & 0 \end{bmatrix}$;
- $\tilde{\boldsymbol{\Gamma}}$ is a 3×3 matrix with all zeros except $\tilde{\boldsymbol{\Gamma}}_{31} = \boldsymbol{\Gamma}_3(1)$ and $\tilde{\boldsymbol{\Gamma}}_{32} = \boldsymbol{\Gamma}_3(2)$.

Let S^m , S^b and S^{hom} denote respectively the strength domains of mortar (or more properly of the interface between mortar and bricks, see Lourenço and Rots [4]), of the units and of the homogenized macroscopic material. S^{hom} domain of the equivalent medium is defined in the space of the macroscopic stresses as follows (Suquet [16]):

$$S^{\text{hom}} \equiv (\mathbf{N} \quad \mathbf{T} \quad \mathbf{M}) \left\{ \begin{array}{l} \mathbf{N} / t = \langle \boldsymbol{\sigma} \rangle = \frac{1}{V} \int_V \boldsymbol{\sigma} dV \quad (a1) \\ \mathbf{M} / t = \langle \boldsymbol{\sigma} y_3 \rangle = \frac{1}{V} \int_V \boldsymbol{\sigma} y_3 dV \quad (a2) \\ \mathbf{T}_3 / t = \langle \boldsymbol{\tau}_3 \rangle = \frac{1}{V} \int_V \boldsymbol{\tau}_3 dV \quad (a3) \\ \text{div} \boldsymbol{\sigma} = \mathbf{0} \quad (b) \\ [[\boldsymbol{\sigma}]] \mathbf{n}^{\text{int}} = \mathbf{0} \quad (c) \\ \boldsymbol{\sigma} \mathbf{n} \text{ anti-periodic on } \partial Y \quad (d) \\ \boldsymbol{\sigma}(\mathbf{y}) \in S^m \quad \forall \mathbf{y} \in Y^m ; \boldsymbol{\sigma}(\mathbf{y}) \in S^b \quad \forall \mathbf{y} \in Y^b \quad (e) \end{array} \right. \quad (2.3)$$

Here, $[[\boldsymbol{\sigma}]]$ denotes the jump of micro-stresses across any discontinuity surface of normal \mathbf{n}^{int} . Conditions (a) is typical of homogenization, condition (d) is derived from anti-periodicity, condition (b) imposes the micro-equilibrium and condition (e) represents the yield criteria for the components (brick and mortar).

The kinematic definition of S^{hom} , used in this chapter, is obtained by means of the dual formulation of (2.3), assuming in the elementary cell a velocity field \mathbf{v} equal to $\dot{\mathbf{E}}\mathbf{y} + \dot{\boldsymbol{\chi}}\mathbf{y} + \dot{\mathbf{\Gamma}}\mathbf{y} + \mathbf{v}^{\text{per}}$, where $\dot{\mathbf{D}}$ is a macroscopic strain rate field, $\dot{\boldsymbol{\chi}}$ contains the macroscopic curvature rate field, $\dot{\mathbf{\Gamma}}$ contains the macroscopic out-of-plane sliding rate, and \mathbf{v}^{per} is a periodic velocity field. Under these hypotheses, the so called support function π^{hom} can be evaluated as follows:

$$\pi^{\text{hom}}(\dot{\mathbf{E}}, \dot{\boldsymbol{\chi}}, \dot{\mathbf{\Gamma}}) = \inf_{\mathbf{v}} \left\{ P(\mathbf{v}) \mid \mathbf{v} = \dot{\mathbf{E}}\mathbf{y} + y_3 \dot{\boldsymbol{\chi}}\mathbf{y} + \dot{\mathbf{\Gamma}}\mathbf{y} + \mathbf{v}^{\text{per}} \right\} \quad (2.4)$$

Where $P(\mathbf{v})$ is the power dissipated in the elementary cell for a given \mathbf{v} .

From (2.4), it has been shown that a kinematic definition of S^{hom} can be obtained as follows:

$$S^{\text{hom}} \equiv (\mathbf{N} \quad \mathbf{M} \quad \mathbf{T}) \left| \begin{cases} \mathbf{N} : \dot{\mathbf{E}} + \mathbf{M} : \dot{\boldsymbol{\chi}} + \mathbf{T}^T \dot{\boldsymbol{\Gamma}} = 1 \leq \pi^{\text{hom}}(\dot{\mathbf{E}}, \dot{\boldsymbol{\chi}}, \dot{\boldsymbol{\Gamma}}) \quad \forall \dot{\mathbf{E}}, \dot{\boldsymbol{\chi}}, \dot{\boldsymbol{\Gamma}} \\ \pi^{\text{hom}}(\dot{\mathbf{E}}, \dot{\boldsymbol{\chi}}, \dot{\boldsymbol{\Gamma}}) = \inf_{\mathbf{v}} \left\{ P(\mathbf{v}) \mid \mathbf{v} = \dot{\mathbf{E}}\mathbf{y} + y_3 \dot{\boldsymbol{\chi}}\mathbf{y} + \dot{\boldsymbol{\Gamma}}\mathbf{y} + \mathbf{v}^{\text{per}} \right\} \\ P(\mathbf{v}) = \int_Y \pi(\dot{\mathbf{d}}) dY + \int_S \pi([\![\mathbf{v}]\!] ; \mathbf{n}) dS \end{cases} \quad (2.5)$$

where:

S is any discontinuity surface of \mathbf{v} in Y , \mathbf{n} is the normal to S ;

$$\pi([\![\mathbf{v}]\!] ; \mathbf{n}) = 1/2([\![\mathbf{v}]\!] \otimes \mathbf{n} + \mathbf{n} \otimes [\![\mathbf{v}]\!]);$$

$$\pi(\dot{\mathbf{d}}) = \max_{\boldsymbol{\sigma}} \{ \boldsymbol{\sigma} : \dot{\mathbf{d}} ; \boldsymbol{\sigma} \in S(\mathbf{y}) \};$$

\mathbf{N} , \mathbf{M} and \mathbf{T} are the ultimate homogenized membrane, bending and out-of-plane shear actions respectively.

It is worth noting that, using the kinematic definition given by (2.5), it is possible to explicitly determine the homogenized strength domain of masonry in the space of the macroscopic stresses using a FE limit analysis discretization of the elementary cell (Figure 2.4 -b).

In particular, S^{hom} is obtained by means of the following constrained minimization problem:

$$S^{\text{hom}} \equiv \left\{ \begin{array}{ll} \lambda = \min_{\mathbf{v}^{\text{per}}, \dot{\mathbf{E}}, \dot{\boldsymbol{\chi}}, \dot{\boldsymbol{\Gamma}}} \frac{1}{V} \int_V P(\dot{\mathbf{d}}) dV & \dot{d}_{ij} = \frac{1}{2} \left(\frac{\partial v_i}{\partial y_j} + \frac{\partial v_j}{\partial y_i} \right) \quad (a) \\ \mathbf{N}^0 : \dot{\mathbf{E}} + \mathbf{M}^0 : \dot{\boldsymbol{\chi}} + \mathbf{T}^{0T} \dot{\boldsymbol{\Gamma}} = 1 & (b) \\ \mathbf{v} = \dot{\mathbf{E}}\mathbf{y} + y_3 \dot{\boldsymbol{\chi}}\mathbf{y} + \dot{\boldsymbol{\Gamma}}\mathbf{y} + \mathbf{v}^{\text{per}} & (c) \end{array} \right. \quad (2.6)$$

where

- λ is the kinematic limit multiplier of the assigned macroscopic actions (moments, membrane actions or out-of-plane shear);

- \mathbf{M}^0 , \mathbf{N}^0 and \mathbf{T}^0 are respectively unitary bending, membrane actions and out-of-plane shear tensors/vectors (i.e. they define only the direction in the S^{hom} generalized stress space at which λ is evaluated, see also Figure 2.6)
- $P(\dot{\mathbf{d}})$ is the local plastic dissipation over the REV;
- \mathbf{y} is a point of the REV in the local frame of reference.

2.2 Derivation of masonry homogenized failure surfaces by means of a FE discretization of the unit cell

A strategy for obtaining an accurate estimation of S^{hom} is to solve problem (2.6) for several assigned $\mathbf{M}^0 - \mathbf{N}^0 - \mathbf{T}^0$ directions of the macroscopic actions by means of a limit analysis FE approach.

In what follows, a FE upper bound approach is adopted, in which dissipation occurs only at the interfaces between adjoining elements, both for in-plane and out-of-plane actions.

For the study of the masonry structures by means of shell elements (Chapter 3), the discretization of the elementary cell is with a triangular FE infinitely resistant elements, as shown in Figure 2.5-b; plastic dissipation can occur only at interfaces between adjoining elements.

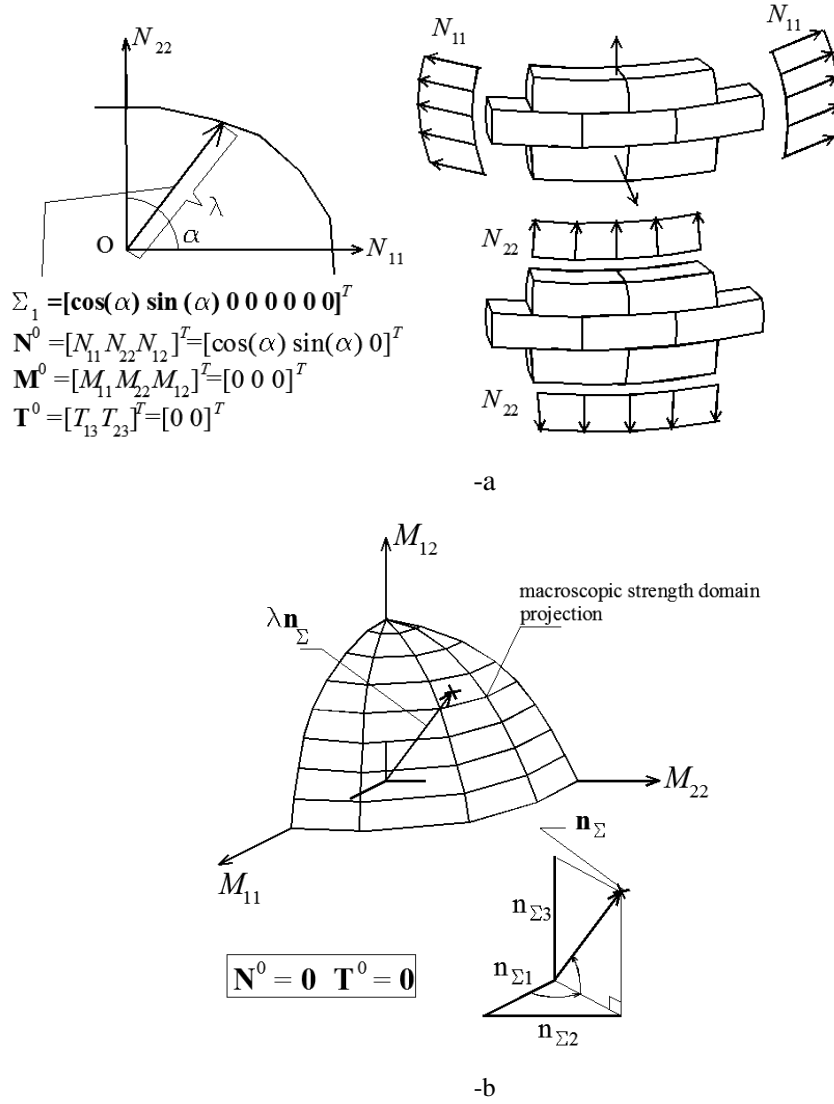


Figure 2.6: Meaning of \mathbf{N}^0 , \mathbf{M}^0 and \mathbf{T}^0 -a vector Σ_1 determines the optimization direction in the homogenized space of in- and out-of-plane actions. In this case $\Sigma_1 = [\cos(\alpha) \sin(\alpha) 0 0 \dots 0]^T$; -b vector \mathbf{n}_{Σ} determines, in this case, $\mathbf{M}^0 = [n_{\Sigma 1} \ n_{\Sigma 3}; \ n_{\Sigma 3} \ n_{\Sigma 2}]$

Instead, for the whole structures studies with wedge elements (Chapter 4), the REV are discretized by means of 3D rigid infinitely resistant six-noded wedge elements, whereas mortar joints are reduced to interfaces with frictional behaviour and limited tensile and compressive strength (Figure 2.7). In this way, plastic dissipation may occur only at bricks-bricks interfaces and on mortar joints. Nonetheless, it is worth noting that, since 3D wedge elements are used at a structural level, only failure surfaces sections in terms of membrane and out-of-plane shear are needed, since flexural and torsional behaviour are derived directly at a structural level by means of an integration along the thickness. In any case, here both in-plane and out-of-plane failure surfaces are recovered for the sake of completeness.

Three different typologies of interfaces occur when a masonry elementary cell is considered, namely internal mortar-mortar, brick-brick and brick-mortar interfaces. Typically, cracking occurs in practice with a cohesive frictional behaviour at the interface between bricks and mortar or directly inside the joint. On the other hand, as experimental evidences show, sliding occurs in mortar joints with almost zero dilatancy with typical non-associated flow rule. This violates one of the hypotheses of classic limit analysis theory (see for instance Ferris and Tin Loi [17], Orduna and Lourenço [18] and [19]), implying that the uniqueness of the ultimate load may be lost and a multiplicity of solutions may exist for limit analysis problems, see for instance Begg and Fishwick [20].

On the other hand, classical limit analysis theorems assure the uniqueness of the ultimate load factor and lead to simple optimization problems. For the above-mentioned reasons, in this case associated flow rules are assumed for the constituent materials.

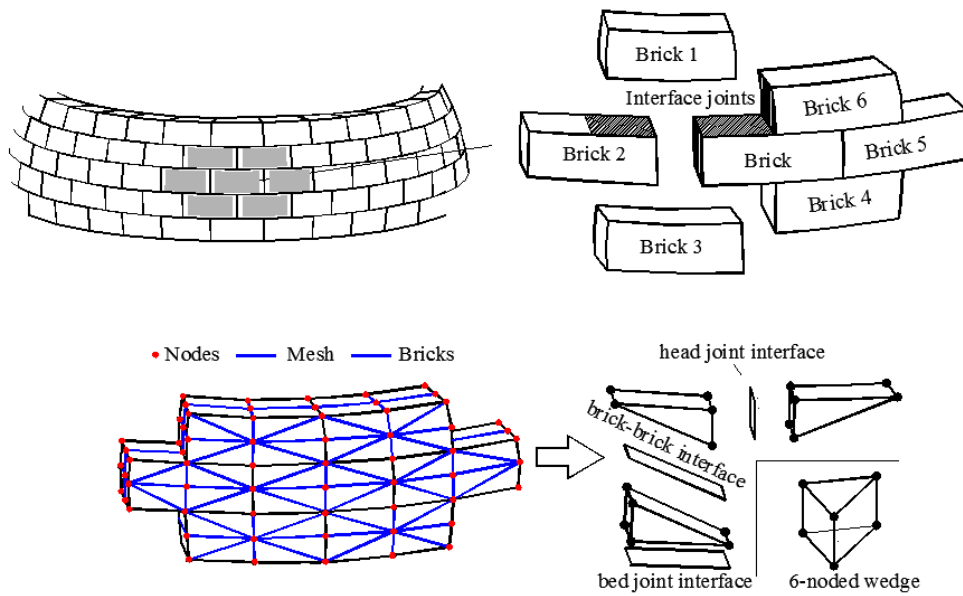


Figure 2.7: Simplified micro-mechanical approach adopted. Brick is supposed to interact with its 6 neighbours and joints are reduced to interfaces with zero thickness. Then, brick with its neighbours is meshed by means of 6-noded wedges.

In general, any non-linear failure criterion $\phi = \phi(\boldsymbol{\sigma})$ for mortar-mortar and bricks-mortar interfaces can be assumed. Nonetheless, as experimental evidences show, basic failure modes for masonry walls with weak mortar are a mixing of sliding along the joints (a), direct tensile splitting of the joints (b) and compressive crushing at the interface between mortar and bricks (c). These modes may be gathered adopting a Mohr-Coulomb failure criterion combined with tension cut-off and cap in compression, see Figure 2.8, as suggested by Lourenço and Rots [4]. For what concerns brick-brick interfaces, a classic Mohr-Coulomb failure criterion in plane stress ($\phi_b = \phi_b(\boldsymbol{\sigma})$) is assumed.

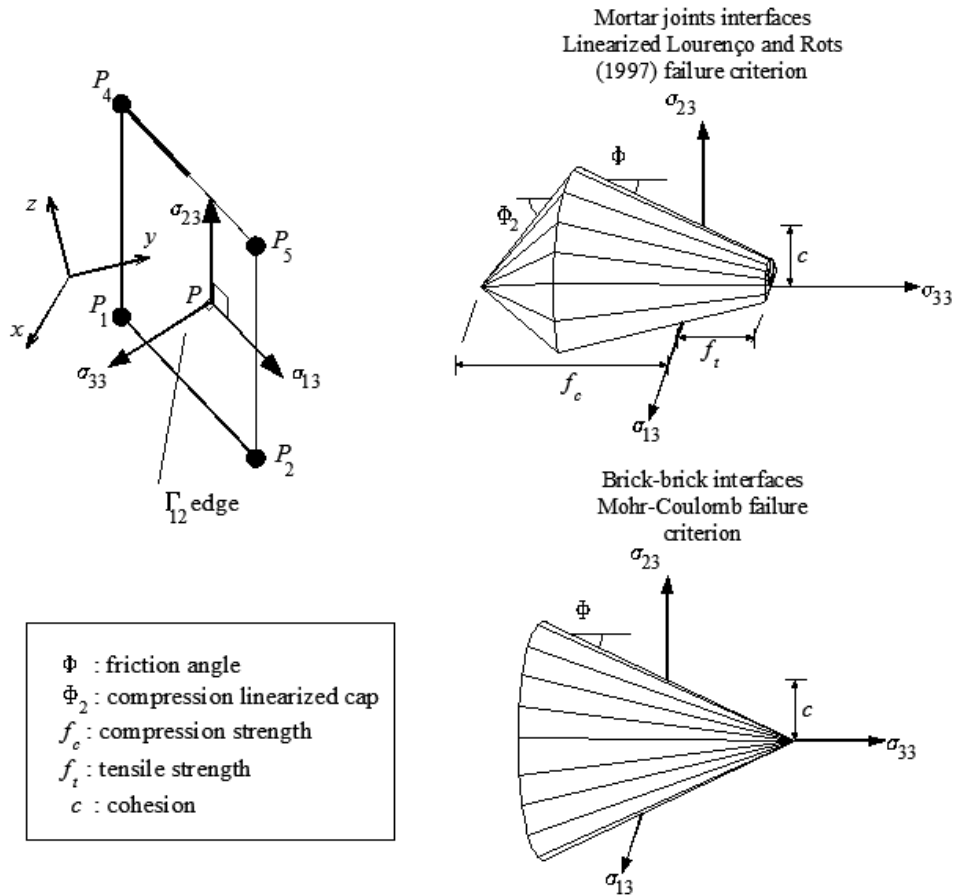
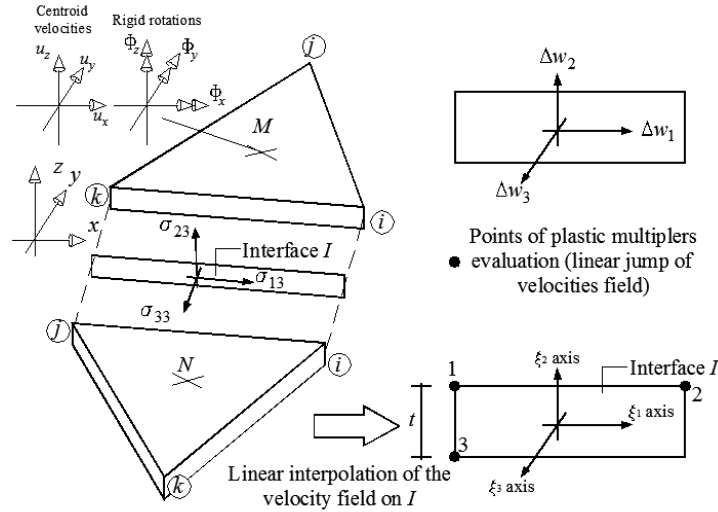
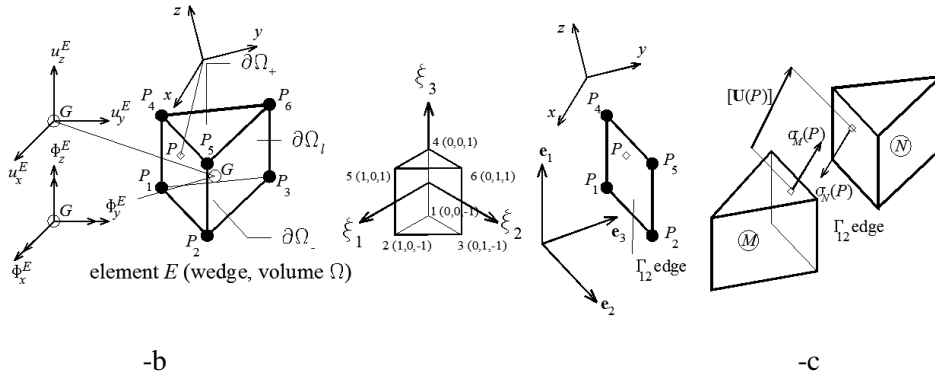


Figure 2.8: Piecewise linear approximation of typical failure criteria adopted for joints and brick-brick interfaces (respectively Linearized Lourenço and Rots 1997 and classic Mohr-Coulomb failure criterion).

Let us consider a generic interface I between adjoining triangular elements M and N , as shown in Figure 2.9.



a-



-b

-c

Figure 2.9: (-a) Triangular three-nodes elements used for the FE discretization of the elementary cell and identification of interface I frame of reference; (-b) Rigid infinitely resistant six-noded wedge element used for the REV discretization and Γ_{12} interface between contiguous elements (-c).

We denote with $\xi_1 - \xi_2 - \xi_3$ an interface local frame of reference, with ξ_3 axis perpendicular to the interface and $\xi_1 - \xi_2$ laying on the interface plane.

$\boldsymbol{\sigma} = [\sigma_{33} \quad \sigma_{13} \quad \sigma_{23}]$ in Figure 2.9. is the stress vector field acting on the interface, with σ_{33} component normal to the interface (i.e. the stress acting parallel to ξ_3 axis) and σ_{13} and σ_{23} the tangential stresses lying on the interface and parallel to axes $\xi_1 - \xi_2$ respectively.

Thus, for each triangular or wedge element, Figure 2.9, six velocities unknown are introduced, namely three centroid velocities (u_x, u_y, u_z) along x, y, z axes and three rotations Φ_x, Φ_y, Φ_z . Let us denote with $[[\mathbf{w}(\xi_1, \xi_2)]] = [\Delta w_1 \quad \Delta w_2 \quad \Delta w_3]^T$ the jump of velocity field on I , Δw_j corresponding to the velocity jump along the direction j with respect to $\xi_1 - \xi_2 - \xi_3$. Trivial algebra permits to conclude that the jump of the velocity field $[[\mathbf{w}]]$ is linear on I .

Aiming at treating the problem within the framework of linear programming, within each interface I of area A^I , a piecewise linear approximation of the failure surface $\phi = \phi(\boldsymbol{\sigma})$ is adopted. $\phi = \phi(\boldsymbol{\sigma})$ is generally constituted by n_{in} planes of equation $\mathbf{A}_i^{I^T} \boldsymbol{\sigma} = c_i^I \quad 1 \leq i \leq n_{in}$. In Figure 2.8, for instance, two different linearized failure surfaces for both mortar-mortar interfaces and brick-mortar interfaces are shown.

Since in the FE model adopted, the jump of velocity on interfaces is assumed to vary linearly, $3 \cdot n_{in}$ independent plastic multiplier rates are assumed as optimization variables for each interface.

Normality rule at the interfaces is expressed by three equality constraints per point of the interface, involving plastic multiplier rates fields $\dot{\lambda}_i^I(P)$ and the jump of velocity $[\tilde{\mathbf{U}}(P)]$ field is given by:

$$[\tilde{\mathbf{U}}(P)] = \sum_{i=1}^{n_{in}} \dot{\lambda}_i^I(P) \frac{\partial \phi}{\partial \boldsymbol{\sigma}} \quad (2.7)$$

Where $\dot{\lambda}_i^I(P)$ is the i^{th} plastic multiplier rate field of I , associated with the i^{th} linearization plane of the failure surface.

In order to satisfy equation (2.7) for each point of I , nine equality constraints must be imposed, i.e. it is necessary to evaluate (2.7) in correspondence of three different positions $P_k = (x_k, y_k, z_k)$ on I (for instance at P_1, P_2, P_3 of Γ_{12} , Figure 2.9):

$$[\tilde{\mathbf{U}}(P_k)] = \sum_{i=1}^{n_{in}} \dot{\lambda}_i^I(P_k) \frac{\partial \phi}{\partial \boldsymbol{\sigma}} \quad k = 1, 2, 3 \quad (2.8)$$

Where $\dot{\lambda}_i^I(P_k)$ is the i^{th} plastic multiplier rate of I corresponding to point $P_k = (x_k, y_k, z_k)$.

From equations (2.8) (2.7) and (2.6), internal power dissipated on the I^{th} interface is expressed by the following equation:

$$\pi_{int}^I = \int_{A^I} [\tilde{\mathbf{U}}(P)]^T \boldsymbol{\sigma} dA^I = \int_{A^I} \sum_{i=1}^{n_{in}} \dot{\lambda}_i^I(P) \left[\frac{\partial \phi}{\partial \boldsymbol{\sigma}} \right]^T \boldsymbol{\sigma} dA^I = \frac{1}{4} \sum_{i=1}^{n_{in}} c_i^I \sum_{k=1}^4 \dot{\lambda}_i^I(P_k) A^I \quad (2.9)$$

It is interesting to notice from equation (2.9) that internal power estimation depends on plastic multiplier rates variables of points P_k only. Finally, it is stressed that the set of plastic multipliers $\dot{\lambda}_i^I(P_k)$, obviously linear dependent with respect to plastic multipliers of points P_1, P_2 and P_3 , is introduced only for the sake of clearness.

External power dissipated may be written as:

$$\pi_{ext} = (\boldsymbol{\Sigma}_0^T + \lambda \boldsymbol{\Sigma}_1^T) \mathbf{v} \quad (2.10)$$

where Σ_0 is the vector of permanent loads, λ is the load multiplier, Σ_1^T is the vector of unitary loads dependent on the load multiplier (i.e. the optimization direction in the space of macroscopic stresses) and \mathbf{V} is the assembled velocity vector of elements, which collects elements centroid velocities and rotations.

Let us remark that, when dealing with masonry vaulted structures, dead loads play a crucial role and contribute in a not negligible manner to the external power.

Obviously, periodicity conditions (2.6) are imposed on \mathbf{V} in the framework of classic FE procedures by means of standard Dirichlet boundary conditions (Pegon and Anthoine [2]).

As the amplitude of the failure mechanism is arbitrary, a further normalization condition $\Sigma_1^T \mathbf{v} = 1$ is usually introduced. Hence, the external power becomes linear in \mathbf{V} and λ and can be written as $\pi_{ext} = \Sigma_0^T \mathbf{v} + \lambda$.

Both by equations (2.7), (2.8), (2.9) and the kinematic formulation of limit analysis, the following constrained minimization problem is obtained:

$$\left\{ \begin{array}{l} \lambda = \min_{\hat{\mathbf{x}}=[\mathbf{v}, \lambda_i^l(P_k)]} \sum_{l=1}^{n^l} \pi_{int}^l - \Sigma_0^T \mathbf{v} \\ \Sigma_1^T \mathbf{v} = 1 \\ [[\mathbf{w}(P_k)]] = \sum_{i=1}^{n_{im}} \lambda_i^l(\xi_1^{P_k}, \xi_2^{P_k}) \frac{\partial \phi}{\partial \sigma} \quad P_k \in I \end{array} \right. \quad (2.11)$$

where n^l is the total number of interfaces considered and $\hat{\mathbf{x}}$ is the vector of total optimization unknowns. In general, problem (2.11) may be easily handled numerically both by means of well know simplex and interior point methods.

2.3 Numerical results

Several structural examples of curved masonry structures are proposed. In particular, two masonry arches experimentally tested by Vermeltoort [21], a ribbed cross vault, a masonry spherical dome and a cloister vault experimentally tested by Faccio et al. [22] and Foraboschi [23][24] are reported. Comparisons with both experimental data available and numerical analyses conducted through the commercial software DIANA 9.3 [25] will be discussed in chapter 3 and 4. In this section, as a preliminary step for the structural analyses, macroscopic masonry failure surface sections for each different structural example analyzed. In general, it is interesting to note that S^{hom} depends not only on the mechanical properties of the constituent materials, but also on the curvature of the elementary cell.

For all the examples presented, a number of two dimensional projections of the eight dimensional macroscopic masonry failure surface, obtained with the numerical procedure previously discussed, are reported. In particular (see Figure 2.10), both the in-plane behaviour of the representative element of volume when subjected to membrane loads (σ_s and σ_r) at different orientations with respect to the bed joint and the out-of-plane response (bending moments along direction 11 and 22 as well as torsion 12, Figure 2.10) at fixed out-of-plane shear (T_{13}, T_{23}) are investigated.

2.3.1 Parabolic arches by Vermeltoort

The representative element of volume (with its geometry and the discretization by means of wedge elements) considered for the analysis of two parabolic masonry arches (a straight and a skew one) tested by Vermeltoort [21] is depicted in Figure 2.11.

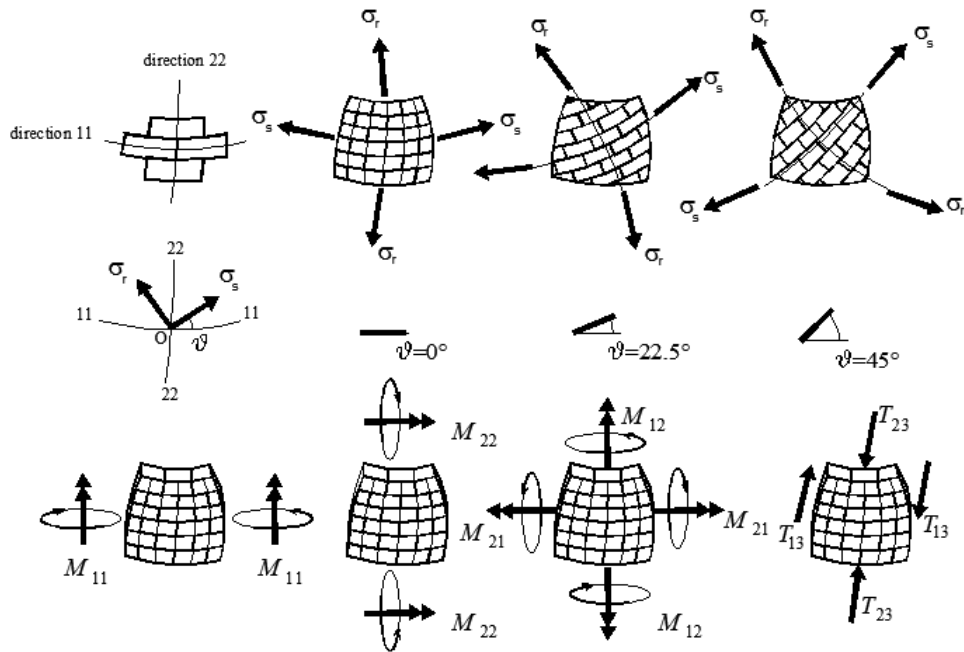


Figure 2.10: Generic curved elementary cell. Meaning of directions 11 and 22, ϑ angle with respect to bed joint orientation, membrane stresses σ_s and σ_r , out-of-plane bending M_{11} and M_{22} , torque M_{12} and out-of-plane shear (T_{13} and T_{23}).

Bricks dimensions are $200 \times 100 \times 52 \text{ mm}^3$ (Rijswaard soft mud bricks) and mortar joints are reduced to interfaces. It is interesting to underline that, since curvature of the arch is not constant, a number of elementary cells should be considered. Nevertheless, here only the REV located at the middle span of the structure (see Figure 2.11) is taken into consideration for the sake of conciseness (differences in curvature from supports to the middle span are, indeed, sufficiently small).

For joints reduced to interfaces, a Lourenço and Rots [4] failure criterion with mechanical properties summarized in Table I has been adopted. For bricks-bricks interfaces, a Mohr-Coulomb failure criterion is assumed, see Table I.

It is worth noting from Table I that joints compressive strength has been taken equal to masonry vertical compressive strength. Such a choice is related to the fact that the rigid plastic model adopted assumes a ductile behaviour of the bricks and 3D effects are neglected. Therefore, it is not possible to reproduce numerically masonry crushing in compression, which results in an ultimate resistance intermediate with respect to bricks and mortar compressive strength. Thus, mechanical properties of joints in compression are assumed with the sole aim of fitting experimental masonry strength. On the other hand, for the structural examples reported in what follows, compression regime is scarcely active and influences marginally failure loads. In Figure 2.12, a synopsis of resultant numerical in- and out-of-plane macroscopic masonry failure surface sections is reported. In particular, in Figure 2.12 –a and -b, in-plane strength in the tension-tension range and in the compression-compression range at different orientations of the bed joint with respect to 11 axis (see Figure 2.12 for the meaning of the symbols) are depicted.

Table I: Parabolic arch. Mechanical characteristic assumed for joints and bricks.

| Joint (Lourenço Rots failure criterion) | | |
|---|--|-----------|
| f_t [N / mm ²] | Tensile strength | 0.32 |
| f_c [N / mm ²] | Compressive strength | 2.5 |
| c | Cohesion | $1.2 f_t$ |
| Φ | Friction angle | 20° |
| Φ_2 | Angle of the linerized compressive cap | 40° |
| Brick (Mohr-Coulomb failure criterion with compressive cutoff) | | |
| f_c [N / mm ²] | Compressive strength | 30 |
| c [N / mm ²] | Cohesion | 1 |
| Φ | Friction angle | 45° |

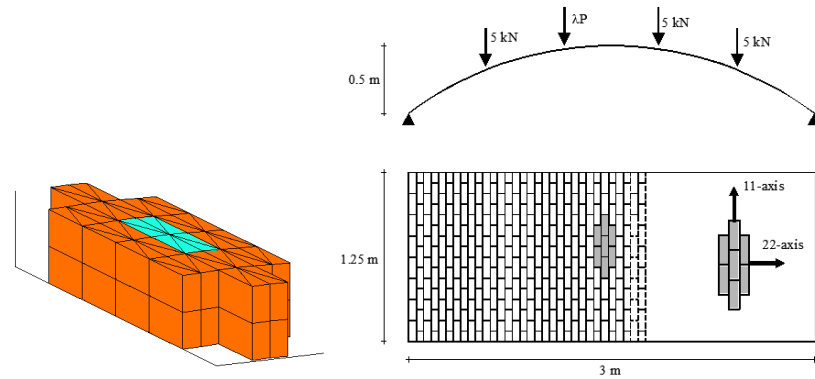


Figure 2.11: Vermeltfoort masonry arches. Representative element of volume adopted for the simulations and FE discretization

Furthermore, in Figure 2.12 from $-c$ to $-f$ M11-M22 and M11-M12 failure surfaces at increasing (imposed) T13 and T23 out-of-plane shear are represented. From an overall analysis of the results, it is particularly evident (1) the anisotropic behavior of the REV at failure and (2) the effect of out-of-plane shear on ultimate bending moment and torsion.

For the sake of completeness, in Figure 2.13, three typical deformed shapes at collapse in presence of N11 membrane action (-a) torsion (-b) and N22 (-c) are illustrated.

The curvature of the elementary cell is, in this case, not particularly pronounced. Furthermore, bricks are disposed with their larger dimension along the direction with null curvature, therefore failure surface sections are very near to those obtained in the flat case (compare, for instance Figure 2.12 with **Errore. L'origine riferimento non è stata trovata.** results).

Only for N22 (see Figure 2.13-c) a marked out-of-plane effect is visible, obviously due to the curvature of the REV.

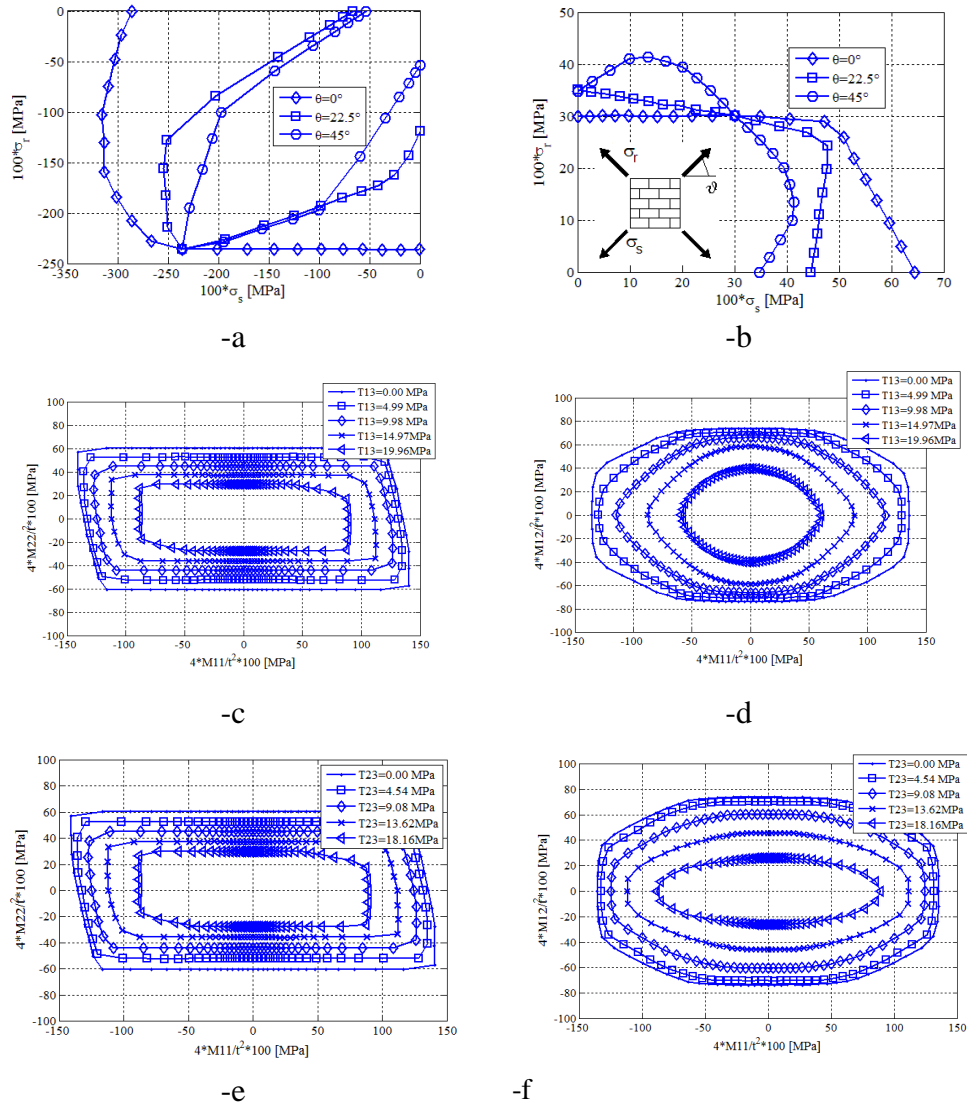


Figure 2.12: Vermeltoort masonry arches. –a and -b: In-plane homogenized failure surface (-a: compression region, -b: tension region) at different orientations of the load with respect to bed joint ϑ direction. –c and -d: M11-M22 (-c) and M11-M12 (-d) failure surfaces at different values of out-of-plane shear T_{13} . –e and -f: M11-M22 (-e) and M11-M12 (-f) failure surfaces at different values of out-of-plane shear T_{23} .

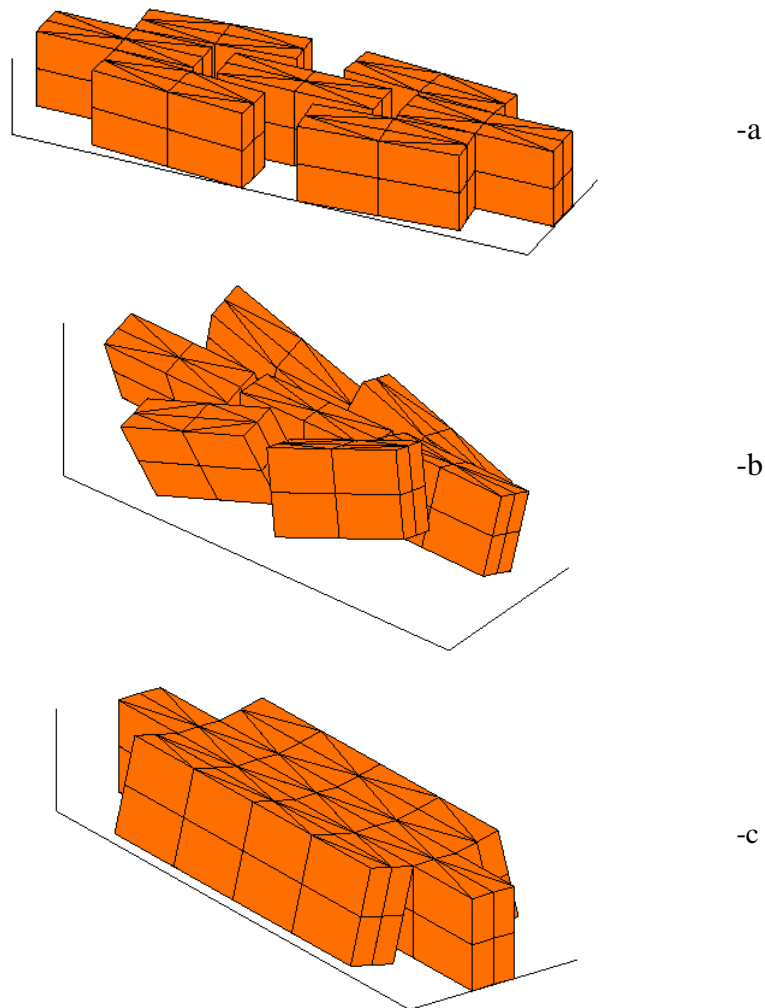


Figure 2.13: Vermeltfoort masonry arches. Typical REV deformed shapes for (-a) N11 membrane action, (-b) pure M12 torsion and (-c) N22 membrane action.

Finally, it is worth noting that, when dealing with membrane actions, being non-null only curvature along 22 direction, ultimate strength along 11 direction remains almost equal to that obtained in the flat case.

2.3.2 Ribbed cross vault

The geometry of the elementary cell utilized for the construction of a ribbed cross vault experimentally tested in [23] is represented in Figure 2.14. The REV geometry presents negligible differences with respect to the cloister vault elementary cell analyzed in the last example. The reader is therefore referred there for a full description of the homogenized failure surface obtained with the model proposed and for a discussion on numerical results. Here, we focus on an alternative disposition of bricks, equally utilized in practice and illustrated in Figure 2.14 (second configuration). Despite the fact that this disposition was not used during experimentation carried out by Faccio et al. [23], it is particularly interesting from a numerical point of view, since the larger dimension of bricks is disposed along axis with non null curvature. For this reason, a meaningful deviation from the flat case is expected.

Common Italian bricks of dimension $250 \times 120 \times 55 \text{ mm}^3$ were used by Faccio et al. [23] to build the vault, with mortar joints of thickness approximately equal to 10 mm (here joints are reduced to interfaces for the sake of simplicity).

11 axis in Figure 2.14 is the direction of non null curvature, with 22 axis perpendicular to 11. 11 curvature is, in this case constant, therefore only one representative volume element is needed for the analysis of the cross vault at a cell level.

Mechanical properties adopted for the constituent materials are summarized in Table II. As in the previous case, a Lourenço-Rots failure criterion is adopted for joints reduced to interfaces whereas for bricks a Mohr-Coulomb strength domain is assumed.

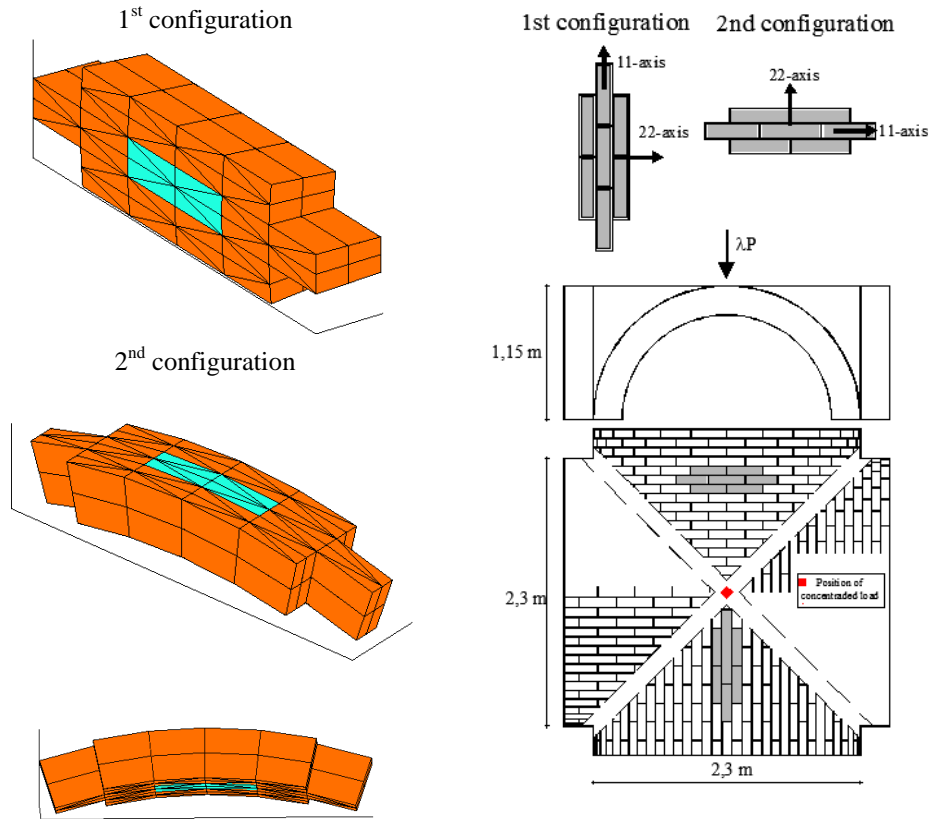


Figure 2.14: Ribbed cross vault. Representative element of volume adopted for the simulations and FE discretization (first experimental bricks configuration and second disposition with bricks larger length along the axis of non-null curvature).

Similarly to the previous example, in- and out-of-plane homogenized failure surfaces obtained with the model proposed are reported in Figure 2.16. Also in this example, masonry homogenized failure surface and in-plane failure mechanisms on the curved elementary cell are reported in Figure 2.15 and Figure 2.17, obtained by means of the homogenization technique with flat triangular element.

Nevertheless, due to bricks disposition (REV longer dimension is disposed along the non null curvature axis, see Figure 2.14) differences between present failure surfaces and those obtained for a flat elementary cell are rather evident. In particular, observing failure surfaces involving M11 bending moment (Figure 2.16 from $-c$ to $-f$), it is rather evident the anisotropic behaviour between positive and negative M11, corresponding to compression of intrados and extrados respectively. Obviously, in this case, curvature reduces masonry strength along 11 direction, whereas REV ultimate resistance along 22 axis remains essentially the same of the flat case. This is confirmed by failure mechanisms observed, for instance, after the application to the REV of N11 membrane action (Figure 2.18-a), pure torsion (Figure 2.18-b) or pure bending moment along 11 direction (Figure 2.18-c). In particular, it is interesting to notice the non negligible out-of-plane velocity components (obviously due to the REV curvature) of bricks resultant solving linear program (2.11) when an external N11 action is applied, see Figure 2.18-a.

Table II: Ribbed cross vault. Mechanical characteristic assumed for joints and bricks.

| Joint (Lourenço Rots failure criterion) | | |
|---|--|-----------|
| f_t [N / mm ²] | Tensile strength | 0.05 |
| f_c [N / mm ²] | Compressive strength | 2.3(*) |
| c | Cohesion | $1.2 f_t$ |
| Φ | Friction angle | 25° |
| Φ_2 | Angle of the linerized compressive cap | 40° |
| Brick (Mohr-Coulomb failure criterion with compressive cutoff) | | |
| f_c [N / mm ²] | Compressive strength | 30 |

(*): the value adopted corresponds to masonry vertical compressive strength adopted by Creazza et al. (2000).

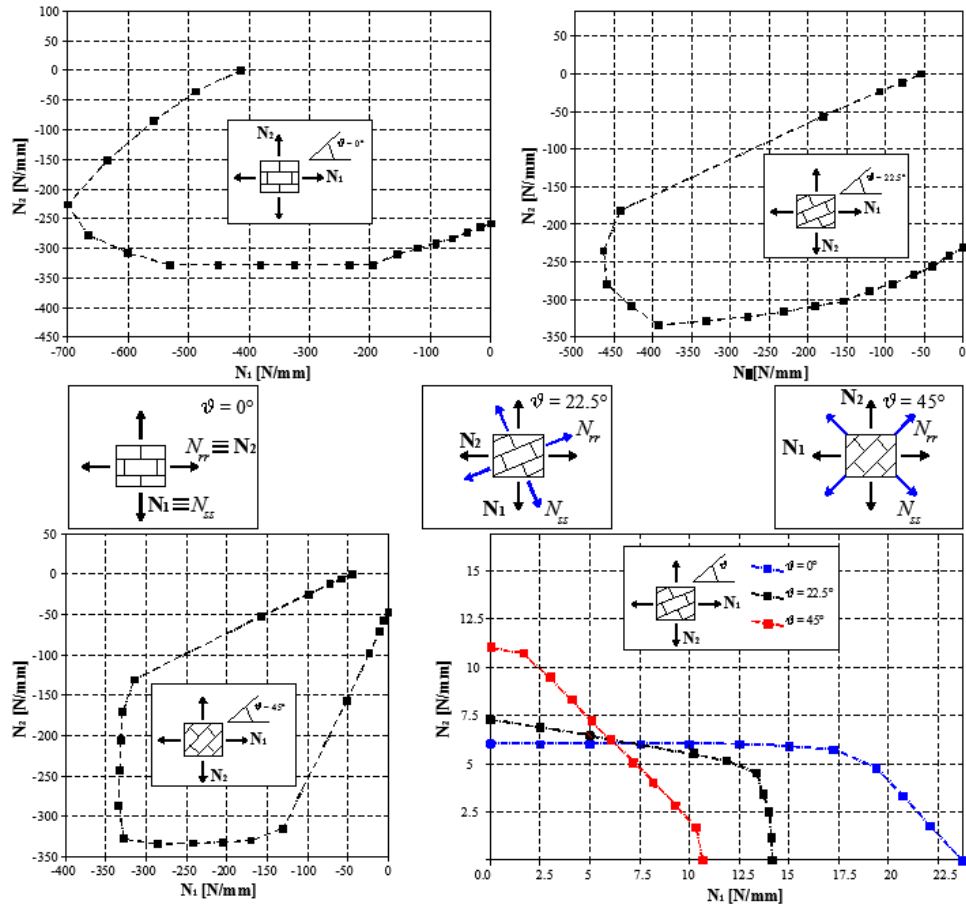


Figure 2.15: In-plane homogenized failure surface at different orientations of the load with respect to bed joint ϑ direction, ribbed cross vault.

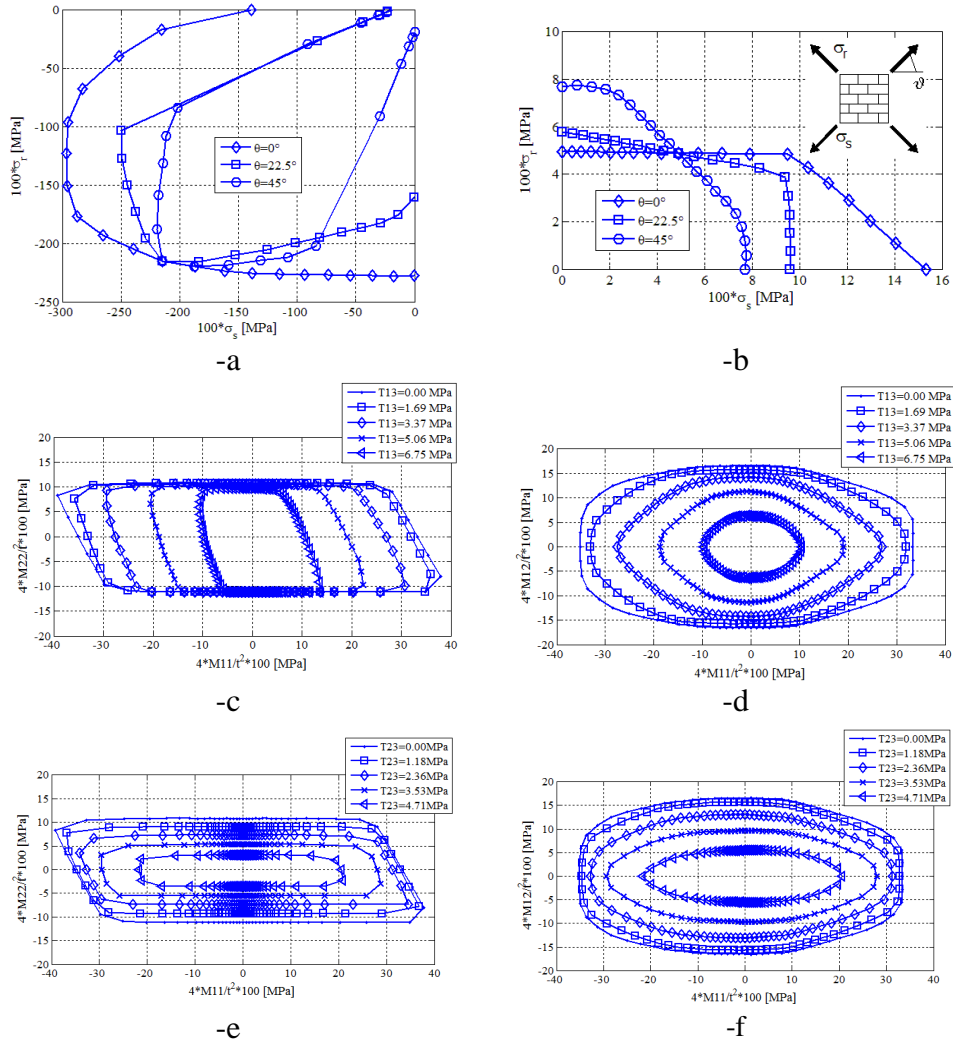


Figure 2.16: Ribbed cross vault. –a and –b: In-plane homogenized failure surface (–a: compression region, –b: tension region) at different orientations of the load with respect to bed joint ϑ direction. –c and –d: M11-M22 (–c) and M11-M12 (–d) failure surfaces at different values of out-of-plane shear T13. –e and –f: M11-M22 (–e) and M11-M12 (–f) failure surfaces at different values of out-of-plane shear T23.

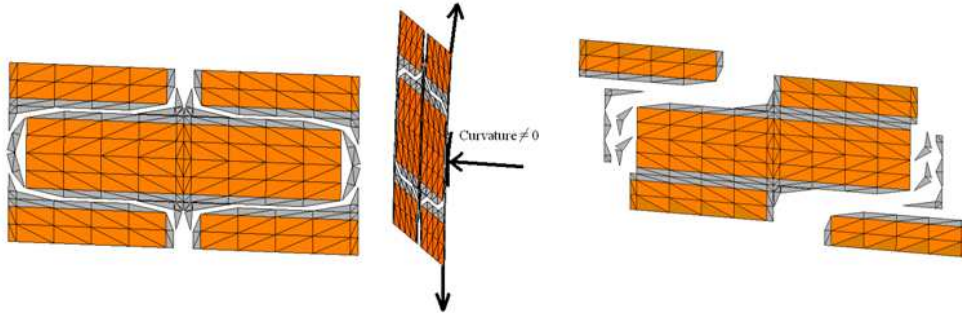


Figure 2.17: In-plane failure mechanisms on the curved elementary cell. –a: pure N_{rr} action and detail of elementary cell out-of-plane curvature (ribbed cross vault elementary cell). –b: complex in-plane failure in presence of N_{rr} , N_{rs} , N_{ss} .

2.3.3 Emi-spherical dome

The double curvature representative element of volume with its discretization in Finite Elements, considered for the analysis at a cell level of a spherical dome experimentally tested in [24], is depicted in Figure 2.19. Bricks dimensions are $250 \times 120 \times 55 \text{ mm}^3$ and mortar joints are reduced to interfaces. We denote with the symbol “11” the direction tangent to the REV in correspondence of the centroid of the central brick and laying on a horizontal plane and with the symbol “22” axis tangent to the elementary cell and perpendicular to “11”.

It is interesting to notice that, differently from previous examples, both 11 and 22 directions correspond to axes of non null curvature. As already discussed, in this case the REV chosen for the simulation should be suitably scaled passing from the supports to the top of the dome, if we suppose that the cupola is generated by repetition of the REV here considered.

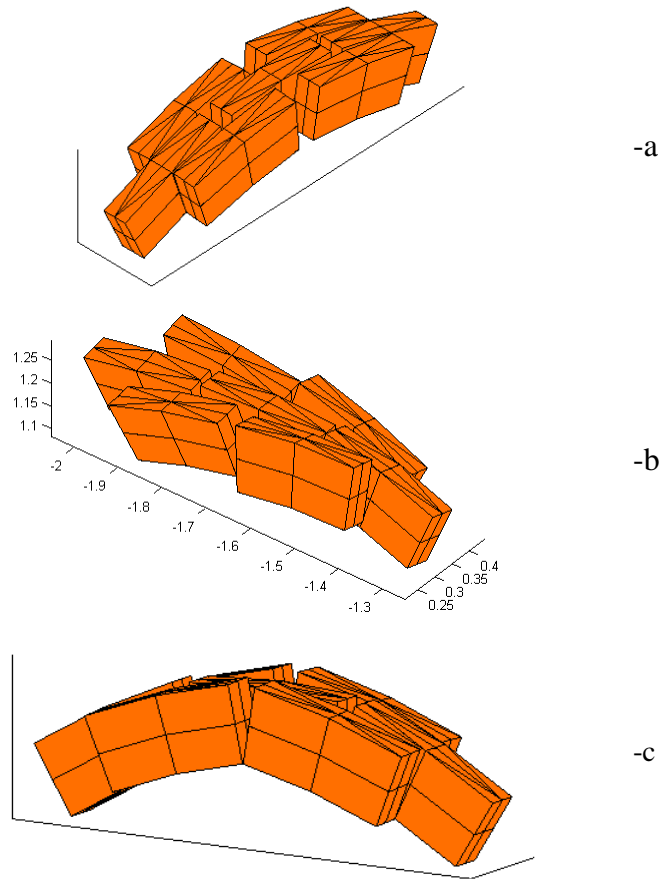


Figure 2.18: Ribbed cross vault. Typical REV deformed shapes for (-a) N11 membrane action, (-b) pure M12 torsion (-c) pure M11 bending moment.

Obviously, this should require that bricks dimensions are scaled from their original dimensions (an approximation here accepted in order to have a numerical estimation of masonry behaviour).

Mechanical properties adopted for the constituent materials are summarized in Table III and correspond to experimental data collected by Foraboschi [23][24], see also [26].

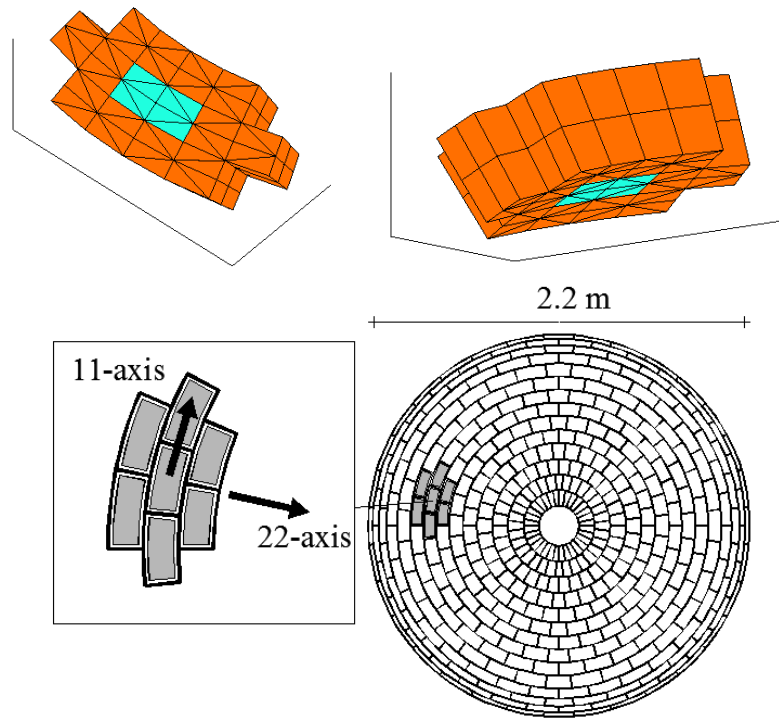


Figure 2.19: Masonry dome. Representative element of volume adopted for the simulations and FE discretization

Membrane and out-of-plane homogenized failure surfaces obtained solving optimization problem (2.11) for a number of different directions of the unitary vector Σ_1^T (representing the load direction in the 8-dimensional space of in-, out-of-plane and shear actions) are depicted in Figure 2.20 following the scheme adopted in the previous examples. Due to the double curvature of the elementary cell, the homogenized masonry failure surface is clearly different from the flat case, remaining sensibly anisotropic. The different strength when respectively positive or negative M11 and M22 bending moments are considered (see for

instance Figure 2.20-c and -e) are obviously a direct consequence of the REV curvature.

This is confirmed by deformed shapes at collapse represented in Figure 2.21. In particular, in Figure 2.21-a field of velocities at collapse for bending along 11 axis (both positive and negative) is depicted, whereas in Figure 2.21-b failure mechanism corresponding to pure torsion (M12) is represented.

2.3.4 Cloister vault

The single curvature REV constituting by repetition a cloister vault with square plane and experimentally tested by Foraboschi [24] is here analyzed. REV with its discretization by means of six-noded wedge elements is depicted in Figure 2.22. Common Italian bricks of dimension $250 \times 120 \times 55 \text{ mm}^3$ were used by Foraboschi [24] to build the vault, with mortar joints of thickness approximately equal to 10 mm (here joints are reduced to interfaces for the sake of simplicity).

Table III: Hemispherical dome. Mechanical characteristic assumed for joints and bricks.

| <i>Joint (Lourenço Rots failure criterion)</i> | | |
|---|--|------------|
| f_t [N / mm^2] | Tensile strength | 0.1 |
| f_c [N / mm^2] | Compressive strength | 1.8 |
| c | Cohesion | $1.2 f_t$ |
| Φ | Friction angle | 20° |
| Φ_2 | Angle of the linerized compressive cap | 45° |
| <i>Brick (Mohr-Coulomb failure criterion with compressive cutoff)</i> | | |
| f_c [N / mm^2] | Compressive strength | 30 |
| c [N / mm^2] | Cohesion | 1 |
| Φ | Friction angle | 45° |

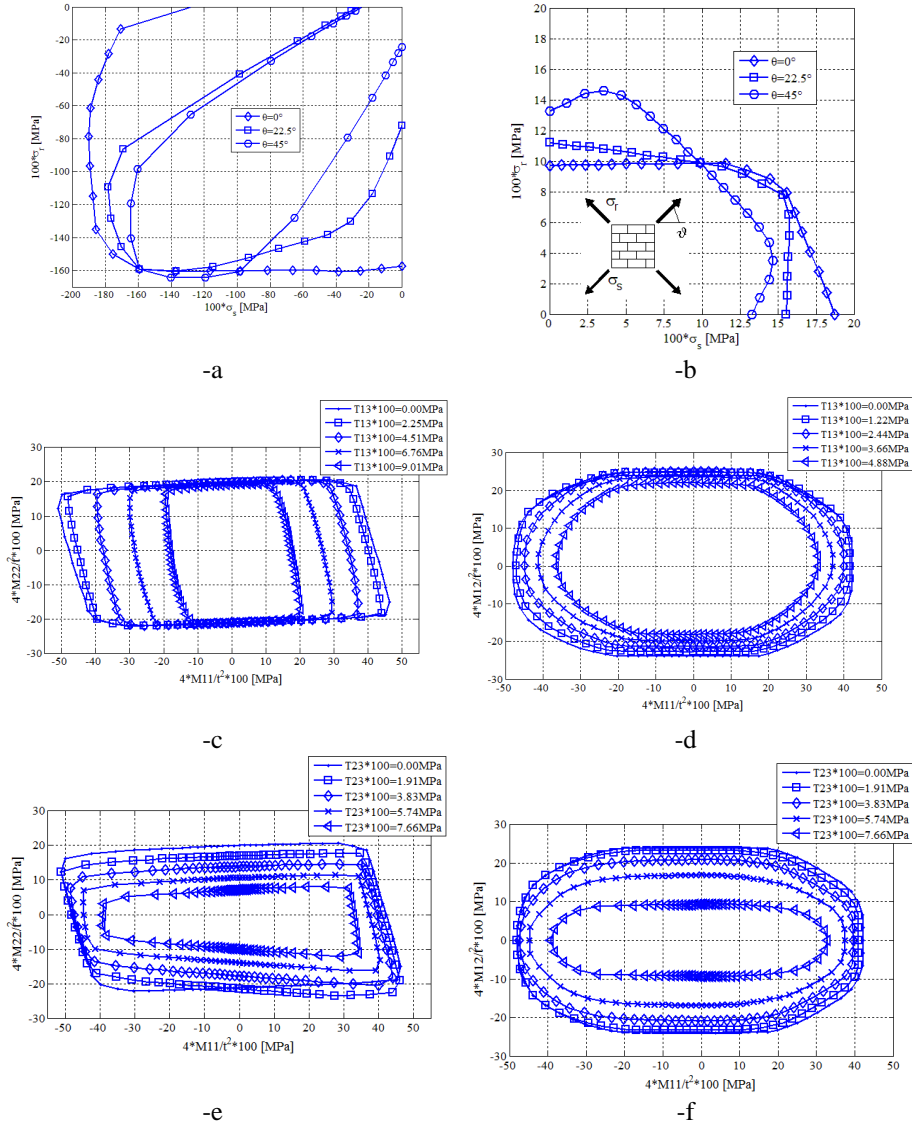


Figure 2.20: Masonry dome. –a and –b: In-plane homogenized failure surface (–a: compression region, –b: tension region) at different orientations of the load with respect to bed joint ϑ direction. –c and –d: M11-M22 (–c) and M11-M12 (–d) failure surfaces at different values of out-of-plane shear T13. –e and –f: M11-M22 (–e) and M11-M12 (–f) failure surfaces at different values of out-of-plane shear T23.

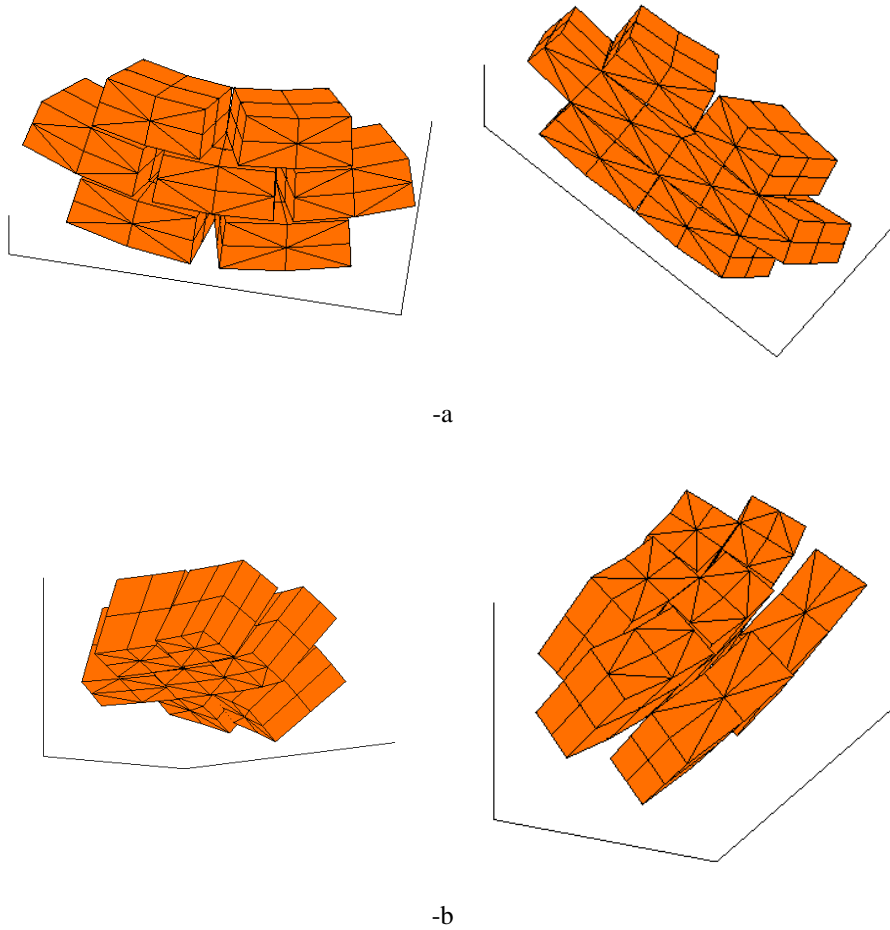


Figure 2.21: Masonry dome. Typical REV deformed shapes for (-a) pure M11 horizontal bending moment (left: intrados compressed; right: extrados compressed), (-b) pure M12 torsion.

We indicate with the symbol “11” the horizontal axis (curvature equal to zero) and with the symbol “22” the axis perpendicular to “11” and tangent to the elementary cell in the centroid of the central brick.

Analogously to previous cases, a Lourenço-Rots failure criterion is adopted for joints reduced to interfaces (mechanical properties, where available, are collected from Foraboschi [23][24]), whereas for bricks a Mohr-Coulomb strength domain is assumed (see Table IV).

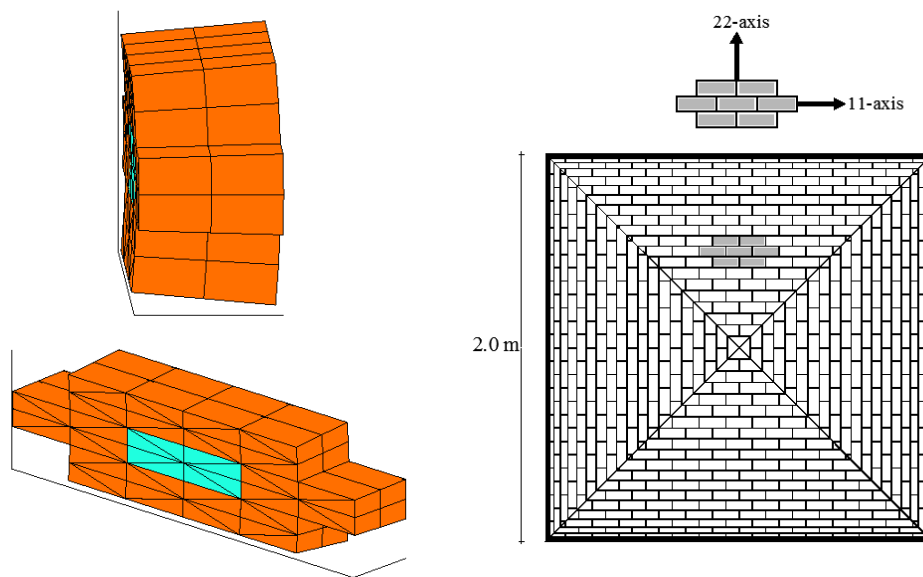


Figure 2.22: Cloister vault. Representative element of volume adopted for the simulations and FE discretization

Homogenized failure surfaces obtained applying the numerical approach previously presented are reported in Figure 2.23. In particular, in Figure 2.23-a and -b, in-plane masonry ultimate behavior at different orientations of the bed joints with respect to load direction in the compression-compression and tension-tension region respectively are represented.

Table IV: Cloister vault. Mechanical characteristic assumed for joints and bricks.

| Joint (Lourenço Rots failure criterion) | | |
|---|--|------------|
| f_t [N / mm^2] | Tensile strength | 0.018 |
| f_c [N / mm^2] | Compressive strength | 2.3 |
| c | Cohesion | $1.2 f_t$ |
| Φ | Friction angle | 20° |
| Φ_2 | Angle of the linerized compressive cap | 40° |
| Brick (Mohr-Coulomb failure criterion with compressive cutoff) | | |
| f_c [N / mm^2] | Compressive strength | 20 |
| c [N / mm^2] | Cohesion | 1 |
| Φ | Friction angle | 45° |

Similarly, in Figure 2.23 from $-c$ to $-f$, out-of-plane ultimate strength (for both 11 and 22 directions) is evaluated at increasing assigned out-of-plane shear actions T13 and T23.

As it is possible to notice, results are similar to those obtained for the parabolic arch by Vermetfoort [21], being REV almost flat in this case. Small differences occur between present results and Cecchi et al.[11] analyses, except for a reduction of 22 axis ultimate strength, consequent to a small out-of-plane effect due to the non null curvature. Such a behaviour is confirmed by the deformed shape at collapse observed loading the REV with a membrane action along 22 axis, as illustrated in Figure 2.24.

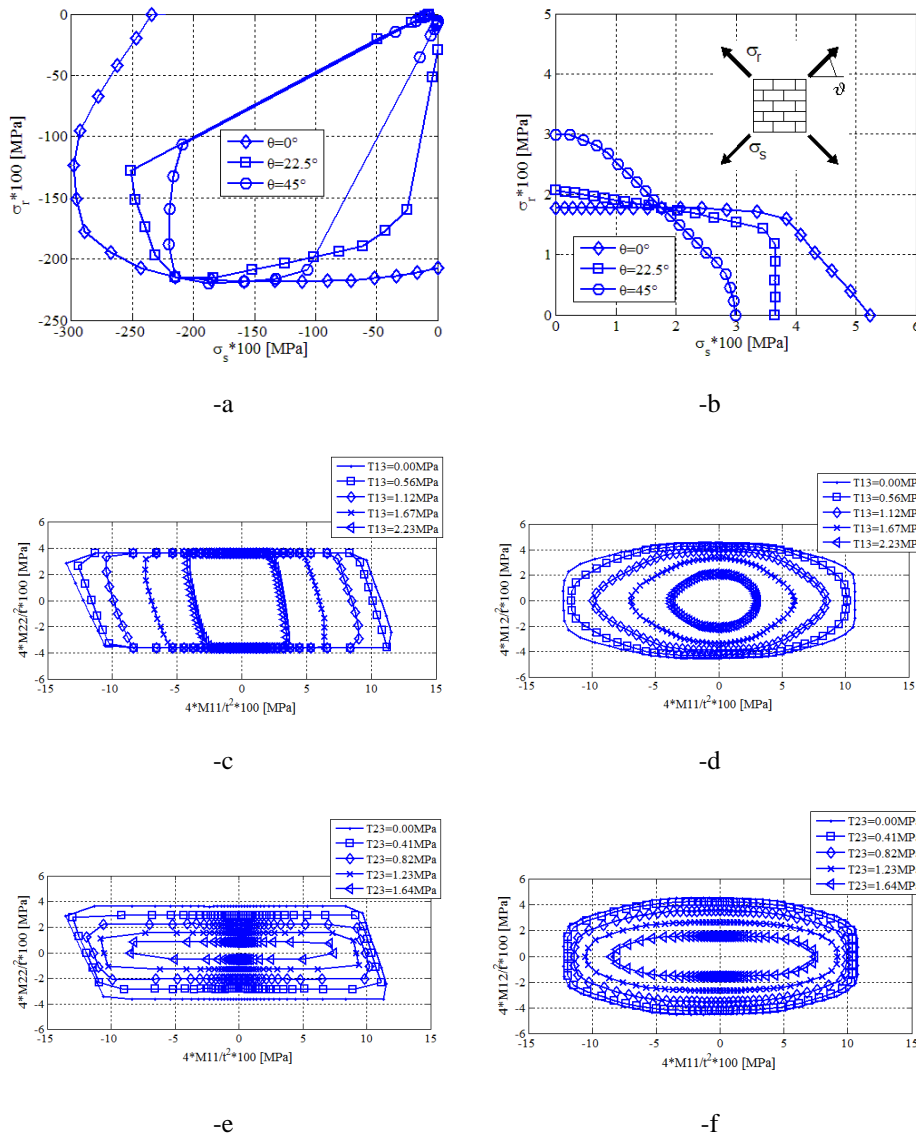


Figure 2.23: Cloister vault. –a and -b: In-plane homogenized failure surface (–a: compression region, –b: tension region) at different orientations of the load with respect to bed joint ϑ direction. –c and -d: M11-M22 (–c) and M11-M12 (–d) failure surfaces at different values of out-of-plane shear T13. –e and -f: M11-M22 (–e) and M11-M12 (–d) failure surfaces at different values of out-of-plane shear T23.

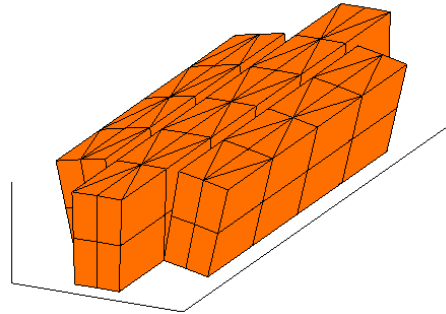


Figure 2.24: Cloister vault. Typical REV deformed shape at collapse for pure membrane action along 22 axis

2.4 Conclusion

In the present chapter, a kinematic simplified identification model for the determination of averaged masonry macroscopic properties at failure has been discussed.

The model assumes as representative element of volume (REV) a central brick interconnected with its six neighbours by means of mortar joints reduced to interfaces with frictional behaviour and limited tensile and compressive strength. Suitable macroscopic internal actions have been imposed on the REV in order to comply, at least in an approximate manner, the homogenization theory requirements. In order to numerically evaluate a piecewise linear approximation of masonry failure surface to use at a structural level, the REV has been discretized by means of flat six-nodded wedge rigid elements and a flat three-nodded triangular rigid element for the study of ribbed cross vault. Since no dissipation is allowed inside the element, failure may occur only at the interfaces between contiguous elements. A possible failure of bricks has been also taken into account assuming a limited strength for brick-brick interfaces. A simple linear programming problem

has been obtained at the micro-scale, which allowed, solving several optimization problems at fixed internal actions combinations, to numerically evaluate a piecewise linear approximation of masonry failure surface.

Four cases of technical relevance have been discussed in detail, namely a parabolic arch, a ribbed cross vault, a dome and a cloister vault. For each case, macroscopic masonry behaviour at failure in presence of membrane and flexural loads has been investigated. The differences with respect to the flat case are sometimes rather evident, especially when bricks are disposed with their longer dimension along the axis with non null curvature or when double curvature REV's are considered.

2.5 References

- [1] Luciano R, Sacco E. Homogenization technique and damage model for old masonry material. *International Journal of Solids and Structures* 1997; 34(4): 3191–208.
- [2] Pegon P, Anthoine A. Numerical strategies for solving continuum damage problems with softening: application to the homogenization of masonry. *Computers and Structures* 1997; 64(4): 623-642.
- [3] Massart T, Peerlings RHJ, Geers MGD. Mesoscopic modeling of failure and damage-induced anisotropy in brick masonry. *European Journal of Mechanics A/Solids* 2004; 23: 719–735.
- [4] Lourenço PB, Rots J. A multi-surface interface model for the analysis of masonry structures. *Journal of Engineering Mechanics ASCE* 1997; 123(7): 660-668.
- [5] Lourenço PB, de Borst R, Rots J. A plane stress softening plasticity model for orthotropic materials. *International Journal for Numerical Methods in Engineering* 1997; 40: 4033-4057.
- [6] Milani G, Lourenço PB, Tralli A. Homogenised limit analysis of masonry walls. Part I: failure surfaces. *Computers and Structures* 2006; 84: 166-180.
- [7] Lourenço PB, de Borst R, Rots J. A plane stress softening plasticity model for orthotropic materials. *International Journal for Numerical Methods in Engineering* 1997; 40: 4033-4057.
- [8] Anthoine A. Derivation of the in-plane elastic characteristics of masonry through homogenisation theory. *International Journal of Solids and Structures* 1995; 32 (2): 137-163.

- [9] Milani G, Lourenço PB, Tralli A. Homogenised limit analysis of masonry walls. Part II: structural examples. *Computers and Structures* 2006; 84: 181-195.
- [10] Cecchi, A., Milani, G., 2007. A kinematic FE limit analysis model for thick English bond masonry walls. *International Journal of Solids and Structures*, in press.
- [11] Cecchi A, Milani G, Tralli A. A Reissner–Mindlin limit analysis model for out-of-plane loaded running bond masonry walls. *International Journal of Solids and Structures* 2007; 44(5): 1438-1460.
- [12] Drosopoulos G A, Stavroulakis G E, Massalas C V. Limit analysis of a single span masonry bridge with unilateral frictional contact interfaces. *Engineering Structures* 2006; 8(13): 1864-1873.
- [13] Slinchenko D, Verijenko V E. Structural analysis of composite lattice shells of revolution on the basis of smearing stiffness. *Composite Structures* 2001;54: 341-448.
- [14] Andrianov I V, Verbonol V M, Awrejcewicz J. Buckling analysis of discretely stringer-stiffened cylindrical shells. *International Journal of Mechanical Sciences* 2006; 48: 1505-1515.
- [15] Habbal A. An effective model for Lipschitz wrinkled arches. *Journal of Mathematical Analysis and Applications* 2003; 285: 155-173.
- [16] Suquet P. Analyse limite et homogénéisation. *Comptes Rendus de l'Académie des Sciences - Series IIB – Mechanics* 1983; 296: 1355-1358.
- [17] Ferris M, Tin-Loi F. Limit analysis of frictional block assemblies as a mathematical program with complementarity constraints. *Int. J. Mech. Sci.* 2001; 43, 209-224.
- [18] Orduna A, Lourenço P B. Cap model for limit analysis and strengthening of masonry structures. *Journal of Structural Engineering, ASCE* 2003; 1367-1375.
- [19] Orduña A, Lourenço P B. Three-dimensional limit analysis of rigid blocks assemblages. Part I: Torsion failure on frictional joints and limit analysis formulation. *Int. J. Solids and Structures* 2005; 42 (18-19): 5140-5160.
- [20] Begg D, Fishwick R. Numerical analysis of rigid block structures including sliding. In: Middleton, J., Pande, G.(Eds.), *Computer Methods in Structural Masonry* 1995; 3, 177–183.
- [21] Vermeltfoort AV. Analysis and experiments of masonry arches. In: *Proc. Historical Constructions*, P.B. Lourenço & P. Roca (Eds.), Guimarães PT, 2001.
- [22] Faccio P, Foraboschi P, Siviero E. Masonry vaults reinforced with FPR strips [In Italian: Volte in muratura con rinforzi in FRP]. *L'Edilizia* 1999; 7/8: 44-50.
- [23] Foraboschi P. Strengthening of masonry arches with fiber-reinforced polymer strips. *Journal of Composites for Construction* 2004; 8: 191-202.

-
- [24] Foraboschi P. *Masonry structures externally reinforced with FRP strips: tests at the collapse [in Italian]. In: Proc. I Convegno Nazionale "Sperimentazioni su Materiali e Strutture", Venice, 2006.*
- [25] *DIANA 9.3 version user's Manual. TNO Building and Construction Research, Department of Computational Mechanics, Delft, The Netherlands, 2008.*
- [26] Creazza G, Saetta A, Matteazzi R, Vitaliani R. *Analyses of masonry vaults: a macro approach based on three-dimensional damage model. Journal of Structural Engineering 2002; 128(5): 646-654.*

Chapter 3.

Limit analysis of masonry vaults by curved shell Finite Elements

Masonry curved elements -as for instance arches, domes and vaults- represent one of the most diffused structural typologies in historical buildings of both Eastern and Western architecture. Moreover, the growing interest in the preservation and rehabilitation of historic constructions has created a need for the development of new efficient tools for the analysis and the evaluation of load-bearing capacity of these structures.

In the present chapter, a novel finite element approach for the limit analysis of masonry vaulted structures is presented. A six-nodes triangular curved element is used in order to correctly take into account, as far is possible, the actual geometry of the vault. For the sake of simplicity, a kinematic approach with possible velocity discontinuities along the edges of adjoining elements is considered. On the other hand, it has been demonstrated (see Sloan and Kleeman [1]) that the introduction of

discontinuities at the interfaces between contiguous elements is suitable for the analysis at collapse of purely cohesive or cohesive-frictional materials, which is the case of masonry.

In Section 3.1, the novel triangular six-nodes curved element is presented, whereas in Section 3.2, several numerical simulations on a number of masonry shells experimentally tested until collapse are performed. In particular, the dependence of the collapse load from the mesh refinement and constituent materials parameters (sensitivity analysis) is thoroughly discussed.

3.1 The curved triangular F. E. model

3.1.1 Basic assumptions

In this Section, a kinematic FE approach for the homogenized upper bound limit analysis of masonry curved shells is presented. A Six-nodes triangular curved rigid element with possible velocities discontinuities along the edges of adjoining elements is developed. Following a general approach widely diffused in the technical literature for the analysis of masonry flat plates (Sinha [2]), in the model, plastic dissipation is allowed only at the interfaces between adjoining element.

The utilization of six-nodes curved elements is particularly important for the structural analyses reported in what follows, since it is possible to accurately approximate the actual shape of curve surfaces even with few elements (Chapelle and Bathe [3]), and therefore permitting a reliable estimation of both internal and external (e.g. dead loads) dissipation.

On the other hand, it is stressed that an important limitation of the limit analysis approach here adopted is its impossibility to give information (required by some codes of practice) on displacements. In any case, once that a failure mechanism is known from limit analysis, an elastic FE analysis of the resistant structure

immediately before the collapse may be used to have information on the displacements.

3.1.2 Six-nodes curved shell elementary

Let a six-nodes triangular curved shell element E be considered, as shown in Figure 3.1-a, with nodes coordinates $(x_i, y_i, z_i), i = 1, \dots, 6$ and node numbers disposed in counter clockwise, with vertex node numbers from 1 to 3. Let the symbol Ω indicate the surface of E , Figure 3.1.

Let us introduce the two natural coordinates t and p varying respectively from 0 to 1 and from 0 to $1-t$ (Zienkiewicz and Taylor [4]). Hence the global coordinate (x, y, z) of a point P within the triangular element E can be expressed as:

$$P \equiv [x \ y \ z]^T = \sum_{i=1}^6 N_i(t, p) [x_i \ y_i \ z_i]^T \tag{3.1}$$

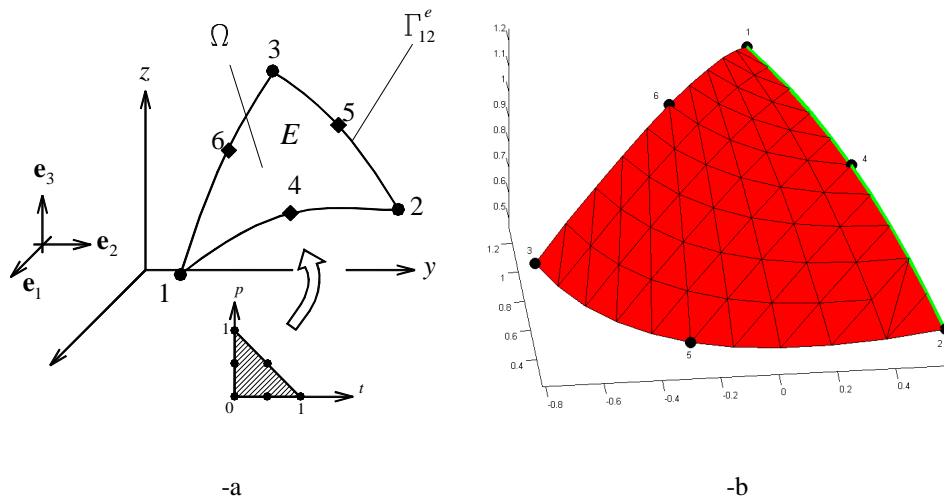


Figure 3.1 Six-nodes curved element (-a) and its implementation in Matlab (-b). The green line refers to Γ_{12}^e edge.

Where x_i , y_i and z_i are global coordinates of node P_i ($i = 1, \dots, 6$) and N_i is the node i shape function. N_i are given by:

$$N_i(t, p) = \begin{cases} \eta_i(2\eta_i - 1) & i = 1, 2, 3 \\ 4\eta_{i-3}\eta_{i-2} & i = 4, 5, 6 \end{cases}$$

$$\eta_i = \begin{cases} 1 - p - t & i = 1, 4 \\ t & i = 2 \\ p & i = 3 \end{cases} \quad (3.2)$$

Natural coordinates of nodal points are respectively $P_1(t, p) = (0, 0)$, $P_2(t, p) = (1, 0)$, $P_3(t, p) = (0, 1)$, $P_4(t, p) = (1/2, 0)$, $P_5(t, p) = (1/2, 1/2)$, $P_6(t, p) = (0, 1/2)$.

Let us consider the Γ_{12}^e edge of the element E , connecting P_1 and P_2 nodes. Similar considerations can be repeated for 1–3 and 2–3 edges respectively, with no conceptual differences. Since the edge is constrained to pass through P_1 , P_4 and P_2 nodes, each point P on Γ_{12}^e is given in parametric form (assuming i.e. $p = 0$) as follows:

$$P = P(t) = \begin{bmatrix} x(t) \\ y(t) \\ z(t) \end{bmatrix} \Big| \begin{cases} x(t) = x_{P_1} + (-3x_{P_1} - x_{P_2} + 4x_{P_4})t + 2[(x_{P_1} + x_{P_2}) - 2x_{P_4}]t^2 \\ y(t) = y_{P_1} + (-3y_{P_1} - y_{P_2} + 4y_{P_4})t + 2[(y_{P_1} + y_{P_2}) - 2y_{P_4}]t^2 \\ z(t) = z_{P_1} + (-3z_{P_1} - z_{P_2} + 4z_{P_4})t + 2[(z_{P_1} + z_{P_2}) - 2z_{P_4}]t^2 \end{cases} \quad (3.3)$$

where x_{P_i} , y_{P_i} and z_{P_i} are respectively x , y and z coordinates of node P_i and $t \in [0 \ 1]$.

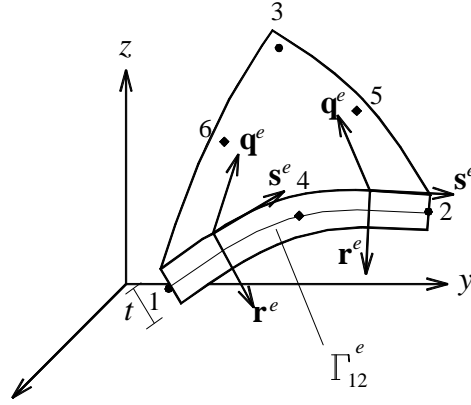


Figure 3.2 Γ_{12}^e edge with thickness t and $\mathbf{s}^e - \mathbf{r}^e - \mathbf{q}^e$ curved local frame of reference

From (3.3), it follows that for an arbitrary edge Γ_{ij}^e of an element E which connects nodes $i - j$, a suitable local curved frame of reference $\mathbf{s}^e - \mathbf{r}^e - \mathbf{q}^e$ with origin on vertex i can be identified, as shown in Figure 3.2.

We consider curved elements as rigid bodies infinitely resistant, with possible plastic dissipation only at the edges between adjoining elements. In this context, thus, it is necessary to evaluate jump of velocities between adjoining elements in the local coordinate system $\mathbf{s}^e - \mathbf{r}^e - \mathbf{q}^e$.

From equations (3.1)-(3.3), we obtain by differentiation vectors $\mathbf{s}^e - \mathbf{r}^e - \mathbf{q}^e$ in the global coordinate system:

$$\begin{aligned}
 \mathbf{r}^e &= -\mathbf{n}_1 \times \mathbf{n}_2 = -(\partial P / \partial t) / \|\partial P / \partial t\| \times (\partial P / \partial p) / \|\partial P / \partial p\| \\
 \mathbf{s}^e &= \frac{dP(t)}{dt} / \left\| \frac{dP(t)}{dt} \right\| \\
 \mathbf{q}^e &= \mathbf{s}^e \times \mathbf{r}^e
 \end{aligned} \tag{3.4}$$

at each point $P(t)$ belonging to the edge Γ_{12}^e .

From (3.4), trivial algebra leads to determine the rotation matrix $\mathbf{T}(t)$ which permits to pass from the global coordinate system to the local (see Figure 3.3).

Since curved triangular elements here adopted are rigid, velocity field interpolation inside each element depends only on 6 independent variables representing centroid velocities $\mathbf{u}_G = [u_x^G \quad u_y^G \quad u_z^G]^T$ and rigid rotations $\Phi_G = [\Phi_x^G \quad \Phi_y^G \quad \Phi_z^G]^T$ along coordinate axes.

Therefore, velocities field of a generic point P on Γ_{12}^e edge is expressed in the global frame of reference as:

$$\begin{bmatrix} u_x(t) \\ u_y(t) \\ u_z(t) \end{bmatrix} = \begin{bmatrix} u_x^G & 0 & 0 & 0 & -\Phi_y^G & \Phi_z^G \\ 0 & u_y^G & 0 & \Phi_x^G & 0 & -\Phi_z^G \\ 0 & 0 & u_z^G & -\Phi_x^G & \Phi_y^G & 0 \end{bmatrix} \begin{bmatrix} x(t) - x_G \\ y(t) - y_G \\ z(t) - z_G \end{bmatrix} = \mathbf{R}_G(P - G) \quad (3.7)$$

From (3.7), it follows that velocity field in the local coordinate system results dependent on t non linearly (see equation (3.3)).

In order to evaluate internal power dissipated at the interfaces by means of S^{hom} , the jump of velocities vector $[\mathbf{u}^{M-N}] = [\dot{\Delta}q \quad \dot{\Delta}s \quad \Delta\dot{\vartheta}_{nn} \quad \Delta\dot{\vartheta}_{nt} \quad \dot{\Delta}r]$ for each point of the interface has to be evaluated as a function of elements centroids velocities and rotations. $\dot{\Delta}q$ and $\dot{\Delta}s$ represent the in-plane normal and tangential velocity jumps, $\Delta\dot{\vartheta}_{nn}$ and $\Delta\dot{\vartheta}_{nt}$ are the flexion and torsion rotation rates jumps, whereas $\dot{\Delta}r$ is the out-of-plane tangential velocity jump (see Figure 3.4).

By means of (3.5) and (3.7), jump of velocities field between elements M and N in the local coordinate system $(\dot{\Delta}q \quad \dot{\Delta}s \quad \dot{\Delta}\tilde{r})$ can be written as follows:

$$\begin{bmatrix} \dot{\Delta}s(s^e) \\ \dot{\Delta}q(s^e) \\ \dot{\Delta}\tilde{r}(s^e) \end{bmatrix} = \mathbf{T}^M(s^e)^{-1} \mathbf{R}_G^M(P(s^e) - G^M) - \mathbf{T}^N(s^e)^{-1} \mathbf{R}_G^N(P(s^e) - G^N) \quad (3.8)$$

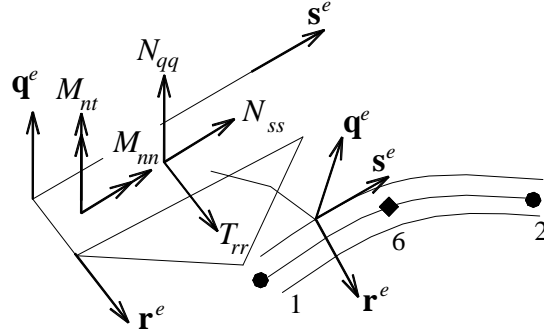


Figure 3.5 Internal actions \mathbf{t}^I at the interface I in the local coordinate system.

Thus, from equations (3.8) and (3.9), for a generic point of abscissa s^e it yields:

$$\dot{\Delta}r(s^e) = \dot{\Delta}\tilde{r}(s^e) - \Delta\dot{\vartheta}_{nt} \left(\frac{L_{12}}{2} - s^e \right) \quad (3.10)$$

Where L_{12} is the interface length.

3.1.3 Plastic flow relationships and power dissipation

We introduce for each interface I between contiguous elements, macroscopic specific actions collected in the vector \mathbf{t}^I , Figure 3.5, defined as $\mathbf{t}^{IT} = [N_{qq}^I \quad N_{ss}^I \quad M_{nn}^I \quad M_{nt}^I \quad T_{rr}^I]$, constituted by membrane actions acting along local axis \mathbf{q}^e (N_{qq}^I) and local axis \mathbf{s}^e (N_{ss}^I), bending moment (M_{nn}^I), torsion (M_{nt}^I) and out-of-plane shear (T_{rr}^I).

$$P^I = \int_0^{L_{12}} (N_{qq}^I \dot{\Delta}q + N_{ss}^I \dot{\Delta}s + M_{nn}^I \dot{\Delta}\vartheta_{nn} + M_{nt}^I \dot{\Delta}\vartheta_{nt} + T_{rr}^I \dot{\Delta}r) ds \quad (3.11)$$

Power dissipated at the interface can be evaluated solving analytically the integral (3.11).

For each interface I of length L_{12} , we suppose to have at disposal the homogenized (linearized) strength domain constituted by m^I planes in the local coordinate system (a generic linearization plane q^I has equation $A_{qq}^{q^I} N_{qq}^I + A_{ss}^{q^I} N_{ss}^I + B_{nm}^{q^I} M_{nm}^I + B_{nt}^{q^I} M_{nt}^I + A_{rr}^{q^I} T_{rr}^I = C_I^{q^I}$ $1 \leq q^I \leq m^I$). Such a linearization for each interface (and, in principle, for each point of the interface) can be obtained from S^{hom} exploiting the procedure recommended by Krabbenhoft et al. [5], and the reader is referred there for further details. Introducing plastic multipliers fields at the interface (one for each linearization plane) from equations (3.11), power dissipated at the interface can be re-written as:

$$P^I = \int_0^{L_{12}} \dot{\lambda}^I(s^e) \left(N_{qq}^I A_{qq}^{q^I} + N_{ss}^I A_{ss}^{q^I} + M_{nm}^I B_{nm}^{q^I} + M_{nt}^I B_{nt}^{q^I} + T_{rr}^I A_{rr}^{q^I} \right) ds \quad (3.12)$$

Obviously, field $\dot{\lambda}_{q^I}^I(s^e)$ assumes the same analytical expression found for the velocity field, i.e. is quadratic in t , see equations (3.3) and (3.7).

Therefore, $\dot{\lambda}_{q^I}^I(s^e)$ field is fully determined introducing only three plastic multipliers for each internal interface and for each linearization plane, corresponding to nodes 1, 6, 3.

On the other hand, the numerical evaluation of integral (3.12) case by case is time consuming and should involve several variables for each interface. Thus, in order both to reduce the computational cost and to be able to tackle complex 3D analyses, a symbolic integration is performed making use of Symbolic MatlabTM toolbox. In this way, plastic dissipation at a generic interface can be obtained with a very limited computation effort as:

$$P^I = \sum_{q^I}^{m^I} (W_1 \dot{\lambda}_{q^I}^{I,1} + W_6 \dot{\lambda}_{q^I}^{I,6} + W_3 \dot{\lambda}_{q^I}^{I,3}) C_I^{q^I} \quad (3.13)$$

where W_i $i=1,6,3$ are predetermined numerical coefficients obtained symbolically.

External power dissipated can be written as $P^{ex} = (\mathbf{P}_0^T + \lambda \mathbf{P}_1^T) \mathbf{w}$, where \mathbf{P}_0 is the vector of permanent loads, λ is the load multiplier for the structure examined, \mathbf{P}_1^T is the vector of variable loads and \mathbf{w} is the vector of assembled centroid elements velocities. As the amplitude of the failure mechanism is arbitrary, a further normalization condition $\mathbf{P}_1^T \mathbf{w} = 1$ is usually introduced. Hence, the external power becomes linear in \mathbf{w} and λ .

3.1.4 The Linear Programming (LP) problem

After some elementary assemblage operations, a linear programming problem is obtained, where the objective function consists in the minimization of the total internal power dissipated:

$$\left\{ \begin{array}{l} \min \left\{ \mathbf{P}_I^{in,ass} \dot{\lambda}^{I,assT} - \mathbf{P}_0^T \mathbf{w} \right\} \\ \text{such that} \left\{ \begin{array}{l} \mathbf{A}^{eq} \mathbf{U} = \mathbf{b}^{eq} \\ \dot{\lambda}^{I,ass} \geq \mathbf{0} \end{array} \right. \end{array} \right. \quad (3.14)$$

where:

\mathbf{U} is the vector of global unknowns and collects the vector of elements centroids velocities (\mathbf{w}) and rotations (Φ) and the vector of assembled interface plastic multiplier rates ($\dot{\lambda}^{I,ass}$).

\mathbf{A}^{eq} is the overall constraints matrix and collects normalization conditions, velocity boundary conditions and constraints for plastic flow in velocity discontinuities.

$\mathbf{P}_I^{in,ass}$ collects the coefficients $W_i C_I^{q^I}$ of equation (3.13) of all the n^I interfaces.

The reader is referred to Sloan and Kleeman [1] for a critical discussion of the most efficient tools for solving the linear programming problem reported in equation (3.14).

It is interesting to note that an estimation of membrane actions and moments associated to the failure mechanism can be obtained via the dual problem of (3.14):

$$\left\{ \begin{array}{l} \min \left\{ -\mathbf{P}_0^T [\mathbf{w} \ \Phi]^T + \mathbf{P}_I^{in,ass} \dot{\lambda}^{I,ass} \right\} \\ \text{such that} \left\{ \begin{array}{l} \mathbf{H}^T [\mathbf{w} \ \Phi]^T + \mathbf{A}^{in^T} \dot{\lambda}^{I,ass} = \mathbf{0} \\ \mathbf{R}^T [\mathbf{w} \ \Phi]^T = 1 \\ \dot{\lambda}^{I,ass} \geq \mathbf{0} \end{array} \right. \end{array} \right. \quad \left\{ \begin{array}{l} \max \{ \hat{\lambda} \} \\ \text{such that} \left\{ \begin{array}{l} \mathbf{H}\Sigma + \mathbf{R}\hat{\lambda} - \mathbf{P}_0 = \\ \mathbf{A}^{in} \Sigma \leq \mathbf{P}_I^{in,ass^T} \end{array} \right. \end{array} \right.$$

primal dual

(3.15)

Where Σ collects elements membrane actions and moment of each element and $\hat{\lambda}$ is the collapse multiplier.

3.2 Structural examples

In this section, several numerical results on a number of masonry vaults are presented and compared with experimental data available from the technical literature.

The first two examples are respectively a barrel rectangular vault and a skew arch, both tested by Vermeltoort [10]. The third example relies on a ribbed cross vault

experimentally tested by Faccio et al. [8], whereas the last example is a hemispherical dome (related experimental results are available from Creazza et al. [6][7]).

For each example, the homogenized limit analysis approach presented in the previous section has been employed to predict ultimate load and failure mechanism, assuming for the constituent materials (where available) mechanical properties experimentally determined (Vermeltfoort [10], Faccio et al. [8], Creazza et al. [7] and [6], Foraboschi [9]).

Both a mesh dependence study and a sensitivity analysis, varying in a wide range mortar cohesion and friction angle, are finally reported.

3.2.1 Barrel rectangular vault

The first analysis relies on the determination of the ultimate strength of a barrel rectangular vault experimentally tested by Vermeltfoort [10]. The vault is a parabolic arch with a clear span of 3 m, an inner radius of 2.5 m, a width of 1.5 m and a sagitta of 0.5 m.

The mechanical properties assumed for joints and bricks to calculate failure surfaces are reported in chapter 2.

In Figure 3.8, a comparison between the numerical failure load and the experimental result is represented: the good agreement between numerical and experimental results is worth noting.

In order to evaluate the influence of the mechanical properties adopted for joints on both collapse load and failure mechanism, a sensitivity analysis has been conducted on the example at hand. Three different values of friction angle Φ have been considered, respectively equal to 20° , 25° and 30° . Similarly, four different values of the tensile strength f_t have been inspected, respectively equal to 0.05, 0.1, 0.3 and 0.5 N/mm^2 .

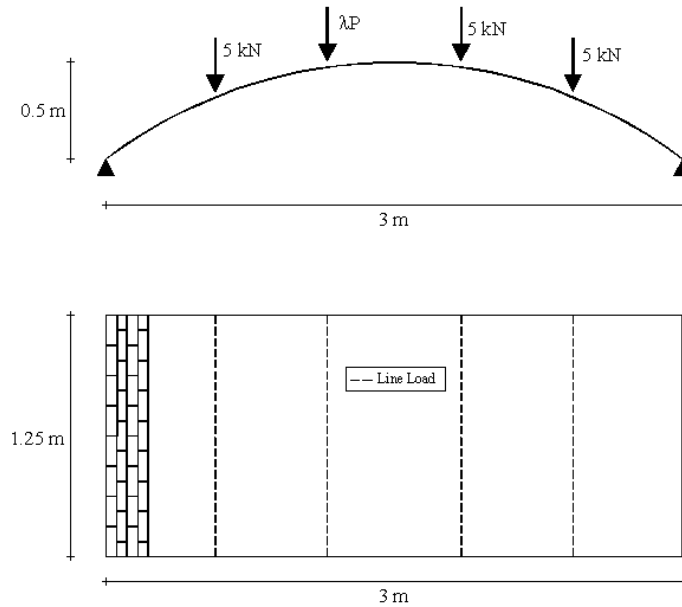


Figure 3.6 Barrel rectangular vault. Geometry and loading condition.

Collapse load numerically evaluated at different friction angles and cohesions is reported in Figure 3.9 -a and -b.

It is interesting to note from the sensitivity analysis that, for high values of tensile strength, the failure load does not depend on mortar friction angle, being failure essentially due to pure bending, as shown in Figure 3.10 -a. In Figure 3.10 -b, the internal power dissipation patch is also represented. As it possible to note, internal dissipation is concentrated under the line of application of the external load, meaning that, in this case, failure occurs as a consequence of the formation of two flexural “plastic” hinges. A total of four hinges is present at collapse (two geometrical and two plastics), a result clearly in agreement with simple mono-dimensional predictions based on at hand calculations (kinematical chains). The numerical collapse load turns out to be very near to that found by Vermeltfoort [10] during experimentation (see Figure 3.8).

Finally, in order to evaluate internal forces acting on the arch, in Figure 3.11 bending moment and axial compressive load eccentricity (defined as the ratio between bending moment and axial load) along arch length are reported.

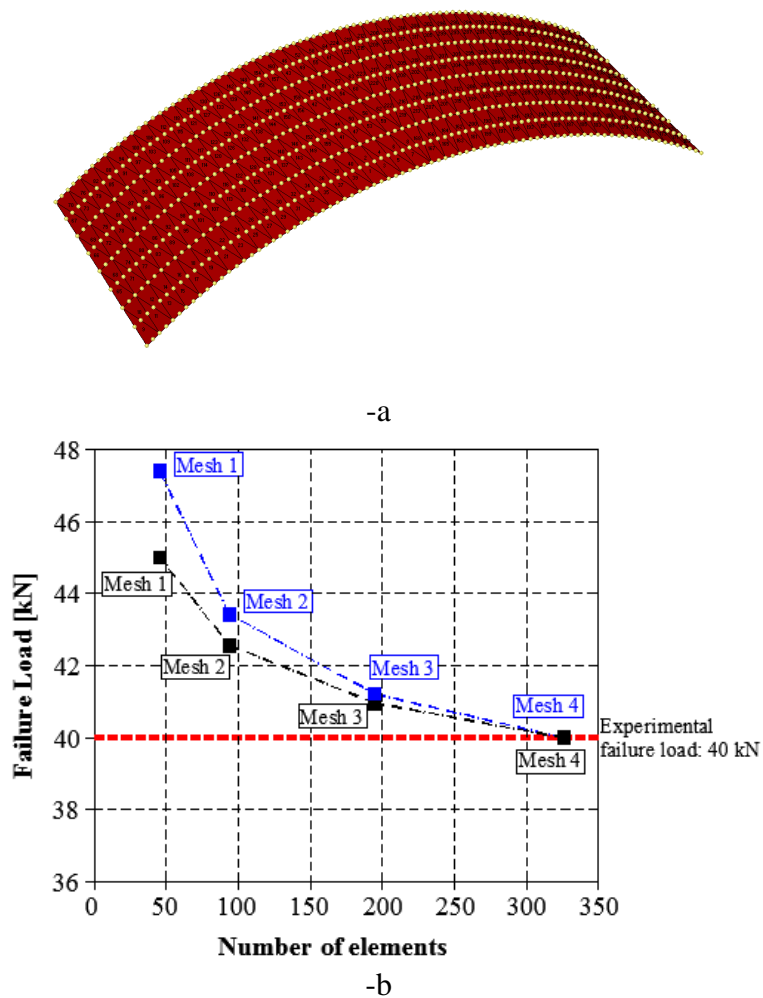


Figure 3.7 Barrel rectangular vault. –a: Mesh 4: 320 elements and 729 nodes –b: Mesh dependence study.

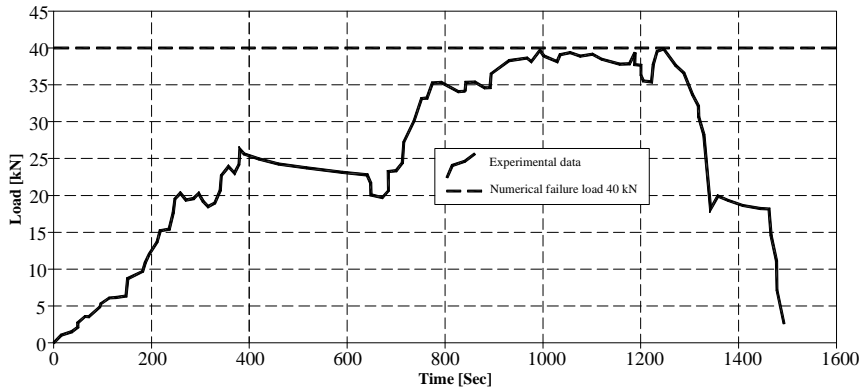


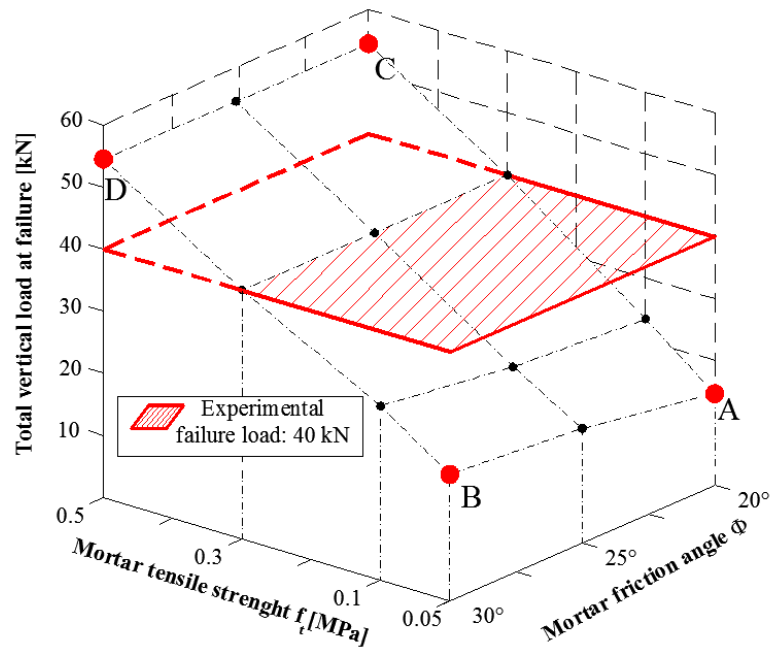
Figure 3.8 Barrel rectangular vault. Comparison between experimental and numerical (dashed line) results.

Numerical data are collected from the solution vector of the dual problem (3.15). It is particularly evident both the formation of two plastic hinges with position corresponding to the maximum positive and negative eccentricities, as well as the effect of the small tensile strength adopted for mortar joints, which allows that maximum eccentricities are major than one half of the arch thickness.

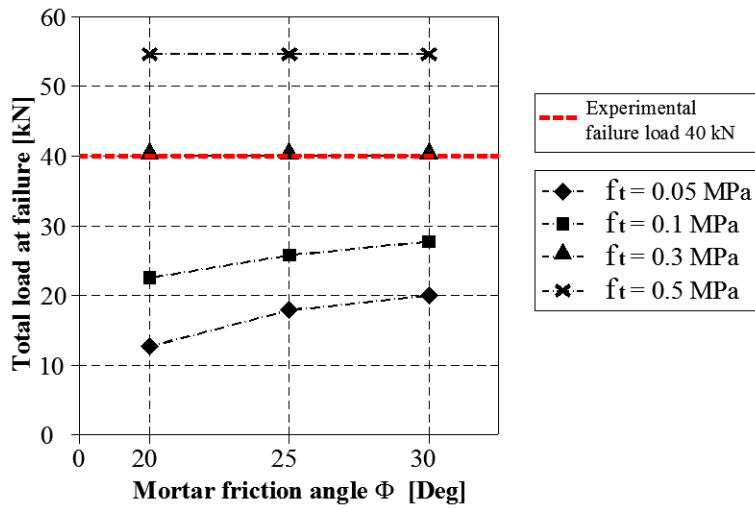
3.2.2 Skew arch

The second numerical simulation relies on a skew parabolic arch with a clear span of 3 m, an inner radius of 2.5 m, a width of 1.5 m, a sagitta of 0.5 m tested by Vermeltfoort [10].

Mechanical properties assumed for joints and bricks are the same of the barrel rectangular vault. In Figure 3.12 the geometry and the loading condition are reported.

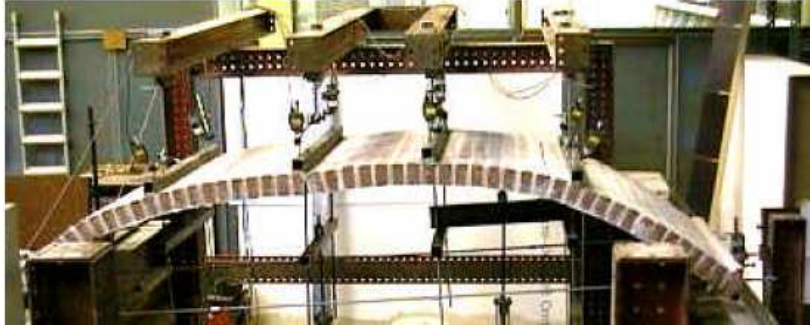


-a

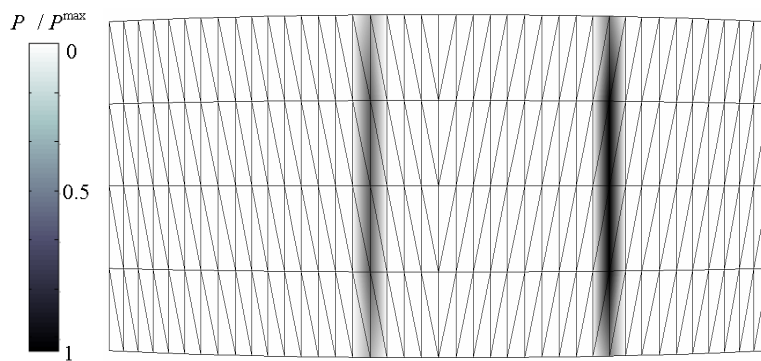
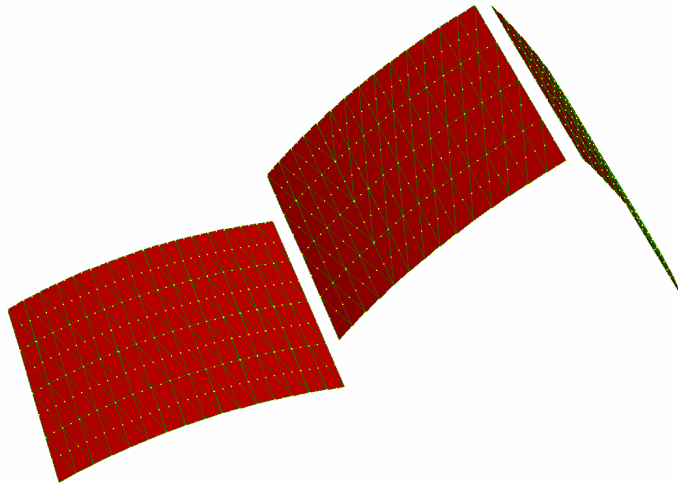


-b

Figure 3.9 Barrel rectangular vault. –a: Sensitivity analysis varying mortar tensile strength and mortar friction angle. –b: Failure load-mortar friction angle diagram.



-a



-b

Figure 3.10 Barrel rectangular vault. -a: Numerical failure mechanism compared with experimental evidences by Vermeltoort (2001). -b: Normalized power dissipated patch (P^{\max} is the maximum nodal power dissipation value).

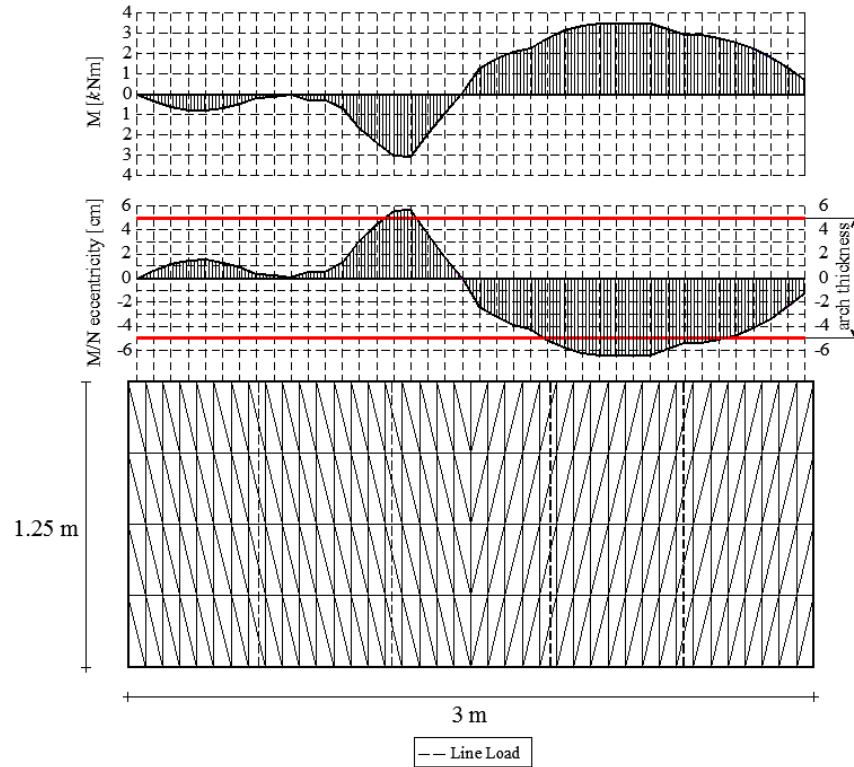


Figure 3.11 Barrel rectangular vault. Bending moment and compressive stress eccentricity evaluated from the dual problem.

Three different meshes, with increasing level of refinement, have been tested (the third mesh is represented in Figure 3.13 –a), in order to perform the mesh dependence study reported in Figure 3.13 –b, where the numerical failure load obtained with the different meshes considered is reported. Failure mechanism and plastic dissipation obtained with mesh 3 is also reported in Figure 3.14.

No experimental force-displacement curves are at disposal for the example at hand. From Vermeltfoort [10], only the experimental collapse load (around 26 kN) is available. When mechanical properties reported in Table I in sub-section 2.3.1 are adopted, a numerical collapse load of 34 kN is obtained, in acceptable agreement

(when an associated limit analysis approach is adopted) with experimental evidences.

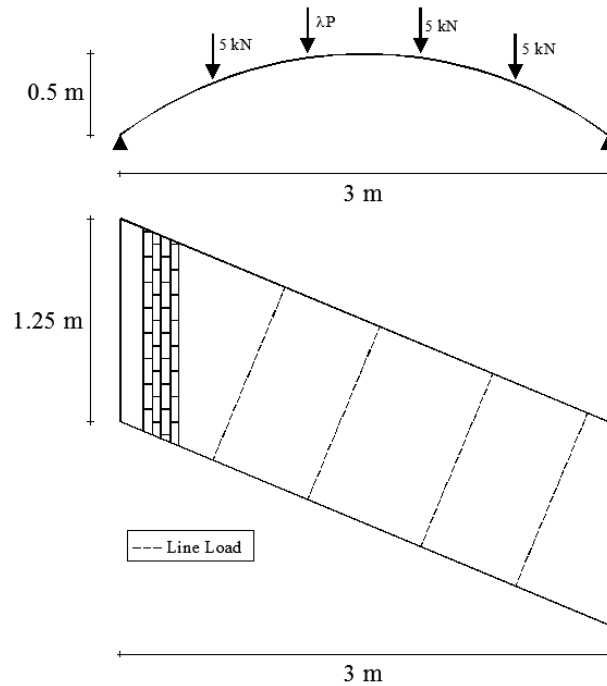


Figure 3.12 Skew vault. Geometry and loading condition.

In order to investigate how joints mechanical properties influence both collapse load and failure mechanism, a sensitivity analysis has been conducted on the example at hand (results are reported in Figure 3.15 -a and -b).

Three different values of friction angle Φ have been considered, respectively equal to 20° , 25° and 30° , with four different values of f_t tensile strength, respectively equal to 0.05, 0.1, 0.3 and 0.5 N/mm^2 .

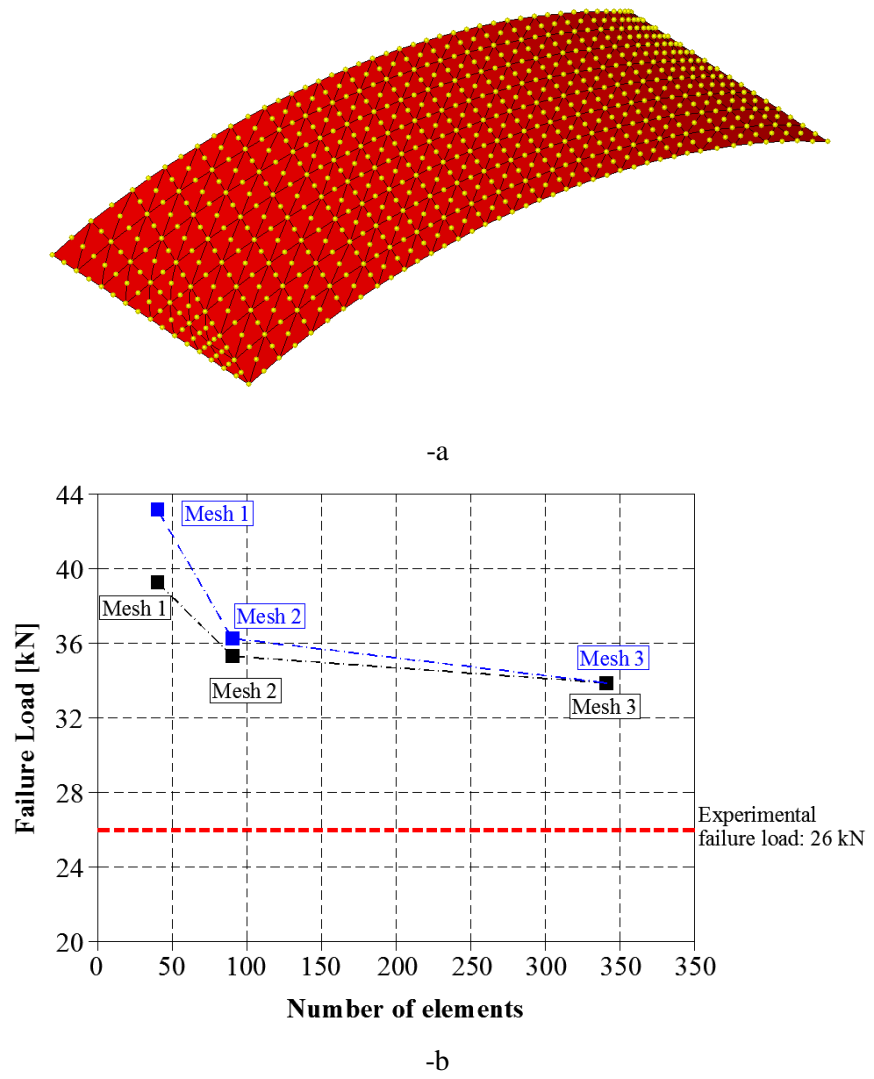


Figure 3.13 Skew vault. –a: Mesh 3: 348 elements (and 755 nodes) –b: Mesh dependence study.

It is interesting to note that, at a fixed value of tensile strength, the failure load varies considerably varying mortar friction angle (see Figure 3.15 -b), meaning that failure is due to a non-trivial combination of out-of-plane shear, bending and torsion, as shown in Figure 3.14 -a, where the failure mechanism of the arch for f_t equal to 0.3 N/mm^2 and Φ equal to 20° is reported. Obviously, in this case, a mono-dimensional analysis would be not useful and a 3D shell model is necessary to reproduce the torsion behaviour of the arch.

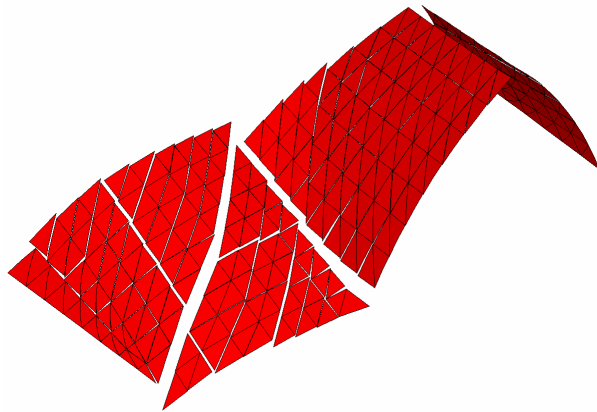
In Figure 3.14 -b, the internal power dissipation patch is also represented. As it is possible to note, internal dissipation is concentrated not only under the line of application of the external load (see detail A in Figure 3.14), but also along two diagonal lines (details B and C), thus demonstrating that failure occurs as a consequence of the limited torsional strength of the arch.

3.2.3 Ribbed cross vault

A ribbed cross vault, experimentally tested by Faccio et al. [8], formed by the intersection of two barrels vaults with an external diameter of 2.3 m, is consider as third example.

Mechanical properties assumed for joints and bricks and the failure surfaces implemented are reported in sub section 2.3.2.

Data not available from experimentation have been chosen from typical values from the literature, whereas the remaining coefficients adopted are taken in agreement with Creazza et al. [7][6]. In Figure 3.16 the geometry and the loading condition of the ribbed cross vault are reported.



-a

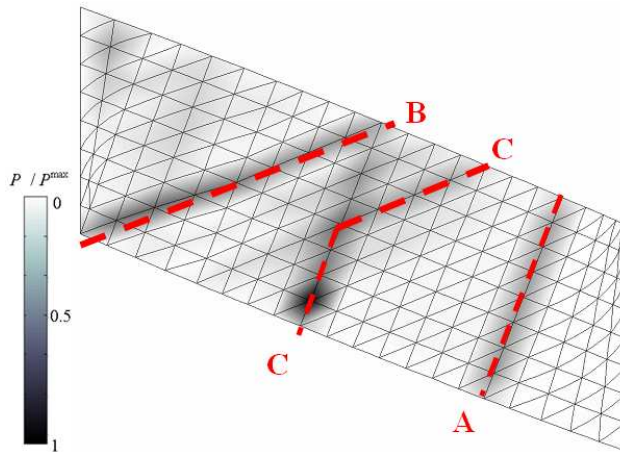
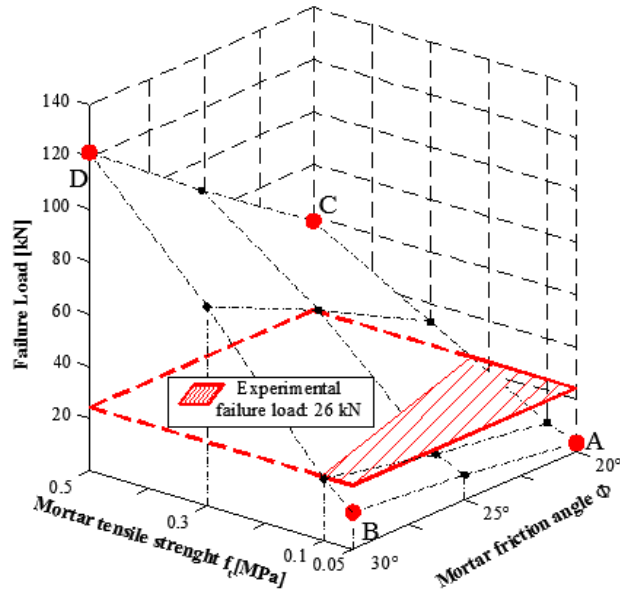
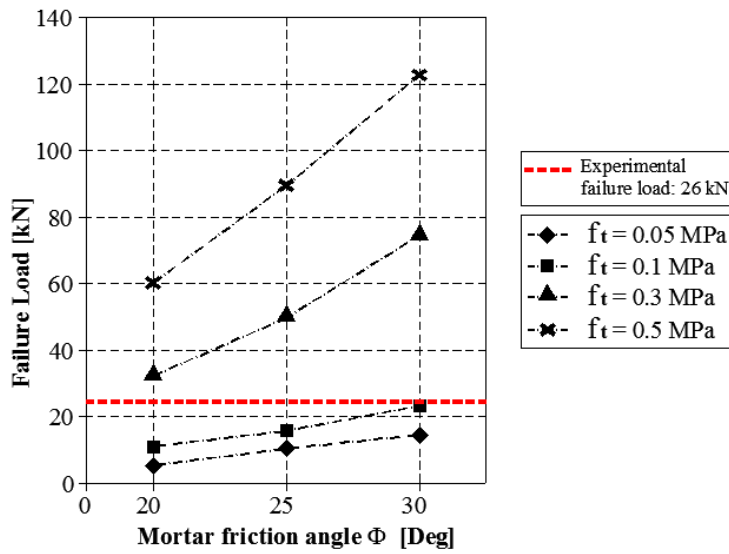


Figure 3.14 Skew vault. -a: Numerical failure mechanism compared with experimental evidences by Vermeltfoort [10]. -b: Normalized power dissipated patch (P^{\max} is the maximum nodal power dissipation value).



-a-



-b-

Figure 3.15 Skew vault. -a: Sensitivity analysis varying mortar tensile strength and mortar friction angle. -b: Failure load-mortar friction angle diagram

Three different meshes, with increasing refinement, have been used (the third mesh is represented in Figure 3.17 -a), in order to perform a mesh dependence study on the numerical collapse load (Figure 3.17 -b). In Figure 3.18, a comparison between numerical failure load obtained with the present model and the experimental load-displacement curves is represented; moreover, numerical results obtained by means of the damage model proposed by Creazza et al. [7][6] are also represented.

The satisfactory agreement among present results, previously Creazza et al. ([7] and [6]) elasto-damaging approach and experimental evidences is worth noting.

As in the previous cases, a sensitivity analysis has been conducted varying both mortar tensile strength f_t (0.05, 0.1, 0.15, and 0.2 N/mm^2) and mortar friction angle Φ (25° , 30° and 35°) in a wide range.

The failure loads P_u so obtained are depicted in Figure 3.19-a and -b. As it is possible to note from Figure 3.19-b, where P_u is reported at a different values of f_t (fixed) varying Φ , failure occurs as a combination of bending and out-of-plane shear for almost all the values of f_t inspected.

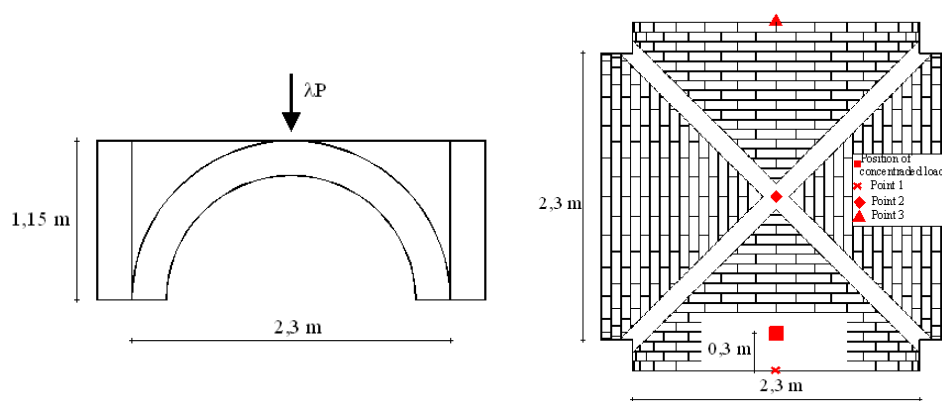


Figure 3.16 Ribbed cross vault. Geometry and loading condition.

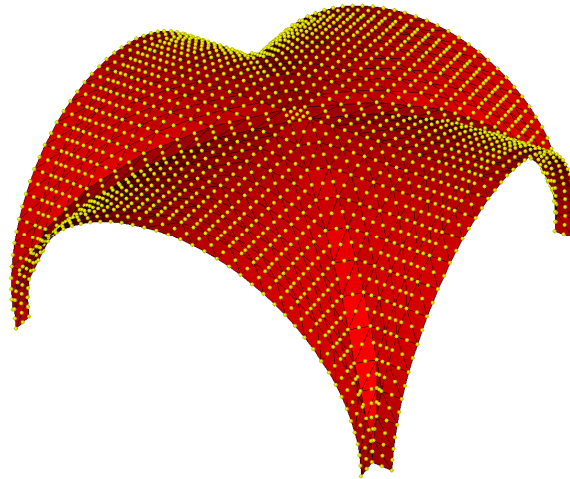
Such a behaviour is confirmed by the failure mechanism observed and the internal power dissipation patch, as shown respectively in Figure 3.20-a and -b, where numerical results obtained assuming f_t equal to 0.1 N/mm^2 and Φ equal to 20° are reported.

Finally, observing the patch of internal power dissipation, it is particularly evident that an out-of-plane sliding of the elements under the zone of the application of external load occurs, with the formation of five bending hinges in the principal arch of the cross vault (see Figure 3.20-c)

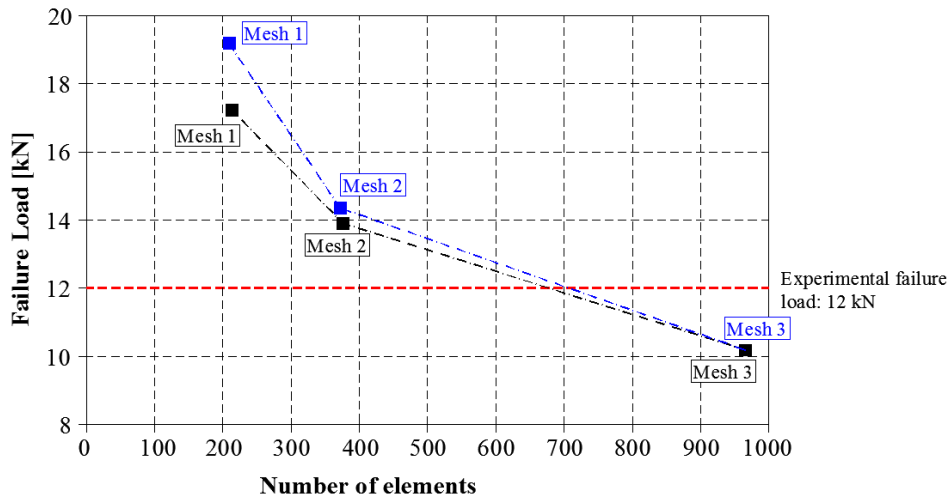
3.2.4 Hemispherical dome

The fourth analysis, which concerns a hemispherical dome with an inner diameter of 2.2m and thickness of 0.12m and experimentally tested by Foraboschi [9], is hereafter discussed.

Mechanical properties assumed for joints and bricks are summarized in Table III in sub section 2.3.3. In Figure 3.21 the geometry and the loading condition are reported. Three different meshes, with increasing refinement, have been used (the third mesh is represented in Figure 3.22 -a), in order to perform a mesh dependence study on the numerical collapse load (Figure 3.22-b). In Figure 3.23, a comparison between the failure load obtained with the present numerical model and experimental load-displacement curves is represented.



-a-



-b-

Figure 3.17 Ribbed cross vault.-a- Mesh 3: 952 elements (and 2009 nodes) -b- Mesh dependence study.

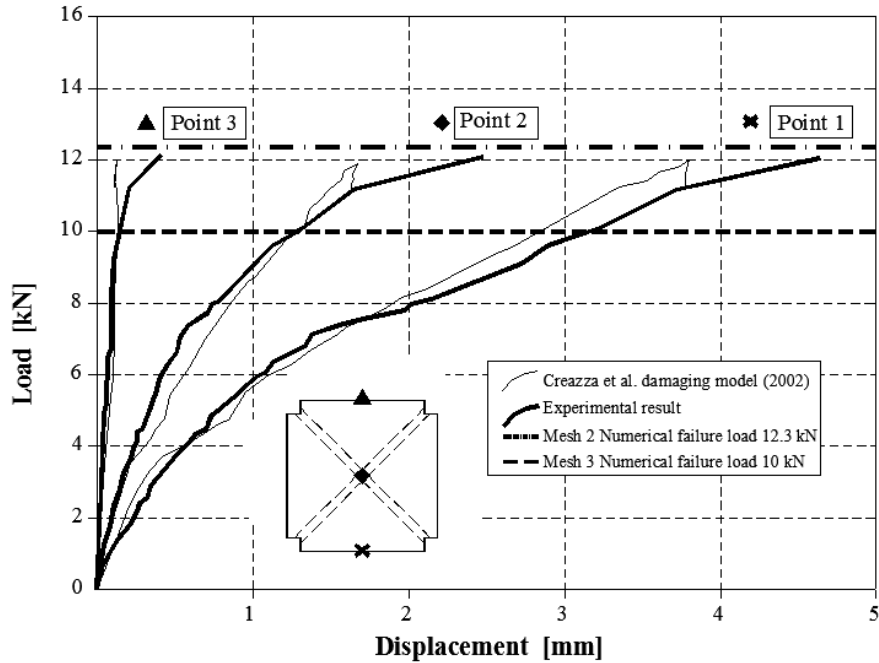
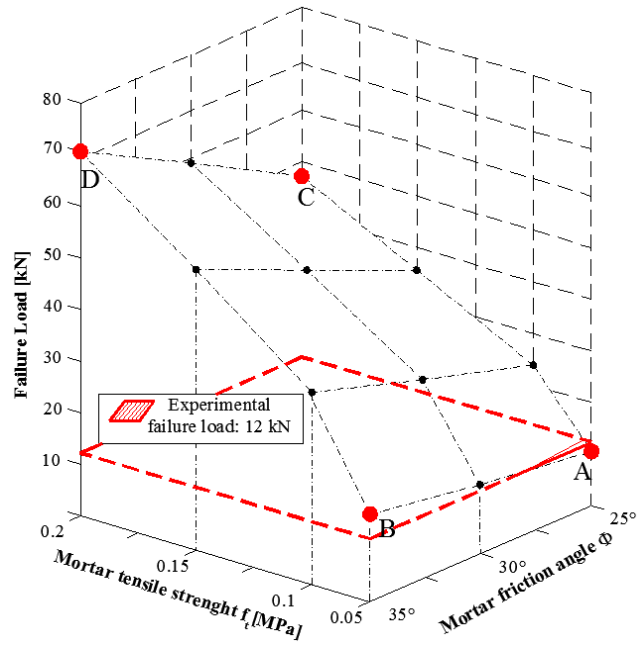


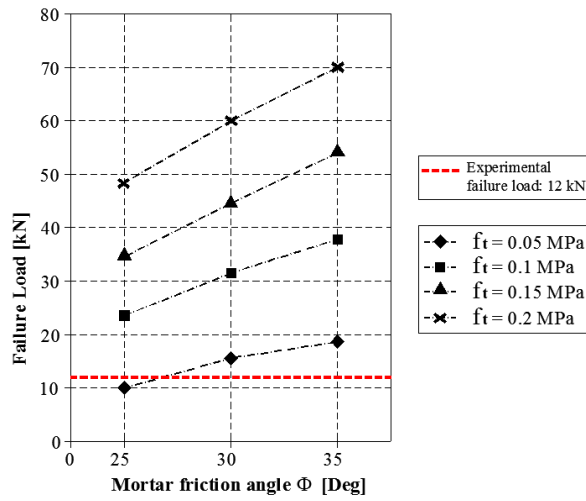
Figure 3.18 Ribbed cross vault. Experimental and numerical (dashed line) results

Load-displacement curves obtained using the elasto-damaging model by Creazza et al. [6] are also depicted. Also in this case a sensitivity analysis (f_t equal to 0.05, 0.1, 0.15, and 0.2 N/mm^2 and Φ equal to 25° , 30° and 35°) has been conducted. Results of such analysis are reported in Figure 3.24-a and -b.

Similarly to the previous cases, the failure load depends considerably on mortar friction angle at assumed tensile strength, meaning that collapse occurs as a combination of bending and in-plane actions, as shown in Figure 3.25 –a (failure mechanism obtained assuming f_t equal to 0.1 N/mm^2 and $\Phi = 20^\circ$).



-a



-b

Figure 3.19 Ribbed cross vault. -a: Sensitivity analysis varying mortar tensile strength and mortar friction angle. -b: Failure load-mortar friction angle diagram.

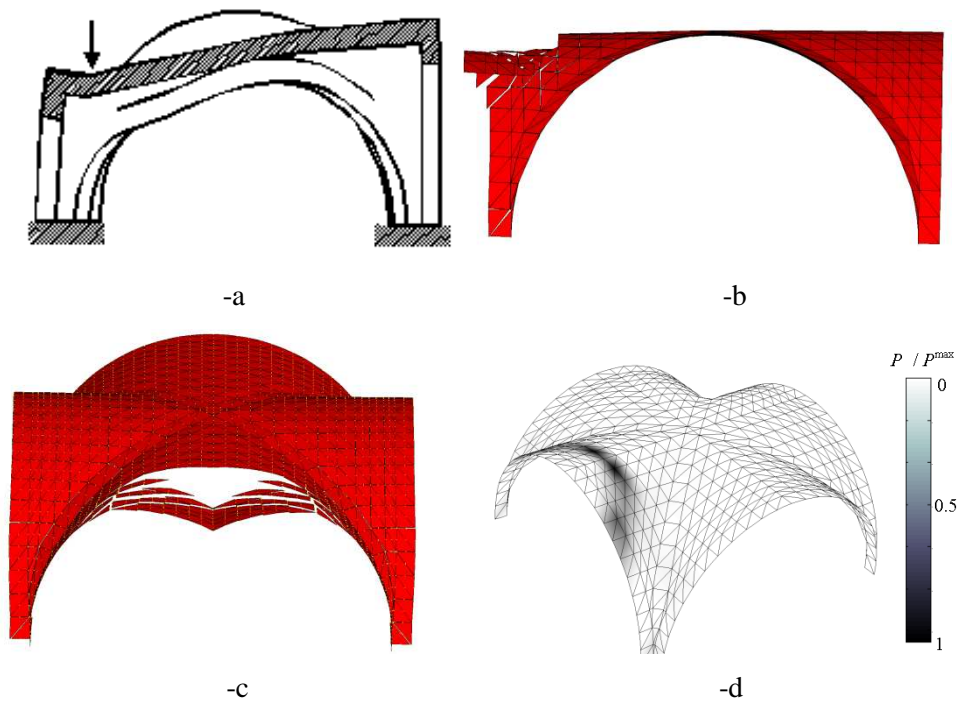


Figure 3.20 Ribbed cross vault: -a: Failure mechanism (Creazza et al. [6]). -b: Failure mechanism, section view, present study. -c: Failure mechanism, front view, present study. -d: Normalized power dissipated patch (P^{\max} is the maximum nodal power dissipation value).

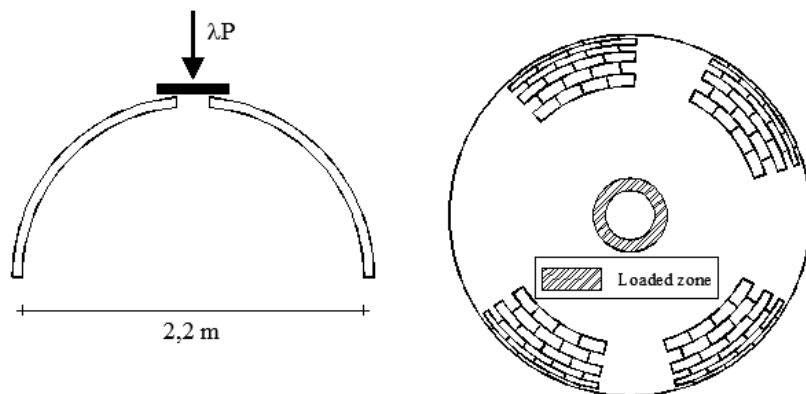


Figure 3.21 Hemispherical dome. Geometry and loading condition.

In Figure 3.25 -b, the internal power dissipation patch is represented. As it possible to note, internal dissipation is concentrated along a circular crown, with the formation of one annular bending hinge; moreover a minor amount appears along the meridians of the hemispherical dome, which vanishes when $f_t \rightarrow 0$.

Finally, in Figure 3.26, the meridian and radial specific membrane actions distributions from the dual problem, as well as meridian actions eccentricity are represented. As it is possible to notice, collapse occurs for the formation of a hinge along the parallel located between the fifth and the sixth row of elements.

3.3 Conclusion

In this chapter, a kinematic limit analysis model for the structural analysis of masonry curved shells has been presented. In the simulations, six-nodes curved triangular elements are used, with possible plastic dissipation at the interfaces between adjoining elements. Curved elements have been used with the aim of taking into account correctly, as far as possible, the actual geometry of the vault.

For the sake of simplicity, a kinematic approach is employed assuming curved six-nodes triangles rigid-infinitely resistant, with possible velocities discontinuities along the edges of adjoining elements. dissipation is allowed only at the interfaces (generalized cylindrical hinges) between adjoining elements. In this way, an upper bound of the collapse load is obtained. In order to take into account all possible failure modes along triangles edges (rotation, stretching, and sliding), it is assumed that dissipation occurs for bending moment, torsion, out-of-plane shear and in-plane actions, as usually accepted for the analysis of thick (Reissner-Mindlin) shells.

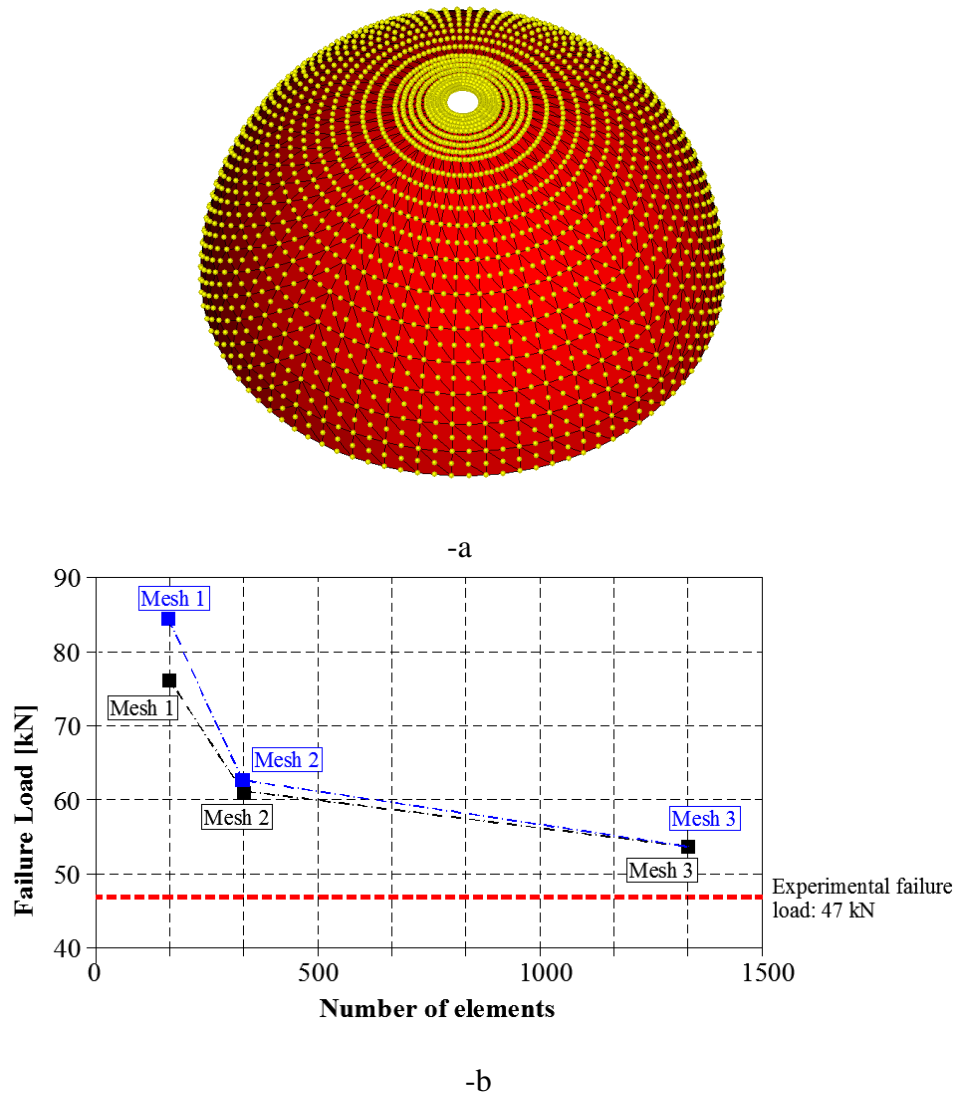


Figure 3.22 Hemispherical dome. –a: Mesh 3:1344 elements (and 2784 nodes). –b: Mesh dependence study.

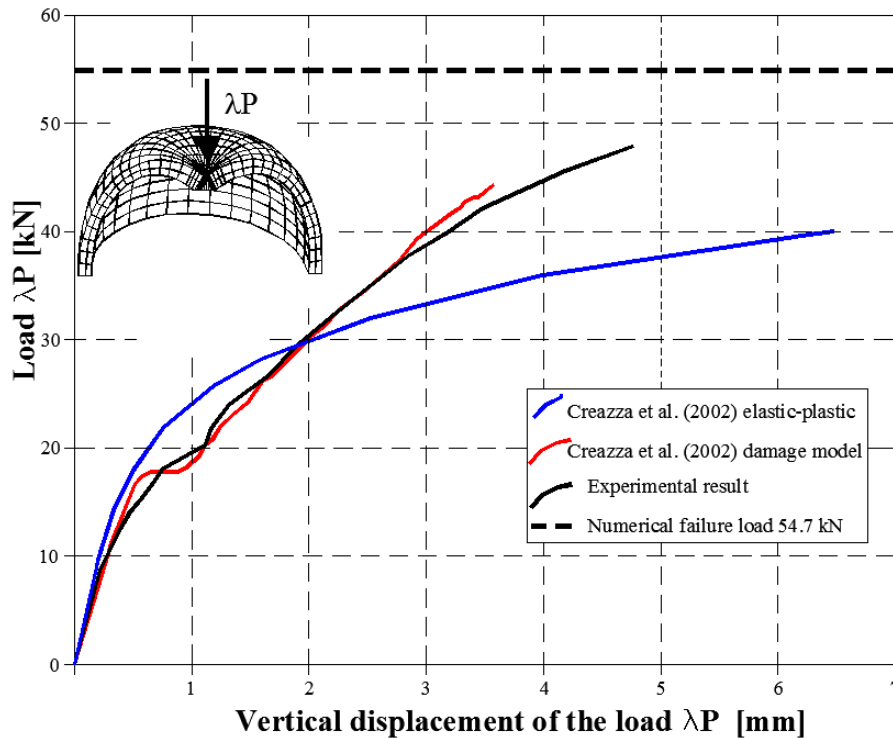
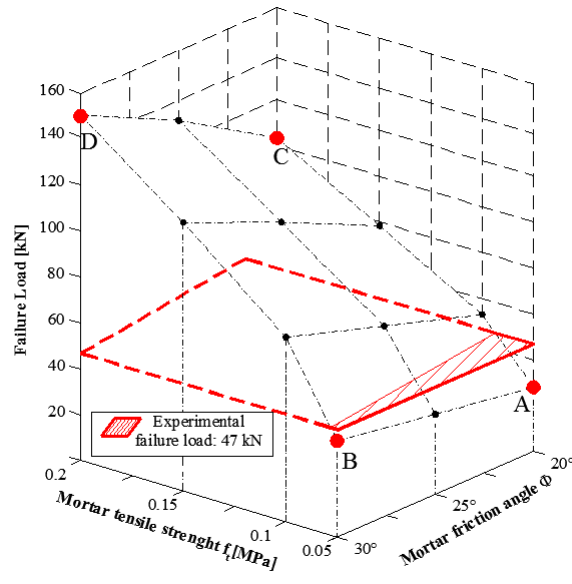
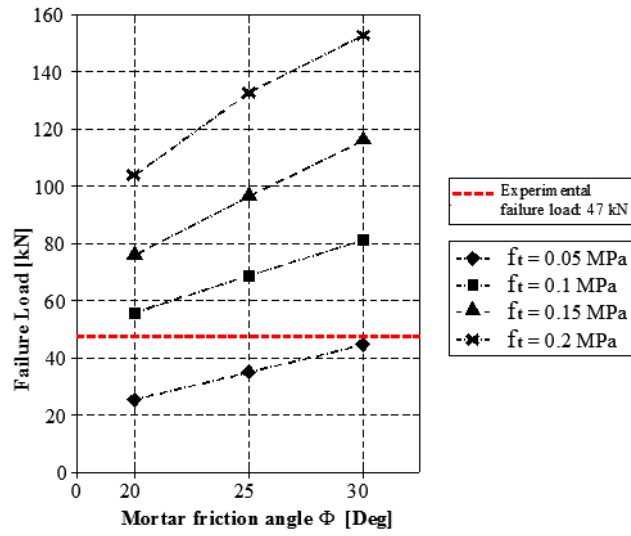


Figure 3.23 Hemispherical dome. Experimental and numerical (dashed line) results.

Plastic dissipation is evaluated assuming for the interfaces between adjoining elements an upper bound approximation of the actual homogenized masonry failure surface, obtained by means of a standard UB finite element procedure, once that a suitable elementary cell is identified for the curved texture under consideration. The model is assessed through several numerical simulations on masonry shells experimentally tested until collapse. In particular, the dependence of the collapse multiplier from the mesh and from the material parameters (sensitivity analysis) is thoroughly discussed.



-a



-b

Figure 3.24 Hemispherical dome. -a: Sensitivity analysis varying mortar tensile strength and mortar friction angle. -b: Failure load-mortar friction angle diagram.

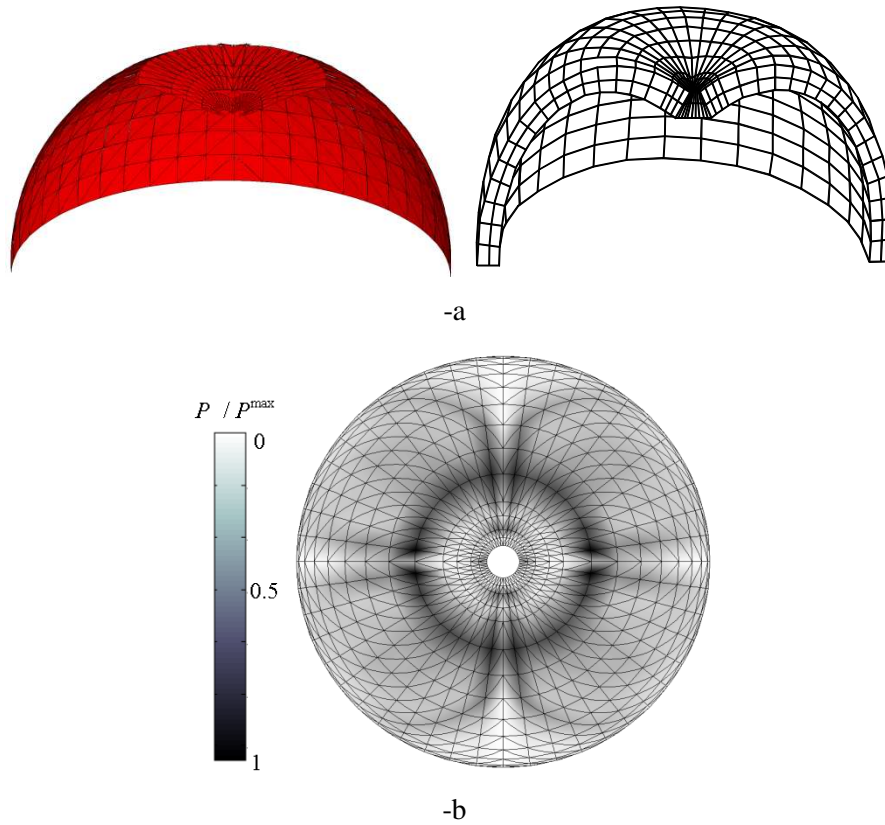


Figure 3.25 Hemispherical dome. -a: Failure mechanism (present study and damage model by Creazza et al. [6]).-b: Normalized power dissipated patch (P^{\max} is the maximum nodal power dissipation value).

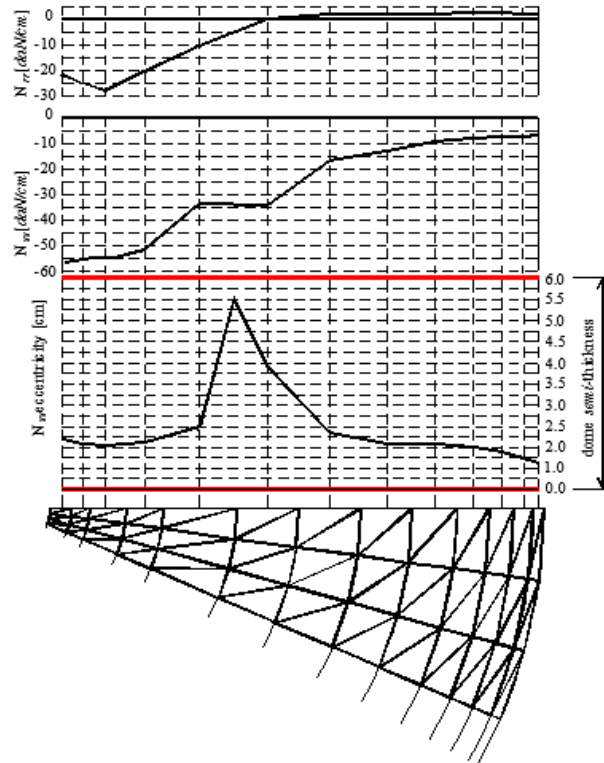


Figure 3.26 Hemispherical dome. Meridian, radial specific membrane actions and eccentricity of radial actions.

3.4 References

- [1] Sloan S W, Kleeman P W. Upper bound limit analysis using discontinuous velocity fields. *Computer Methods in Applied Mechanics and Engineering* 1995; 127(1-4): 293-314.
- [2] Sinha B P. A simplified ultimate load analysis of laterally loaded model orthotropic brickwork panels of low tensile strength. *Journal of Structural Engineering ASCE* 1978; 56B(4), 81-84.
- [3] Chapelle D, Bathe K J. *The Finite Element analysis of shells- fundamentals*. Springer 2003; Berlin.
- [4] Zienkiewicz O C, Taylor R L. *The finite element method. Vol. I. Basic formulations and linear problems*. McGraw-Hill, London 1989.
- [5] Krabbenhoft K, Lyamin AV, Hjiiaj M, Sloan SW. A new discontinuous upper bound limit analysis formulation. *International Journal for Numerical Methods in Engineering* 2005; 63: 1069-1088.
- [6] Creazza G, Saetta A, Matteazzi R, Vitaliani R. Analyses of masonry vaults: a macro approach based on three-dimensional damage model. *Journal of Structural Engineering ASCE* 2002; 128(5): 646-654.
- [7] Creazza G, Saetta A, Matteazzi R, Vitaliani R. Analyses of masonry vaulted structures by using a 3-D damage model. *European Congress on Computational Methods in Applied Sciences and Engineering, ECCOMAS 2000, Barcelona, SP*.
- [8] Faccio P, Foraboschi P, Siviero E. Masonry vaults reinforced with FRP strips [In Italian: Volte in muratura con rinforzi in FRP]. *L'Edilizia* 1999; 7/8: 44-50.
- [9] Foraboschi P. Masonry structures externally reinforced with FRP strips: tests at te collapse [in Italian]. In: *Proc. I Convegno Nazionale "Sperimentazioni su Materiali e Strutture"*, Venice 2006.
- [10] Vermeltoort A V. Analysis and experiments of masonry arches. In: *Proc. Historical Constructions 2001*, P.B. Lourenço & P. Roca (Eds.), Guimarães PT.

Chapter 5.

Application of numerical model proposed on an entire masonry building

The recent devastating earthquake occurred in Abruzzo (Italy 2009) indicated once again that the historical Italian buildings, essentially constituted by masonry structures, are scarcely resistant to horizontal loads and highly vulnerable to seismic actions. Such inadequate behaviour under earthquake excitation is a common issue of masonry buildings in many countries worldwide and is essentially due to mortar joints low strength when loaded out-of-plane [1].

The utilization of FRP strips as reinforcement instead of conventional methods seems the most suitable solution for the seismic upgrading, thanks to the limited invasiveness, durability and good performance at failure [2]-[8] of carbon fibers.

As discussed in previous chapter, the new and efficient numerical tool proposed is able to predict the ultimate load bearing capacity not only for domes but also for entire masonry buildings with or without FRP strips. In order to fully validate the

numerical model proposed, a set of numerical simulations on an entire building reinforced with FRP strips and experimentally tested until collapse by Yi et al. [10][11] is reported, in this chapter, in presence and absence of reinforcement. Results, obtained with the model proposed fit well both experimental data and alternative non linear FEM simulations results. From an overall analysis of the performance of the numerical tool proposed, it can be deduced that the approach presented may be a valuable software for practitioners involved in an inexpensive evaluation of ultimate loads of masonry buildings reinforced with FRP strips.

5.1 Masonry test structure: geometry description

A 3D FE limit analysis on a two story unreinforced-reinforced masonry building experimentally tested by Yi et al. and Moon et al. in [10]-[12] is considered.

The structure reproduces some structural characteristics of typically existing masonry buildings in the mid-America area. The dimensions of the structure are 7.32×7.32 m in plan, with story heights of 3.6 m for the first story and 3.54 m for the second story. The structure is constituted by four masonry walls labeled as walls A, B, 1, and 2, respectively, see Figure 5.1.

The walls have different thicknesses and opening ratios to represent typical masonry walls.. Walls 1 and 2 are composed of brick masonry with thickness 20 cm. Wall 1 has relatively small openings, whereas wall 2 contains a large door opening and larger window openings. Therefore, the large difference in stiffness between walls 1 and 2 allows the torsional behavior of the building to be investigated. Walls A and B are identical, and with a nominal thickness equal to 30 cm. The moderate opening ratios in these two walls are representative of many existing masonry buildings. The aspect ratios of piers range from 0.4 to 4.0. The

four masonry walls are considered perfectly connected at the corners, a feature not always reproduced in the existing structures. This allows to investigate also the contribution of the transverse walls to the strength of the overall building. For walls A and B, Yi et al. [10][11] employed masonry arch lintels, whereas for walls 1 and 2, steel lintels were used. A wood diaphragm and a timber roof are present in correspondence of the floors. Both solid bricks and hollow cored bricks were employed in the structure. The nominal dimensions of both types of bricks are 200×89 mm (length \times width). The cored bricks contain a longitudinal hole through the center with a diameter of 22 mm. Solid bricks were used for the lower 54 courses in the first story of the test structure to approximately the 3.8 m level, whereas cored bricks were used for the remaining parts of the structure.

5.1.1 Reinforced building

When dealing with the reinforced case, each wall was strengthened with different typologies and dispositions of strips.

For Wall 1, unidirectional glass FRP (GFRP) strips epoxy bonded to the interior face were used (Figure 5.2 -a), whereas two bidirectional glass fiber reinforcement cement sheets bonded to the internal faces were applied on Wall 2 (Figure 5.2 -b). Pre-stressing bars (17.5 mm diameter and 690 MPa yield strength) were located vertically at the center of each pier of Wall A (Figure 5.2 -c).

Finally, unidirectional vertical and diagonal GFRP strips were bonded to the interior face of Wall B (Figure 5.2 -d).

5.1.2 Loading condition and material properties

Two different loading conditions are investigated numerically, corresponding to horizontal loads dependent on the load multiplier applied along X (i.e. parallel to Walls 1 and 2) and Y direction (parallel to A and B) respectively, see Figure 5.1.

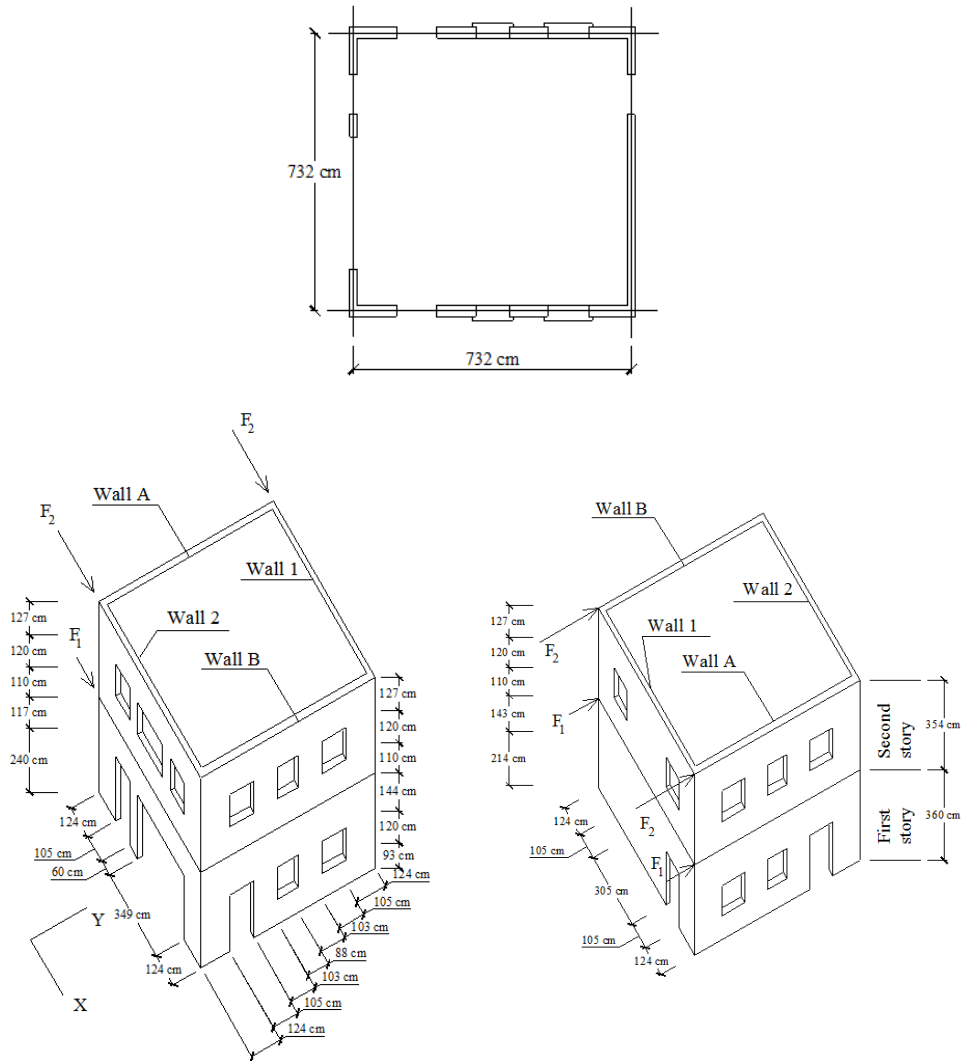


Figure 5.1 Unreinforced masonry test structure

The test setup of [10] was obtained locating two 1000 kN actuators at the roof level and two 450 kN actuators at the first floor, thus reproducing a first vibration mode static distribution of horizontal loads in both directions.

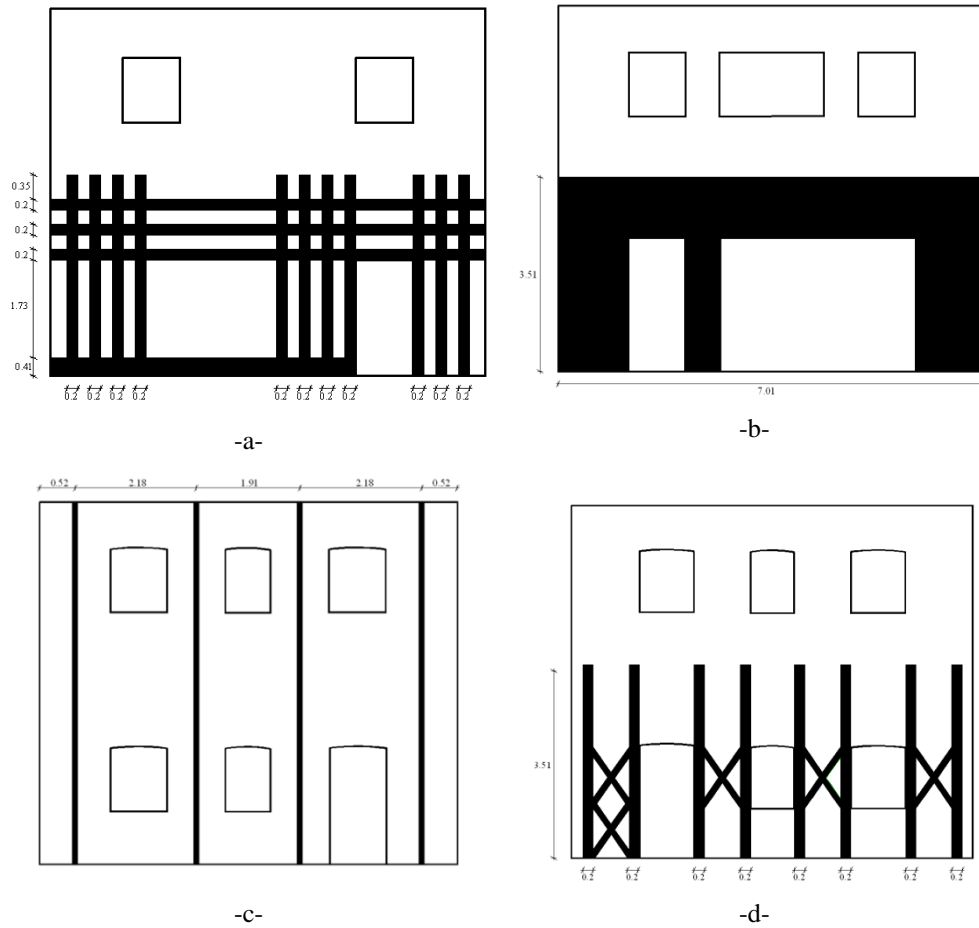


Figure 5.2 Reinforced masonry test structure: -a- Wall 1; -b- Wall 2; -c- Wall A; -d- Wall B

In the numerical model, vertical loads consist only of walls' self weight and permanent loads of the first floor and of the roof.

The experimental compressive strength of bricks and mortar reported in [10] is 41.6 MPa and 0.283 MPa respectively. Mechanical properties assumed in the numerical model for masonry are summarized in Table 5.1.

Table 5.1: Entire building reinforced with FRP strips. Mechanical characteristic assumed for joints and bricks.

Joint (Lourenço Rots failure criterion)

| | | |
|----------------|---|------------|
| $f_t [N/mm^2]$ | Tensile strength | 0.15 |
| $f_c [N/mm^2]$ | Compressive strength | 4 |
| c | Cohesion | $1.2 f_t$ |
| Φ | Friction angle | 20° |
| Φ_2 | Angle of the linearized compressive cap | 40° |

Brick (Mohr-Coulomb failure criterion with compressive cutoff)

| | | |
|----------------|----------------------|------------|
| $f_c [N/mm^2]$ | Compressive strength | 4.5 |
| $c [N/mm^2]$ | Cohesion | 1 |
| Φ | Friction angle | 45° |

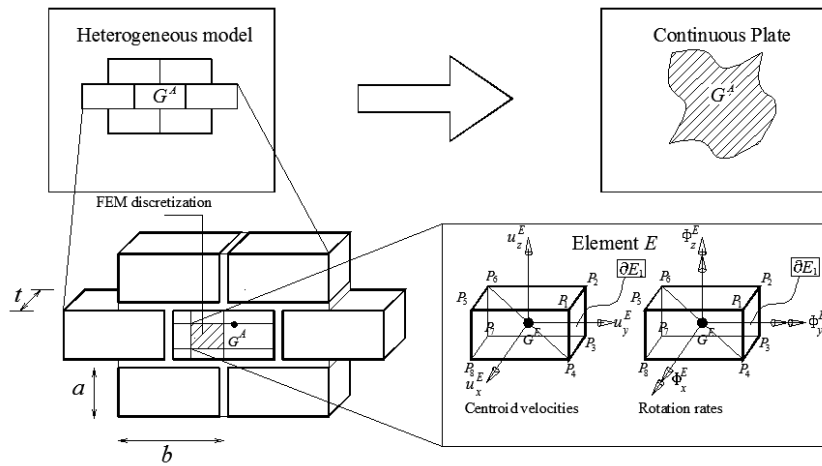


Figure 5.3 REV adopted to model unreinforced masonry and its FE discretization

The failure surfaces adopted for analysis on macro-scale level at step II, calculated with the procedure explained in Chapter 2 (see Figure 5.3 for REV adopted to model unreinforced masonry) are reported in Figure 5.4.

5.2 Numerical results

5.2.1 X direction

For the numerical limit analyses performed in what follows, a model with 5920 wedge shaped elements (masonry) and 2176 triangles has been used, see Figure 5.5. The 3D deformed shapes at collapse, both in presence and absence of reinforcement, obtained through the FE limit analysis proposed are represented in Figure 5.5 and Figure 5.6. The corresponding numerical and the experimental collapse loads are reported in Table 5.2. As can be noted, limit analysis simulations are in satisfactory agreement with experimental results, providing collapse loads not exceeding 10% of error with respect to the experimental ones in the most unfavourable case. Considering the obvious limitations and inaccuracies introduced using a homogenized limit analysis approach, such a discrepancy may be regarded as acceptable. From a detailed inspection of the deformed shape at collapse, it can be observed a symmetric behaviour of the building, being Walls A and B almost geometrically identical (except for the application of a different reinforcement typology in the strengthened case). Figure 5.7 and Figure 5.8 show a comparison between the deformed shape of Walls A and B and the experimental crack pattern. As can be noted, while in the unreinforced case, collapse occurs for rocking and shear failure of the piers of the first story with a rigid body motion of the second story, the introduction of FRP at the first level has the obvious consequence of transferring plastic dissipation also at the second story.

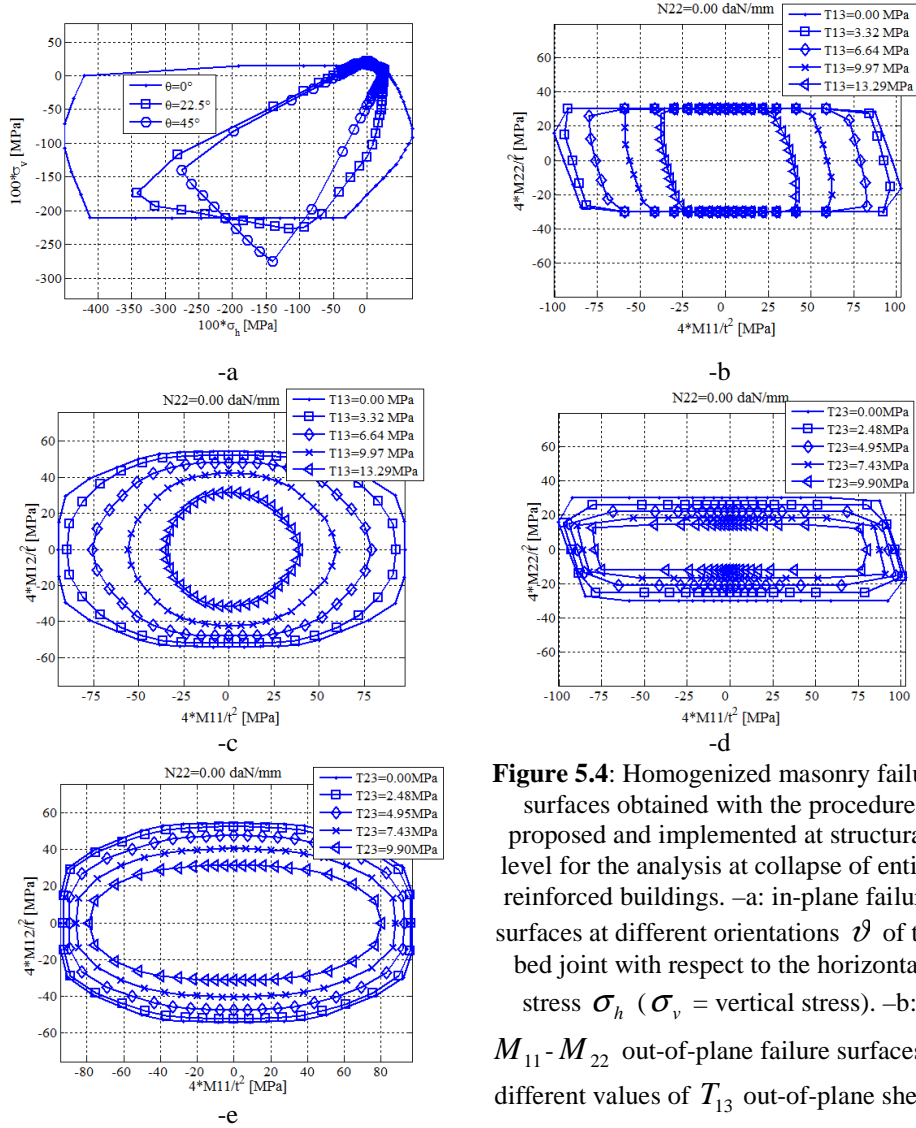


Figure 5.4: Homogenized masonry failure surfaces obtained with the procedure proposed and implemented at structural level for the analysis at collapse of entire reinforced buildings. -a: in-plane failure surfaces at different orientations ϑ of the bed joint with respect to the horizontal stress σ_h (σ_v = vertical stress). -b: $M_{11} - M_{22}$ out-of-plane failure surfaces at different values of T_{13} out-of-plane shear. -c: $M_{11} - M_{12}$ failure surfaces at different values of T_{13} . -d: $M_{11} - M_{22}$ out-of-plane failure surfaces at different values of T_{23} out-of-plane shear. -e: $M_{11} - M_{12}$ out-of-plane failure surfaces at different values of T_{23} .

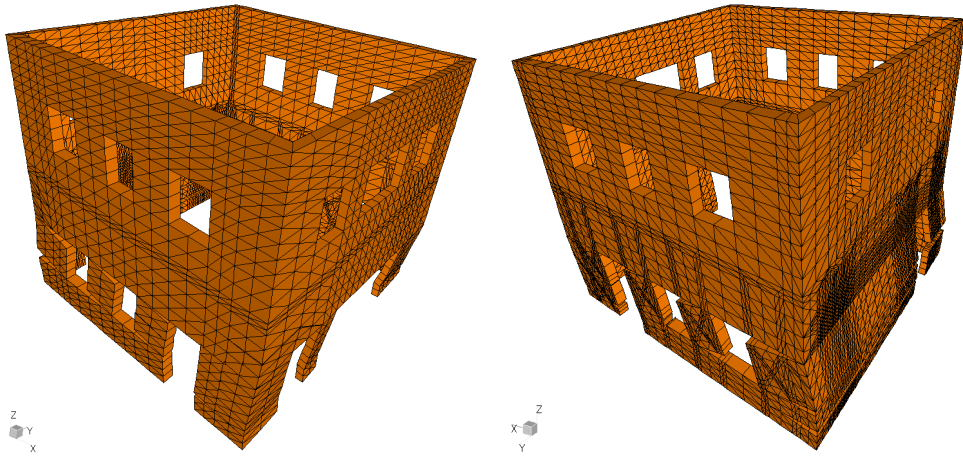


Figure 5.5 Collapse mechanisms in absence of reinforcement: +X direction

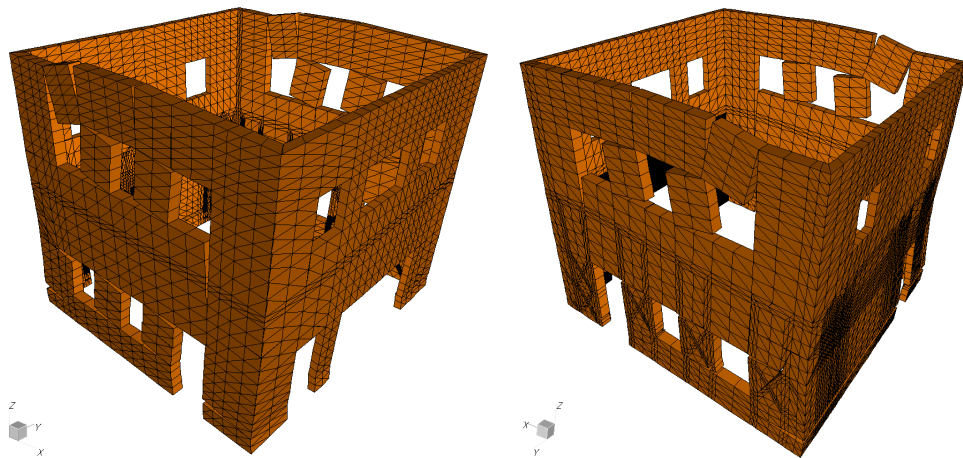
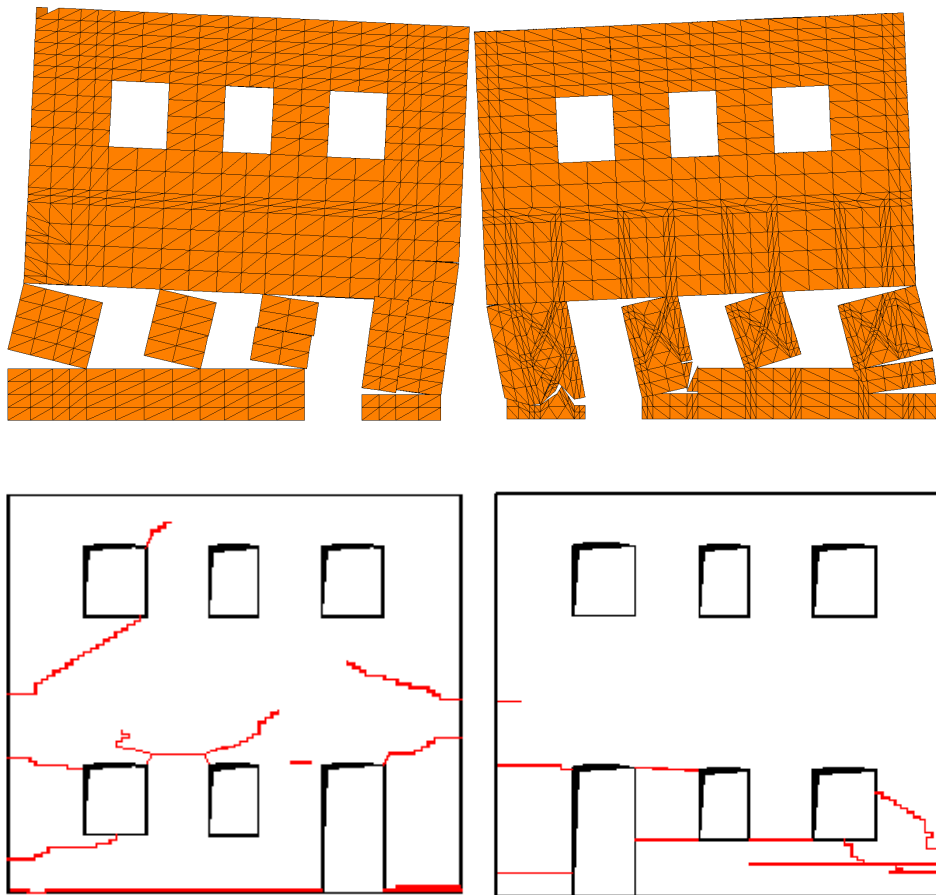


Figure 5.6 Collapse mechanisms in presence of reinforcement: +X direction

Table 5.2: Collapse load

| | <i>Numerical model</i> | <i>Experimental</i> | <i>Variation</i> |
|--------------------|--------------------------|-------------------------|--|
| | (λ_{num}) | (λ_{ex}) | $[(\lambda_{\text{num}}) - (\lambda_{\text{ex}})] / (\lambda_{\text{ex}})$ |
| Without FRP | 330 | 305 | 8.2% |
| With FRP | 520 | 475 | 9.5% |

**Figure 5.7** +X direction: comparison between numerical and crack pattern without FRP

This is confirmed comparing the normalized plastic dissipation patch reported in Figure 5.9 and Figure 5.10 respectively in absence and presence of FRP reinforcement.

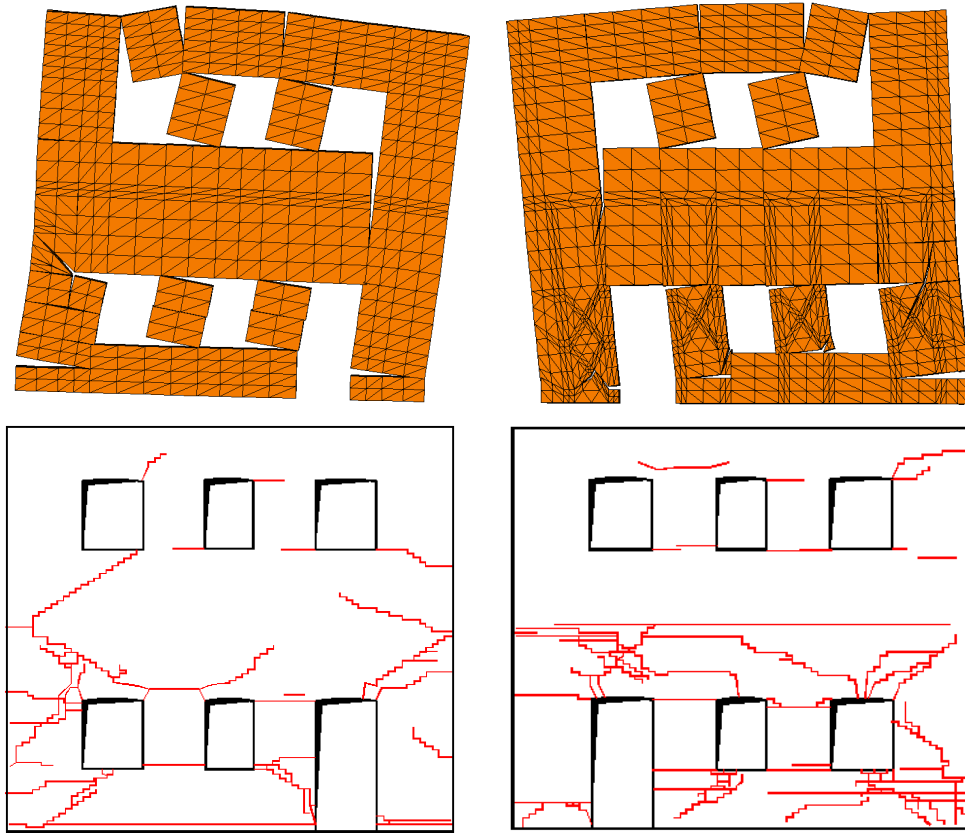


Figure 5.8 +X direction: comparison between numerical and crack pattern with FRP

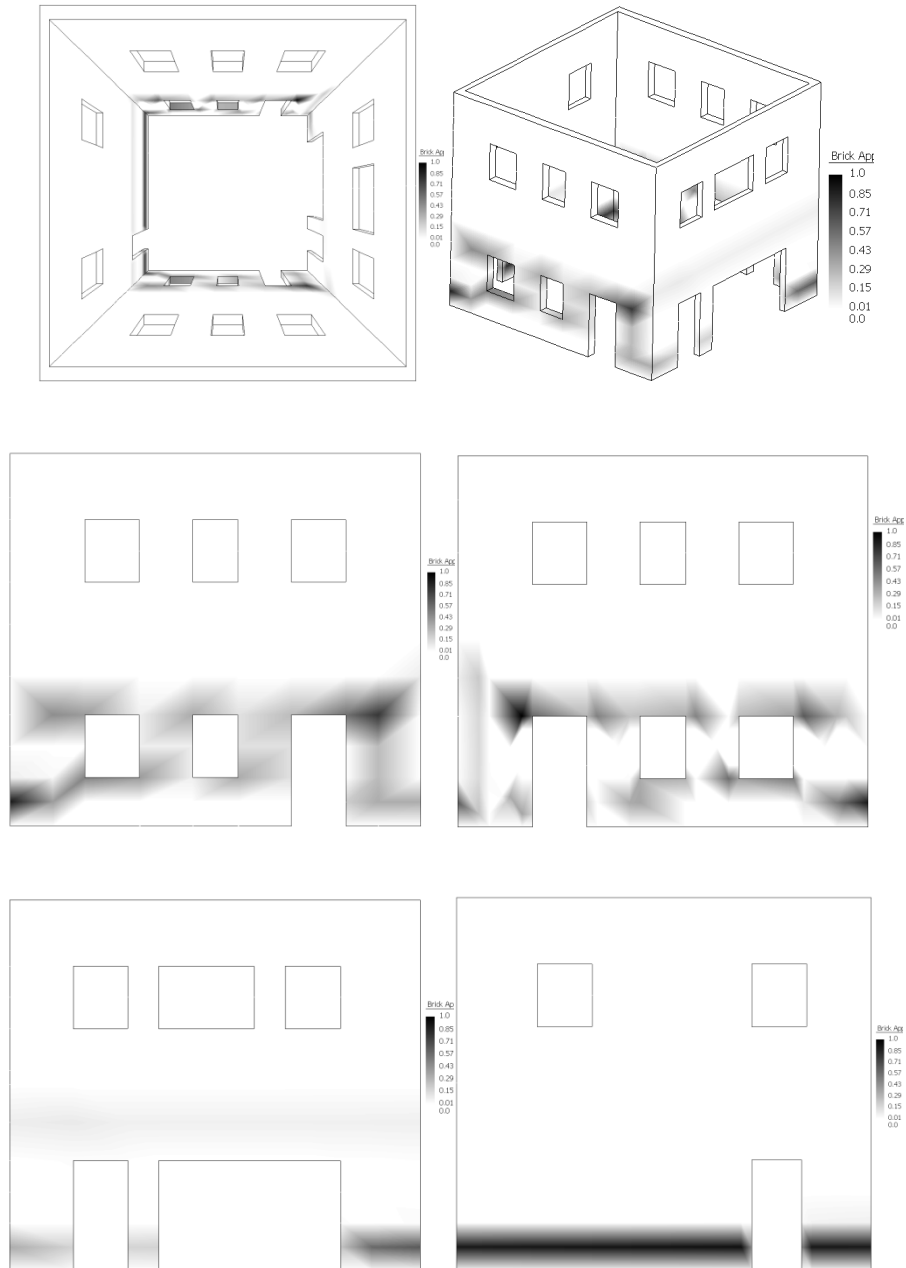


Figure 5.9 Seismic load along +X direction, unreinforced case. Normalized plastic dissipation patch on masonry elements (color range from 0 to 1).

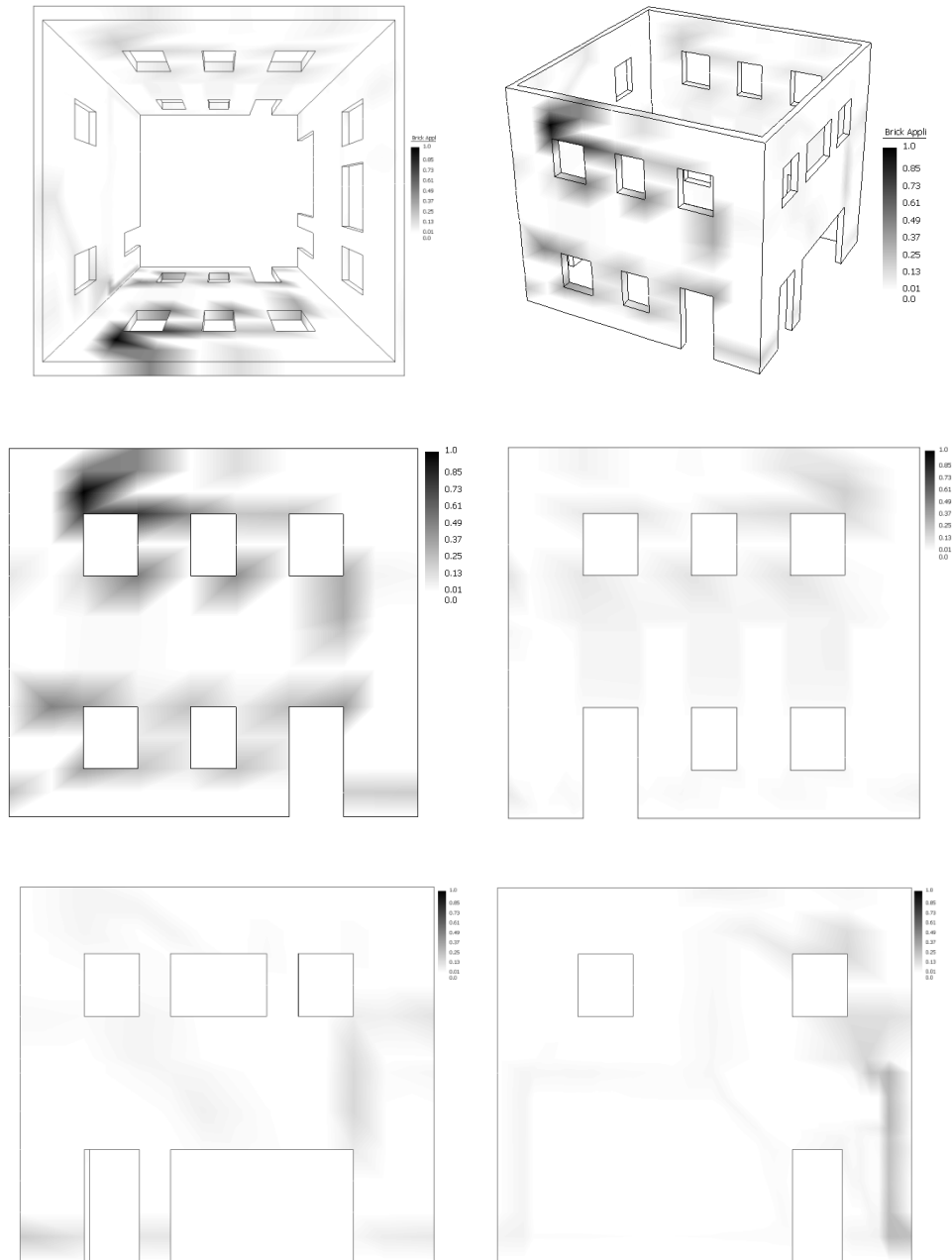


Figure 5.10 Seismic load along +X direction, unreinforced case. Normalized plastic dissipation patch on masonry elements (color range from 0 to 1).

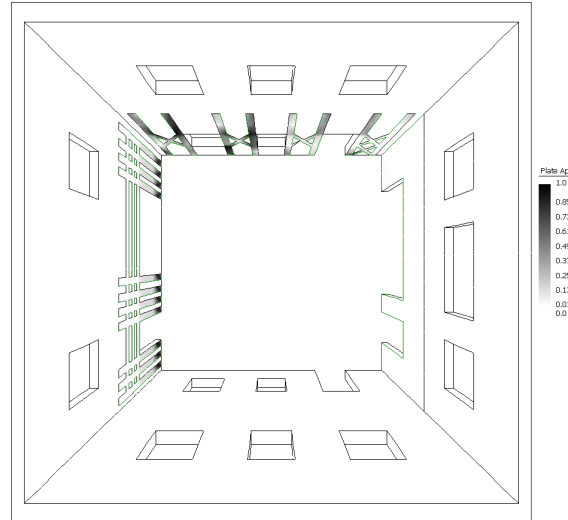


Figure 5.11 Seismic load along +X direction. Normalized plastic dissipation patch on masonry/FRP interfaces (color range from 0 to 1).

In the framework of limit analysis, plastic dissipation simulates the crack zones found at the end of the experimentation and therefore should give a global prediction of the effectiveness of the reinforcement.

Finally, in Figure 5.11, plastic dissipation at the interface between FRP and masonry is represented; it is particularly evident the role played by the strips which delaminate for in-plane actions on Wall A and for out-of-plane rocking of Wall 1.

In order to have a deep insight into the role played by the reinforcement strips on the increase of the ultimate resistance of the building, in Figure 5.12 numerical collapse loads obtained varying f_b masonry/FRP interface strength in a wide range (from 0 to 1 MPa, being 0 MPa the unreinforced case) are represented. First derivative of collapse load with respect to f_b reaches the maximum value approximately in the range 0.3- 0.6 MPa, meaning that this is the optimal value of the bond strength. Finally, it is worth remembering that typical values of bond

strength f_b which can be found in building practice range from 0.15 MPa to 0.50 MPa.

5.2.2 Y direction

Numerical 3D deformed shapes at collapse, with and without reinforcement, obtained when the building is loaded along Y direction are shown in Figure 5.13 and Figure 5.14. The corresponding numerical and the experimental collapse loads are reported in Table 5.3. As can be noted, also in this case, limit analysis failure loads seem in good agreement with experimental results.

Figure 5.15 and Figure 5.16 show a comparison between the deformed shape of Walls 1 and 2 and the experimental crack pattern. As can be noted, the collapse mechanism is similar, in particular the different opening ratio of the Wall 1 and 2 determines torsional effects in the building, see Figure 5.13 and Figure 5.14.

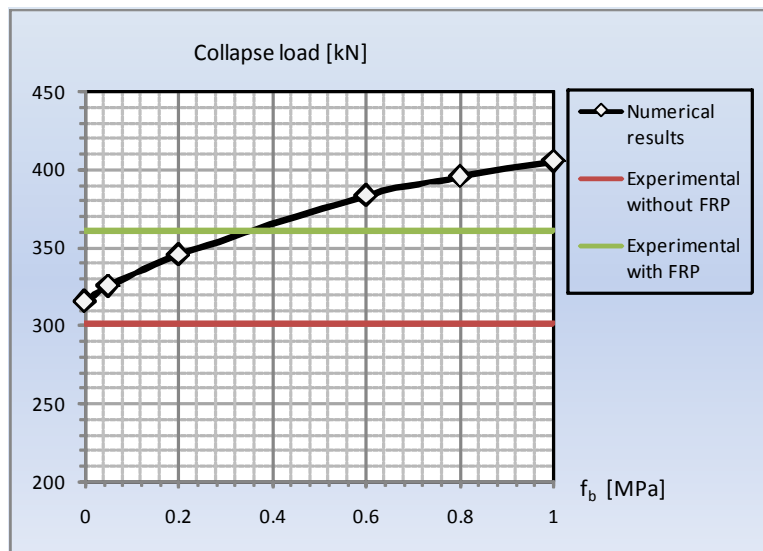


Figure 5.12 Seismic load along +X direction: sensitivity analysis on the collapse load varying f_b masonry/FRP interface strength.

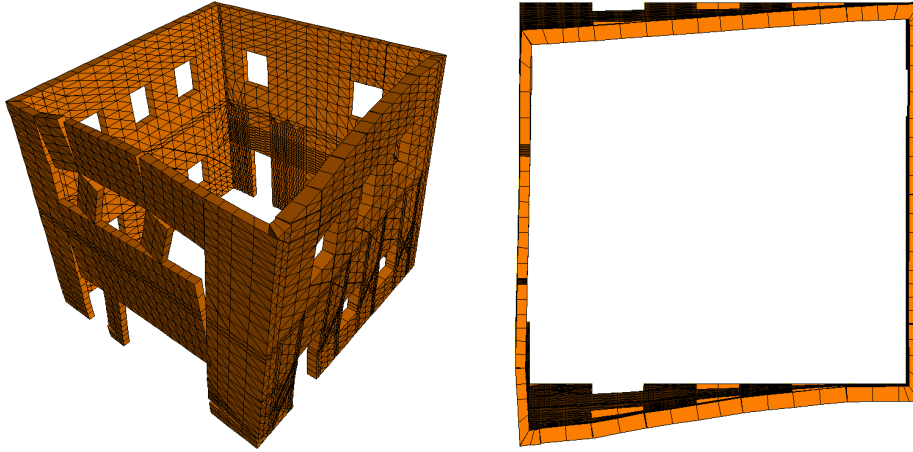


Figure 5.13 Collapse mechanisms in absence of reinforcement: +Y direction

When dealing with the FRP reinforced structure, a moderate increment of the collapse load (around 15-20%) is observed, a consequence of the fact that the failure mechanism does not change considerably with respect to the unreinforced case, except for a more evident plastic dissipation concentrated on Wall 2.

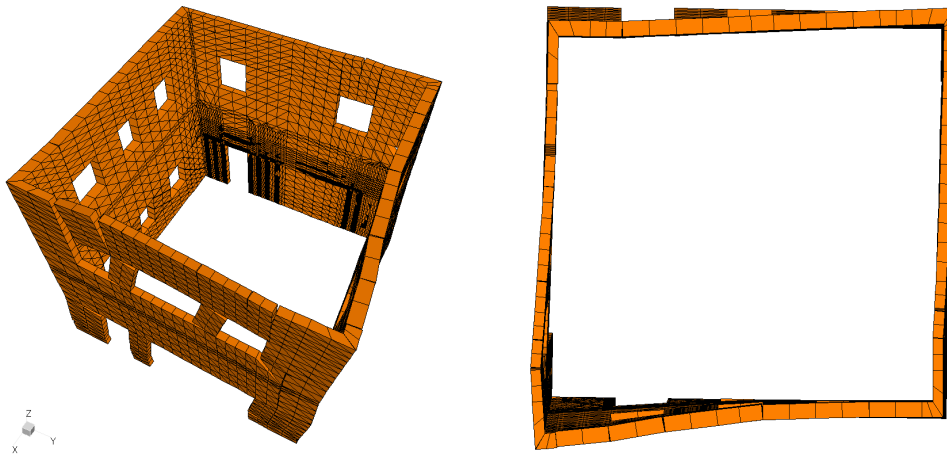
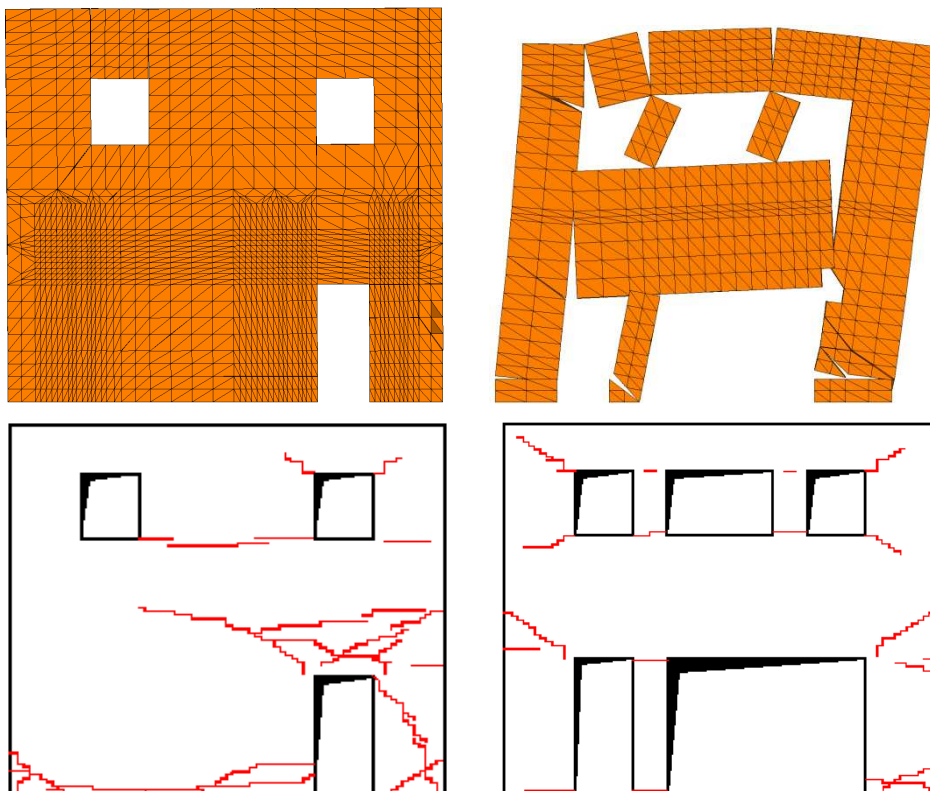


Figure 5.14 Collapse mechanisms in presence of reinforcement: +Y direction

Table 5.3: Collapse load +Y Direction

| | <i>Numerical model</i> | <i>Experimental</i> | <i>Variation</i> |
|--------------------|------------------------|---------------------|---|
| | (λ_{num}) | (λ_{ex}) | $[(\lambda_{num}) - (\lambda_{ex})] / (\lambda_{ex})$ |
| Without FRP | 315 | 301 | 4.6% |
| With FRP | 395 | 361 | 9.4% |

As can be observed from the Table 5.3, a very good agreement is found between experimental and numerical collapse loads, both in presence and absence of FRP strips.

**Figure 5.15** +Y direction: comparison between numerical and crack pattern without FRP

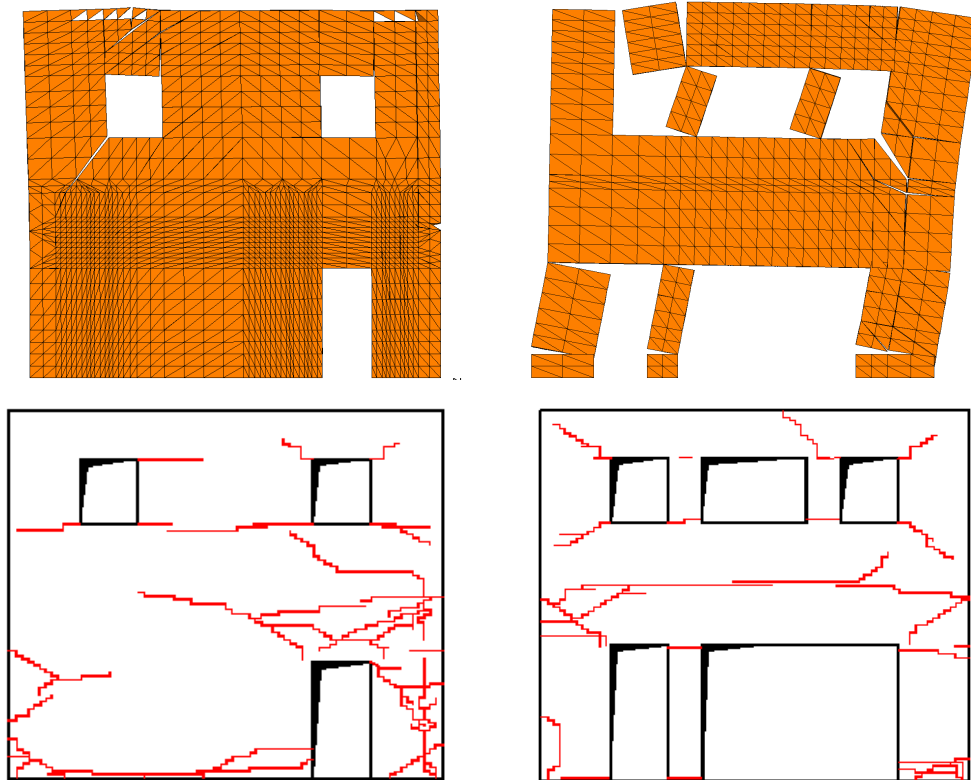


Figure 5.16 +Y direction: comparison between numerical and crack pattern with FRP

As already discussed, within limit analysis, plastic dissipation simulates the crack zones found at the end of the experimentation. Considering that a homogenized approach has been used (i.e. a precise crack pattern zigzagging between bricks can not be reproduced), plastic dissipation patch results quite satisfactory, see Figure 5.17 and Figure 5.18.

Finally, in, plastic dissipation at the interface between FRP and masonry is represented; it is particularly evident the role played both by the continuous tendon which delaminates for in-plane actions and by the reinforcement loaded out-of-plane on Wall B.

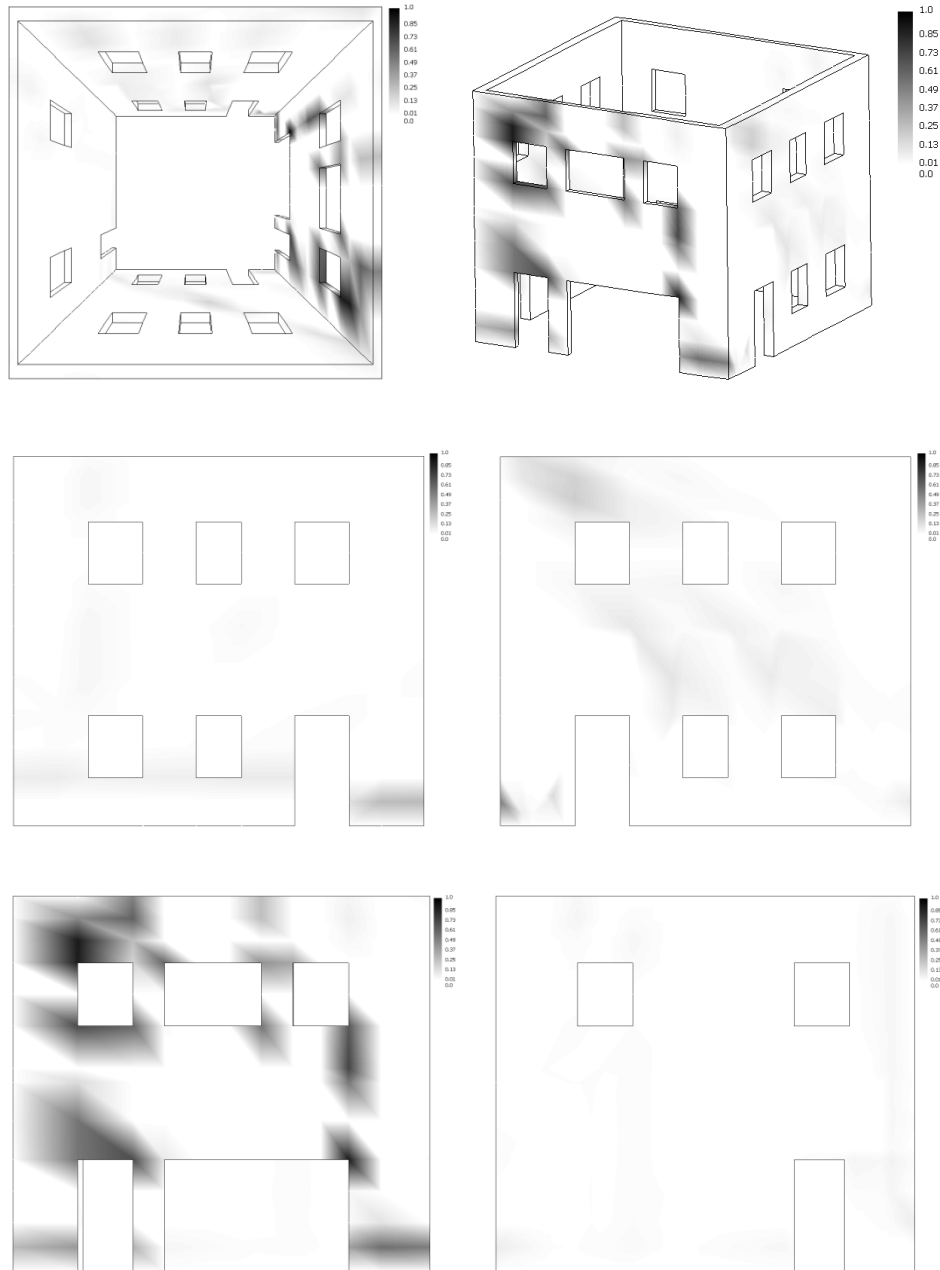


Figure 5.17 Seismic load along +Y direction, unreinforced case. Normalized plastic dissipation patch on masonry elements (color range from 0 to 1).

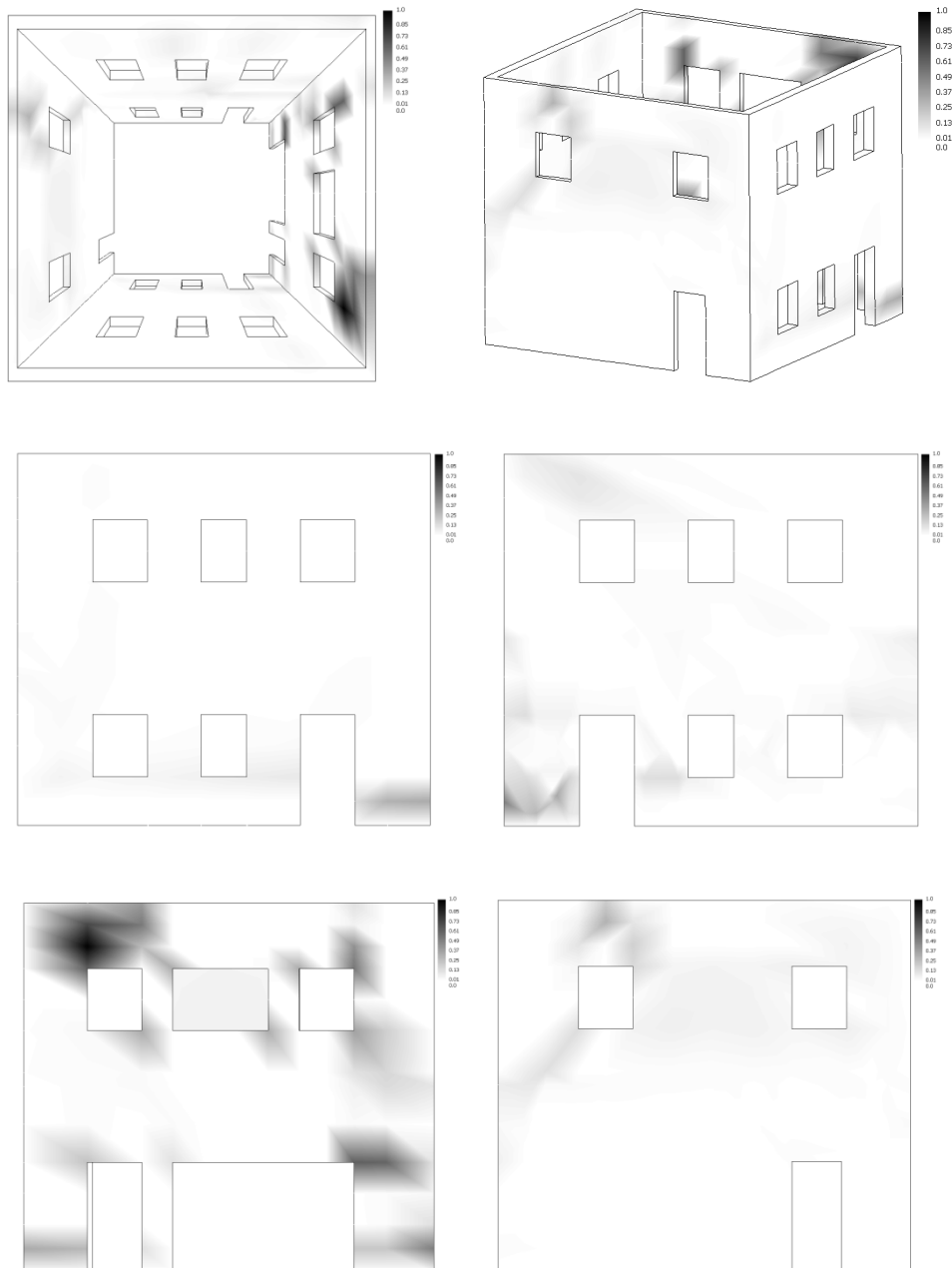


Figure 5.18 Seismic load along +Y direction, reinforced case. Normalized plastic dissipation patch on masonry elements (color range from 0 to 1).

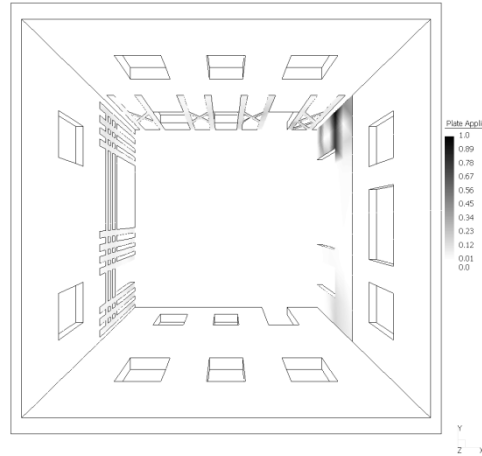


Figure 5.19 Seismic load along +Y direction. Normalized plastic dissipation patch on masonry/FRP interfaces (color range from 0 to 1).

In order to fully assess the numerical results obtained with the present model, in Figure 5.20 numerical collapse loads obtained varying masonry/FRP interface strength f_b in a wide range (from 0 to 1 MPa, being 0 MPa the unreinforced case) are represented. It is worth noting that a satisfactory increase of the collapse load is obtained in the range 0.3- 0.6 MPa. This result is both in agreement with experimental evidences on the bond strength and codes of practice specifics, and indicates once again that high resistance masonry/FRP interfaces do not allow to increase proportionally the collapse load of the entire building. Failure for delamination is, indeed, a consequence of the limited masonry strength, see [9], since f_b peak strength is evaluated from masonry tensile and compressive strength.

5.3 Conclusions

In order to validate the numerical model proposed, an entire two story masonry building reinforced in various ways with FRP strips and experimentally tested at Georgia Tech under earthquake excitation has been extensively analyzed.

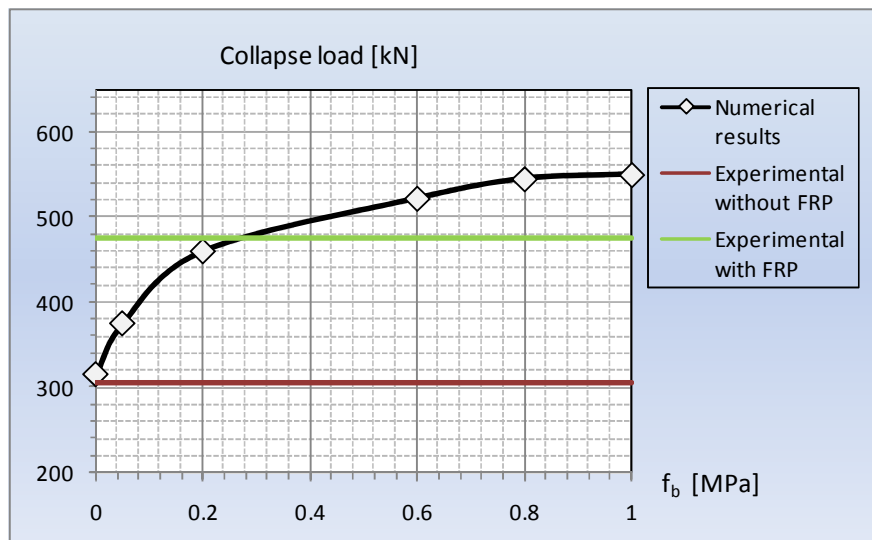


Figure 5.20 Seismic load along +Y direction: sensitivity analysis on the collapse load varying f_b masonry/FRP interface strength.

Good agreement between present results and available data has been found both in presence and absence of reinforcement, meaning that the procedure proposed may be used by practitioners for a reliable evaluation of collapse loads and failure mechanisms of complex 3D strengthened masonry structures.

5.4 References

- [1] Casolo S. *Modelling the out of plane seismic behaviour of masonry walls by rigid elements*, *Earthquake Engineering and Structural Dynamics* 2000; 29(12): 1797-1813.

- [2] Corradi M, Borri A, Vignoli A. *Strengthening techniques tested on masonry structures struck by the Umbria–Marche earthquake of 1997–1998. Construction and Building Materials* 2002; 16: 229–239.
- [3] Schwegler G. *Masonry construction strengthened with composites in seismically endangered zone. In Proc.: 10th European Conference on Earthquake Engineering, Wien 1994: 2299–2303.*
- [4] Eshani MR. *Strengthening of earthquake damaged masonry structures with composite materials. In Proc.: Nonmetallic (FRP) reinforcement for concrete structures. Proceedings of the Second International RILEM Symposium FRPRCS-2 1997; 681–687.*
- [5] Saadmantesh H. *Fiber composites of new and existing structures. ACI Structural Journal* 1991; 91(3): 346–354.
- [6] El-Dakhkhni WW, Hamid AA, Hakam ZHR, Elgaaly M. *Hazard mitigation and strengthening of unreinforced masonry walls using composites. Composite Structures* 2006; 73: 458–477.
- [7] Pendhari SS, Kant T, Desai YM. *Application of polymer composites in civil construction: A general review. Composite Structures* 2008; 84(2): 114–124.
- [8] Triantafillou TC. *Composites: a new possibility for the shear strengthening of concrete, masonry and wood. Composites Science and Technology* 1998; 58: 1285–1295
- [9] CNR-DT200, 2006. *Guide for the design and construction of externally bonded FRP systems for strengthening existing structures. C.N.R., National Research Council, Italy, 2006.*
- [10] Yi T, Moon FL, Leon RT, Khan LF. *Lateral load tests on a two story unreinforced masonry building. ASCE J Struct Engrg* 2006;132(5): 643–52.
- [11] Yi T, Moon FL, Leon RT, Khan LF. *Analyses of a two-story unreinforced masonry building. ASCE J Struct Engrg* 2006;132(5): 653–62.
- [12] Moon FL, Yi T, Leon RT, Khan LF. *Testing of a full scale unreinforced masonry building following seismic strengthening. ASCE J Struct. Engrg.* 2007; 133(9): 1215–1226.

Chapter 6.

Conclusion

The aim of this thesis is to propose a new efficient numerical tool, based on the kinematic theorem of limit analysis, for the study of masonry shell and 3D structures with or without FRP reinforcement.

The approach consists of two steps. In step I unreinforced masonry strength domains are obtained by means of FE limit analysis procedure applied to a representative element of volume constituted by a central brick interacting with its six neighbours through rigid plastic interfaces (mortar joint). In step II, the unreinforced strength domains are implemented in a novel upper bound FE limit analysis code for the analysis at collapse of entire masonry curved and 3D structures.

Two structural models are proposed:

- 1) A Six-nodes triangular curved rigid element with possible velocities discontinuities along the edges of adjoining elements is developed;
- 2) Rigid infinitely resistant wedge-shaped 3D elements with possible velocities discontinuities along the edges of adjoining elements is developed.

After a brief introduction reported in Chapter 1, in Chapter 2 a kinematic simplified identification model for the determination of averaged masonry macroscopic properties at failure has been discussed. The model assumes as representative element of volume (REV) a central brick interconnected with its six neighbours by means of mortar joints reduced to interfaces with frictional behaviour and limited tensile and compressive strength. Suitable macroscopic internal actions have been imposed on the REV in order to comply, at least in an approximate manner, the homogenization theory requirements. In order to numerically evaluate a piecewise linear approximation of masonry failure surface to use at a structural level, the REV has been discretized by means of flat six-nodded wedge rigid elements and a flat three-nodded triangular rigid element for the study of ribbed cross vault. Since no dissipation is allowed inside the element, failure may occur only at the interfaces between contiguous elements. A possible failure of bricks has been also taken into account assuming a limited strength for brick-brick interfaces. A simple linear programming problem is obtained at the micro-scale, which allows, solving several optimization problems at fixed internal actions combinations, to numerically evaluate a piecewise linear approximation of masonry failure surface. In Chapter 3 a kinematic limit analysis model for the structural analysis of masonry curved shells is presented. In the simulations, six-nodes curved triangular elements are used, with possible plastic dissipation at the interfaces between adjoining

elements. For the sake of simplicity, a kinematic approach is employed assuming curved six-nodes triangles rigid-infinitely resistant, with possible velocities discontinuities along the edges of adjoining elements. Dissipation is allowed only at the interfaces (generalized cylindrical hinges) between adjoining elements. In this way, an upper bound of the collapse load is obtained. In order to take into account all possible failure modes along triangles edges (rotation, stretching, and sliding), it is assumed that dissipation occurs for bending moment, torsion, out-of-plane shear and in-plane actions, as usually accepted for the analysis of thick moderately (Reissner-Mindlin) shells.

Plastic dissipation is evaluated assuming for the interfaces between adjoining elements an upper bound approximation of the actual homogenized masonry failure surface, obtained by means of a standard UB finite element procedure, once that a suitable elementary cell is identified for the curved texture under consideration.

In chapter 4 a homogenized FE limit analysis approach for the numerical evaluation of collapse loads and failure mechanisms of FRP-reinforced masonry curved structures is presented.

Unreinforced masonry homogenized failure surfaces obtained in chapter 2 have been used to evaluate plastic dissipation at the interfaces between adjoining wedge-shaped elements. A possible dissipation at the triangular interfaces between FRP and masonry elements is also considered in order to model, in an approximate but effective way, the possible delamination of the strips from the supports. Italian code CNR DT 200/2006 formulas have been used to evaluate peak interface tangential strength.

Several numerical examples are analyzed, consisting of two different typologies of masonry arches (a barrel vault and an arch in a so-called “skew” disposition), a ribbed cross vault, a hemispherical dome and a cloister vault.

For all the cases, both the unreinforced and FRP reinforced case are discussed, analyzed with six-nodes triangular curved rigid element (Chapter 3) and rigid infinitely resistant wedge-shaped 3D elements. Additional non-linear FE analyses are conducted (employing DIANA F.E. program) for all the examples presented, modelling masonry through both a heterogeneous and an equivalent macroscopic material with orthotropic behaviour, in order to assess limit analysis results.

Finally, an entire two story masonry building reinforced in various ways with FRP strips and experimentally tested at Georgia Tech is discussed.

References

- Alfano G, Rosati L, Valoroso N. A numerical strategy for finite element analysis of no-tension materials. *Int. Jour. Num. Meth. Eng.* 2000; 48: 317-350.
- Andrianov I V, Verbonol V M, Awrejcewicz J. Buckling analysis of discretely stringer-stiffened cylindrical shells. *International Journal of Mechanical Sciences* 2006; 48: 1505-1515.
- Anthoine A. Derivation of the in-plane elastic characteristics of masonry through homogenisation theory. *International Journal of Solids and Structures* 1995; 32 (2): 137-163.
- Begg D, Fishwick R. Numerical analysis of rigid block structures including sliding. In: Middleton, J., Pande, G.(Eds.), *Computer Methods in Structural Masonry* 1995; 3, 177 –183.
- Benvenuto E. An introduction to the history of structural mechanics. Volume II: vaulted structures and elastic systems 1991; 307-554, Springer-Verlag Berlin-New-York.
- Berto L, Saetta A, Scotta R, Vitaliani R. An orthotropic damage model for non linear masonry walls analysis: irreversible strain and friction effects. *Third International Seminar Structural Analysis of Historical Constructions*. Guimaraes, Portugal, 2001.
- Berto L, Saetta A, Scotta R, Vitaliani R. Shear behaviour of masonry panel: parametric FE analyses. *Int. Jour. Solids Struct.* 2004;41(16-17): 4383-4405.
- Block P, Ciblac T, Ochsendorf J. Real-time limit analysis of vaulted masonry buildings. *Computers & Structures* 2006; 84(29-30): 1841-1852.
- Caporale A, Luciano R, Rosati L. Limit analysis of masonry arches with externally bonded FRP reinforcements. *Computer Methods in Applied Mechanics and Engineering* 2006; 196: 247-260.
- Casolo S. Modelling the out of plane seismic behaviour of masonry walls by rigid elements", *Earthquake Engineering and Structural Dynamics* 2000; 29(12): 1797-1813.
- Cecchi A, Milani G, Tralli A. A Reissner–Mindlin limit analysis model for out-of-plane loaded running bond masonry walls. *International Journal of Solids and Structures* 2007; 44(5): 1438-1460.
- Cecchi, A., Milani, G., 2007. A kinematic FE limit analysis model for thick English bond masonry walls. *International Journal of Solids and Structures*, in press.
- Ceroni F, Pecce MR, Manfredi G, Marcari G. Experimental bond behaviour in masonry elements externally reinforced with FRP laminates. In: *Proc. of International Conference Composites in Constructions*, Cosenza, Italy, 2003.

- Chapelle D, Bathe K J. *The Finite Element analysis of shells- fundamentals*. Springer 2003; Berlin.
- CNR-DT200, 2006. *Guide for the design and construction of externally bonded FRP systems for strengthening existing structures*. C.N.R., National Research Council, Italy, 2006.
- Como M, Grimaldi A. A unilateral model for limit analysis of masonry walls. *II Meeting on Unilateral Problems in Structural Analysis*. CISM Courses and Lectures, Springer Verlag 1985; 288:223-238.
- Corradi M, Borri A, Vignoli A. Strengthening techniques tested on masonry structures struck by the Umbria–Marche earthquake of 1997–1998. *Construction and Building Materials* 2002; 16: 229–239.
- Creazza G, Saetta A, Matteazzi R, Vitaliani R. Analyses of masonry vaults: a macro approach based on three-dimensional damage model. *Journal of Structural Engineering* 2002; 128(5): 646-654.
- Creazza G, Saetta A, Matteazzi R, Vitaliani R. Analyses of masonry vaulted structures by using a 3-D damage model. *European Congress on Computational Methods in Applied Sciences and Engineering, ECCOMAS 2000, Barcelona, SP, 2000*.
- Creazza G, Saetta A, Matteazzi R, Vitaliani R. Analyses of masonry vaults: a macro approach based on three-dimensional damage model. *Journal of Structural Engineering* 2002; 128(5): 646-654.
- Cuomo M, Ventura G. A complementary energy formulation of no-tension masonry-like solids. *Comp. Meth. Appl. Mech. Eng.* 2000;189: 313-339.
- D.M.LL.PP. (1987) *Norme tecniche per la progettazione, esecuzione e collaudo degli edifici in muratura e per il loro consolidamento [Technical norms for the design, execution and test of masonry buildings and for their rehabilitation]*, Italy, 1987.
- de Buhan P, de Felice G. A homogenisation approach to the ultimate strength of brick masonry. *Journal of the Mechanics and Physics of Solids* 1997; 45(7): 1085-1104.
- De Lorenzis L, Dimitri R, La Tegola A. Reduction of the lateral thrust of masonry arches and vaults with FRP composites. *Construction and Building Materials* 2007; 21(7): 1415-1430
- Del Piero G. Constitutive equation and compatibility of the external loads for linear elastic masonry-like materials. *Meccanica* 1989; 24: 150-162.
- Del Piero G. Limit analysis and no-tension materials. *Int. J. of Plasticity* 1998; 14:259-271.
- Di Pasquale S. *New trends in the analysis of masonry structures*. *Meccanica* 1992; 27: 173-184.
- DIANA 9.3 version *User's Manual*. TNO Building and Construction Research, Department of Computational Mechanics, Delft, The Netherlands, 2008.

Drosopoulos G A, Stavroulakis G E , Massalas C V. *Limit analysis of a single span masonry bridge with unilateral frictional contact interfaces. Engineering Structures* 2006; 8(13): 1864-1873.

El-Dakhkhni WW, Hamid AA, Hakam ZHR, Elgaaly M. *Hazard mitigation and strengthening of unreinforced masonry walls using composites. Composite Structures* 2006; 73: 458-477.

Eshani MR. *Strengthening of earthquake damaged masonry structures with composite materials. In Proc.: Nonmetallic (FRP) reinforcement for concrete structures. Proceedings of the Second International RILEM Symposium FRPRCS-2 1997; 681-687.*

Faccio P, Foraboschi P, Siviero E. *Masonry vaults reinforced with FPR strips [In Italian: Volte in muratura con rinforzi in FRP]. L'Edilizia* 1999; 7/8: 44-50.

Ferris M, Tin Loi F. *Limit analysis of frictional blocks assemblies as a mathematical problem with complementarity constraints. Int.J. Mech. Sci.* 2001; 43: 209-224.

Focacci F. *Rinforzo delle murature con materiali compositi [Masonry strengthening with composite materials]. Flaccovio*, 2008.

Foraboschi P. *Masonry structures externally reinforced with FRP strips: tests at the collapse [in Italian]. In: Proc. I Convegno Nazionale "Sperimentazioni su Materiali e Strutture", Venice* 2006.

Foraboschi P. *Strengthening of masonry arches with fiber-reinforced polymer strips. Journal of Composites for Construction* 2004; 8: 191-202.

Gambarotta L, Lagomarsino S. *Damage models for the seismic response of brick masonry shear walls. Part I: the mortar joint model and its applications. Earthquake Engineering and Structural Dynamics* 1997; 26: 423-439.

Gambarotta L, Lagomarsino S. *Damage models for the seismic response of brick masonry shear walls. Part II: the continuum model Introduction and its applications. Earthquake Engineering and Structural Dynamics* 1997; 26: 440-462.

Giuffrè A. *Lecture sulla Meccanica delle murature storiche. Kappa Eds., Rome*, 1990.

Habbal A. *An effective model for Lipschitz wrinkled arches. Journal of Mathematical Analysis and Applications* 2003; 285: 155-173.

Heyman J. *Equilibrium of shell structures. Oxford, Oxford University Press* 1977.

Heyman J. *The safety of masonry arches. International Journal of Mechanical Sciences* 1969; 43: 209-224.

Huerta S. *Mechanics of masonry vaults: the equilibrium approach. In: Proc. Historical Constructions 2001, P.B. Lourenço & P. Roca (Eds.), Guimarães PT.*

JSCE, *Japan Society of Civil Engineers. Recommendations for upgrading of concrete structures with use of continuous fiber sheets. Concrete Engineering Series 41*, 2001.

- Korany Y, Drysdale R. *Load-Displacement of Masonry Panels with Unbonded and Intermittently Bonded FRP. I: Analytical Model. J. Compos. for Constr.* 2007; 11(1): 15-23.
- Krabbenhoft K, Lyamin AV, Hjiij M, Sloan SW. *A new discontinuous upper bound limit analysis formulation. International Journal for Numerical Methods in Engineering* 2005; 63: 1069-1088.
- Lotfi HR, Shing PB. *Interface model applied to fracture of masonry structures. Jour. Struct. Eng. ASCE* 1994; 120(1): 63-80.
- Lourenço PB, de Borst R, Rots J. *A plane stress softening plasticity model for orthotropic materials. International Journal for Numerical Methods in Engineering* 1997; 40: 4033-4057.
- Lourenço PB, Rots J. *A multi-surface interface model for the analysis of masonry structures. Journal of Engineering Mechanics ASCE* 1997; 123(7): 660-668.
- Lourenço PB. *An orthotropic continuum model for the analysis of masonry structures. Report 03.21.1.31.27 1995, University of Delft, Delft, Holland.*
- Lucchesi M, Padovani C, Pasquinelli G, Zani N. *On the collapse of masonry arches. Meccanica* 1997; 32: 327-346
- Lucchesi M, Padovani C, Pasquinelli G, Zani N. *The maximum modulus eccentricity surface for masonry vaults and limit analysis. Mathematics and Mechanics of Solids* 1999; 4: 71-87.
- Luciano R, Sacco E. *A damage model for masonry structures. Eur.Jour. Mech.-A/Solids* 1998; 17(2): 5-303.
- Luciano R, Sacco E. *Damage of masonry panels reinforced by FRP sheets. International Journal of Solids and Structures* 1998; 35(15): 1723-1741.
- Luciano R, Sacco E. *Homogenization technique and damage model for old masonry material. International Journal of Solids and Structures* 1997; 34(4): 3191-208.
- Luciano R, Sacco E. *Homogenization technique and damage model for old masonry material. Int. Jour. Solids Struct.* 1997; 34(24):3191-3208.
- Marfia S, Sacco E. *Modeling of reinforced masonry elements. Int.Jour. Solids Struct.* 2001; 38(24-25): 4177-4198.
- Marfia S, Sacco E. *Modelling of reinforced masonry elements. International Journal of Solids and Structures* 2001; 38: 4177-4198.
- Massart T, Peerlings RHJ, Geers MGD. *Mesoscopic modeling of failure and damage-induced anisotropy in brick masonry. European Journal of Mechanics A/Solids* 2004; 23: 719-735.

Massart TJ, Peerlings RHJ, Geers MGD. Mesoscopic modeling of failure and damage-induced anisotropy in brick masonry. *Eur. Jour. Mech.-A/Solids* 2004; 23(5): 719-735.

Massart TJ. Multi-scale modeling of damage in masonry structures. PhD Thesis University of Bruxelles 2003.

Milani E, Milani G, Tralli A. Limit analysis of masonry vaults by means of curved shell finite elements and homogenization. *International Journal of Solids and Structures* 2008; 45: 5258-5288.

Milani G, Lourenço PB, Tralli A. Homogenised limit analysis of masonry walls. Part I: failure surfaces. *Computers and Structures* 2006; 84: 166-180.

Milani G, Lourenço PB, Tralli A. Homogenised limit analysis of masonry walls. Part II: structural examples. *Computers and Structures* 2006; 84: 181-195.

Milani G. Homogenized limit analysis of FRP-reinforced masonry walls out-of-plane loaded. *Computational Mechanics* 2009; 43(5): 617-639.

Moon FL, Yi T, Leon RT, Khan LF. Testing of a full scale unreinforced masonry building following seismic strengthening. *ASCE J Struct. Engrg.* 2007; 133(9): 1215-1226.

O'Dwyer D. Funicular analysis of masonry vaults. *Computers & Structures* 1999; 73 (1-5): 187-197.

Oppenheim I J, Gunaratnam D J, Allen R H. Limit State Analysis of Masonry Domes. *Journal of Structural Engineering ASCE* 1989; 115: 868-882.

Orduna A, Lourenço P B. Cap model for limit analysis and strengthening of masonry structures. *Journal of Structural Engineering, ASCE* 2003; 1367-1375.

Orduña A, Lourenço P B. Three-dimensional limit analysis of rigid blocks assemblages. Part I: Torsion failure on frictional joints and limit analysis formulation. *Int. J. Solids and Structures* 2005; 42 (18-19): 5140-5160.

Pegon P, Anthoine A. Numerical strategies for solving continuum damage problems with softening: application to the homogenization of masonry. *Computers and Structures* 1997; 64(4): 623-642.

Pendhari SS, Kant T, Desai YM. Application of polymer composites in civil construction: A general review. *Composite Structures* 2008; 84(2): 114-124.

Pesciullesi C, Rapallini M, Tralli A, Cianchi A. Optimal spherical masonry domes of uniform strength. *Journal of Structural Engineering ASCE* 1997; 123: 203-209.

Pietruszczak S, Ushaksaraei R. Description of inelastic behavior of structural masonry. *Int. Jour. Solids Struct.* 2003; 40(15): 4003-4019.

Roca P, Lopez-Almansa F, Miquel J, Hanganu A. Limit analysis of reinforced masonry vaults. *Engineering Structures* 2007; 29: 431-439.

- Romano G, Romano M. *Sulla soluzione di problemi strutturali in presenza di legami costitutivi unilateri*. *Atti Acc. Naz. Linc.* 1979; Serie VIII, Vol. LXVII.
- Saadmantesh H. *Fiber composites of new and existing structures*. *ACI Structural Journal* 1991; 91(3): 346–354.
- Schwegler G. *Masonry construction strengthened with composites in seismically endangered zone*. In *Proc.: 10th European Conference on Earthquake Engineering*, Wien 1994: 2299–2303.
- Sinha B P. *A simplified ultimate load analysis of laterally loaded model orthotropic brickwork panels of low tensile strength*. *Journal of Structural Engineering ASCE* 1978; 56B(4), 81-84.
- Slinchenko D, Verijenko V E. *Structural analysis of composite lattice shells of revolution on the basis of smearing stiffness*. *Composite Structures* 2001;54: 341-448.
- Sloan S W, Kleeman P W. *Upper bound limit analysis using discontinuous velocity fields*. *Computer Methods in Applied Mechanics and Engineering* 1995; 127(1-4): 293-314.
- Suquet P. *Analyse limite et homogeneisation*. *Comptes Rendus de l'Academie des Sciences - Series IIB – Mechanics* 1983; 296: 1355-1358.
- Triantafillou TC. *Composites: a new possibility for the shear strengthening of concrete, masonry and wood*. *Composites Science and Technology* 1998; 58: 1285–1295
- Ushaksaraei R, Pietruszczak S. *Failure criterion for structural masonry based on critical plane approach*. *J. Eng. Mech. ASCE* 2002; 128(7): 769 –778.
- Vermeltfoort AV. *Analysis and experiments of masonry arches*. In: *Proc. Historical Constructions*, P.B. Lourenço & P. Roca (Eds.), Guimarães PT, 2001.
- Yi T, Moon FL, Leon RT, Khan LF. *Analyses of a two-story unreinforced masonry building*. *ASCE J Struct Engrg* 2006;132(5): 653–62.
- Yi T, Moon FL, Leon RT, Khan LF. *Lateral load tests on a two story unreinforced masonry building*. *ASCE J Struct Engrg* 2006;132(5): 643–52.
- Zienkiewicz OC, Taylor RL. *The finite element method. Vol. I. Basic formulations and linear problems*. McGraw-Hill, London, 1989.



Registrazione modulo Dichiarazione di conformità

MODULO INVIATO CORRETTAMENTE

Consegnare la copia stampata e debitamente firmata all'Ufficio Dottorato e Alta Formazione in via Scienze 41b Ferrara

Io sottoscritto Dott. (Cognome e Nome)

MILANI ENRICO

nato a

ROVIGO

Provincia

ROVIGO

il giorno

21/12/1980

Your E-Mail Address

enrico.milani@ing3srl.com

avendo frequentato il corso di Dottorato di Ricerca in:

SCIENZE DELL'INGEGNERIA

Ciclo di Dottorato

XXII

Titolo della tesi in Italiano

MODELLI AGLI ELEMENTI FINITI PER ANALISI LIMITE SECONDO IL TEOREMA CINEMATICO DI STRUTTURE E VOLTE IN MURATURA CON E SENZA FIBRORINFORZI

Titolo della tesi in Inglese

A F.E. UPPER BOUND LIMIT ANALYSIS MODEL FOR MASONRY CURVED AND 3D STRUCTURES, WITH AND WITHOUT FRPREINFORCEMENT

Titolo della tesi in altra Lingua Straniera

Tutore - Prof:

TRALLI ANTONIO

Settore Scientifico Disciplinare (SSD)

ICAR/08

Parole chiave (max 10)

MURATURE, ELEMENTI FINITI, FRP, OMOGENEIZZAZIONE, ANALISI LIMITE

Consapevole - Dichiaro

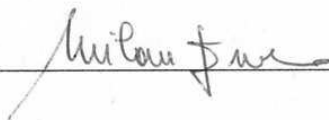
CONSAPEVOLE --- 1) del fatto che in caso di dichiarazioni mendaci, oltre alle sanzioni previste dal codice penale e dalle Leggi speciali per l'ipotesi di falsità in atti ed uso di atti falsi, decade fin dall'inizio e senza necessità di alcuna formalità dai benefici conseguenti al provvedimento emanato sulla base di tali dichiarazioni; -- 2) dell'obbligo per l'Università di provvedere al deposito di legge delle tesi di dottorato al fine di assicurarne la conservazione e la consultabilità da parte di terzi; -- 3) della procedura adottata dall'Università di Ferrara ove si richiede che la tesi sia consegnata dal dottorando in 4 copie di cui una in formato cartaceo e tre in formato .pdf, non

modificabile su idonei supporti (CD-ROM, DVD) secondo le istruzioni pubblicate sul sito : <http://www.unife.it/dottorati/dottorati.htm> alla voce ESAME FINALE – disposizioni e modulistica; -- 4) del fatto che l'Università sulla base dei dati forniti, archiverà e renderà consultabile in rete il testo completo della tesi di dottorato di cui alla presente dichiarazione attraverso l'Archivio istituzionale ad accesso aperto "EPRINTS.unife.it" oltre che attraverso i Cataloghi delle Biblioteche Nazionali Centrali di Roma e Firenze. --- DICHIARO SOTTO LA MIA RESPONSABILITA' --- 1) che la copia della tesi depositata presso l'Università di Ferrara in formato cartaceo, è del tutto identica a quelle presentate in formato elettronico (CD-ROM, DVD), a quelle da inviare ai Commissari di esame finale e alla copia che produrrò in seduta d'esame finale. Di conseguenza va esclusa qualsiasi responsabilità dell'Ateneo stesso per quanto riguarda eventuali errori, imprecisioni o omissioni nei contenuti della tesi; -- 2) di prendere atto che la tesi in formato cartaceo è l'unica alla quale farà riferimento l'Università per rilasciare, a mia richiesta, la dichiarazione di conformità di eventuali copie; -- 3) che il contenuto e l'organizzazione della tesi è opera originale da me realizzata e non compromette in alcun modo i diritti di terzi, ivi compresi quelli relativi alla sicurezza dei dati personali; che pertanto l'Università è in ogni caso esente da responsabilità di qualsivoglia natura civile, amministrativa o penale e sarà da me tenuta indenne da qualsiasi richiesta o rivendicazione da parte di terzi; -- 4) che la tesi di dottorato non è il risultato di attività rientranti nella normativa sulla proprietà industriale, non è stata prodotta nell'ambito di progetti finanziati da soggetti pubblici o privati con vincoli alla divulgazione dei risultati, non è oggetto di eventuali registrazioni di tipo brevettale o di tutela. --- PER ACCETTAZIONE DI QUANTO SOPRA RIPORTATO

Firma Dottorando

Ferrara, li _____

Firma del Dottorando

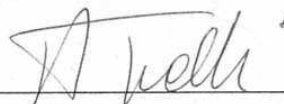


Firma Tutore

Visto: Il Tutore

Si approva

Firma del Tutore



FORMAZIONE POSTLAUREA

Ufficio Dottorato di Ricerca - Ufficio Alta Formazione ed Esami di Stato - IUSS
